Multi-Scroll Chaos Generation via Linear Systems and Hysteresis Function Series

F. Han

Doctor of Philosophy

2004

RMIT

Multi-Scroll Chaos Generation via Linear Systems and Hysteresis Function Series

A thesis submitted in fulfilment of the requirements for
the degree of Doctor of Philosophy

Fengling Han

B.Eng., M.Eng.

School of Electrical and Computer Engineering
Science, Engineering and Technology Portfolio
RMIT University

December 2004

Declaration

I declare that the thesis contains no material which has been accepted for any other academic award in any university and that, to the best of my knowledge, the thesis is original and my own work, it contains no material previously published or written by another person other than where reference has been made in the text. Parts of this thesis have been published in the papers listed in the publication section. And the content of the thesis is the result of work which has been carried out since the official commencement date of the approved research program.

Signed: 

Fengling Han
School of Electrical and Computer Engineering
Royal Melbourne Institute of Technology
Melbourne, VIC 3001, Australia

December 2004

Acknowledgements

My sincere appreciation goes to my supervisors, Prof. Xinghuo Yu and Prof. Guanrong Chen, for their guidance and kind help during the entire process of my research. The progress I made during this research is due to their guidance, motivation, wisdom and critical insights. This was vital to the successful completion of the thesis.

I would like to acknowledge the cooperation and help of Dr. Jinhu Lü, who has collaborated with me at the Royal Melbourne Institute of Technology, and has given me considerable assistance. I also express my thanks to those in the Faculty of Informatics and Communication, Central Queensland University (CQU), Emeritus Professor John Dekkers, Associate Professor Russel Stonier, Mr. Noel Patson, Dr. Zhenwei Cao and Ms. Lily Li, for their kind help, encouragement and friendship when I studied in CQU. I appreciate the assistance of Yuye Wang in Department of Electrical Engineering, Harbin Institute of Technology, who helped me to finish the experimental results. I also thank Dr. Wenbo Liu, Prof. Guoqun Zhong and Centre for Chaos Control and Synchronization, City University of Hong Kong. Without their help, this thesis would never have been completed so smoothly.

Finally, I am indebted to my husband, Yong, to my daughter, Lucy, and to my parents for their assistance, love and deep understanding. Without their support, this work would not have been completed.

Contents

List of Publications

During the candidature of the Ph.D degree, the following publications have been published in journals:

1. Fengling Han, Xinghuo Yu, Yuye Wang, Yong Feng and Guanrong Chen, "*N*-scroll chaotic attractors by second-order system and double-hysteresis blocks," *IEE Journal Electronics Letters*, vol. 39, no. 23, pp.1636-1637, Nov. 2003.
2. Fengling Han, Yuye Wang, Xinghuo Yu and Yong Feng, "Experimental confirmation of a new chaotic attractor," *Chaos, Solitons & Fractals*, vol. 21, pp. 69-74, Jan. 2004.
3. Jinhu Lü, Fengling Han, Xinghuo Yu and Guanrong Chen, "Generating multi-dimensional scroll chaotic attractors: a hysteresis series switching method," Regular paper, *Automatica,* vol. 40, pp.1677-1687, Aug. 2004.
4. Fengling Han, Jinhu Lü, Xinghuo Yu, Guanrong Chen and Yong Feng, "Generating multi-scroll chaotic attractors via a linear second-order hysteresis system," In press. *Dynamics of Continuous, Discrete And Impulsive Systems. Series B: Applications & Algorithms*, vol. 12, pp.95-110, 2005.

The following papers have been either published in international conferences or submitted for publication:

5. Fengling Han, Xinghuo Yu, Huifeng Dong and Yong Feng, "Phase-to-phase Wave parameters measurement of distribution lines based on BP networks," *Developments In Applied Artificial Intelligence, Proceedings of 15th International Conference on Industrial and Engineering Applications of Artificial Intelligence and Expert Systems*, IEA/AIE2002, pp. 284-292, Cairns, Australia, June 2002.
6. Fengling Han, Lixia Sun, Yong Feng, Ping Wang and Xinghuo Yu, "Synchronization of the duffing oscillator by using terminal sliding mode control," *Proceedings of IEEE Region 10 Conference on Computers, Communications, Control and Power Engineering*, vol. 3, pp. 1362-1365, Beijing, China, Oct. 2002.
7. Fengling Han, Xinghuo Yu, Lily Li and Russel Stonier, "Complex dynamic behaviour in a linear third-order continuous system with hysteresis series," *Proceedings of International Symposium on Nonlinear Theory and its Applications*, pp. 933-936, Xi'an, China, Oct. 2002.

8. Dujuan Li, Asm Sajeev and Fengling Han, "Time scheduling using agent technology," *Proceedings of International Symposium on Nonlinear Theory and its Applications*, pp. 555-558, Xi'an, China, Oct. 2002.

9. Fengling Han, Xinghuo Yu, Guanrong Chen, Wenbo Liu and Yong Feng, "Generation of multi-scroll chaos using second-order linear systems with hysteresis," *Proceedings of IEEE International Symposium on Circuits and Systems*, vol.3, pp. 84-87, Bangkok, Thailand, May 2003.

10. Fengling Han, Xinghuo Yu, Yuye Wang, Yong Feng and Guanrong Chen, "Chaotic generator of second-order systems with hysteresis feedback controller," *Proceedings of International Conference on Control Science and Engineering*, Harbin, China, Dec. 2003.

11. Fengling Han, "Study on stability margin of the hysteresis-switched chaotic systems," *Proceedings of Asia-Pacific Workshop on Chaos Control and Synchronization.* Melbourne, July 2004.

12. Fengling Han, Xinghuo Yu, Yi Wang, and Majid Al-Dabbagh, "Sinusoidal steady-state analysis for fault location in power distribution systems," *Proceedings of the 30th Annual Conference of the IEEE Industrial Electronics Society* (IECON'04), Busan, Korea, Nov. 2004.

13. Fengling Han, Xinghuo Yu, Yong Feng and Guanrong Chen, "Domain of attraction of hysteresis-series based chaotic attractors," *Proceedings of the 7th Asia-Pacific Complex Systems Conference*, Cairns, Australia, Dec. 2004.

14. Fengling Han, Jinhu Lü, Xinghuo Yu and Guanrong Chen, "Dynamical behaviours of a 3D hysteresis-based system," Submitted to *Chaos, Solitons & Fractals*.

List of Tables

List of Figures

Abstract

Anti-control of chaos has attracted a lot of attention recently due to its potential applications in science and engineering. How to generate useful chaos that is also practically implementable and useful is a current focus of research. This research aims at developing new chaos generation schemes which demonstrate complex dynamical behaviours using simple linear systems with hysteresis function series.

A continuous-time linear unstable second-order system with a feedback of hysteresis function is first proposed for generating chaos. The design for chaos generation is studied theoretically. A Poincaré map is used to demonstrate the dynamical behaviour of the system. The existence and the analytic solution of the limit cycle that bounds the basin of attraction of the chaotic attractor are derived. Conditions for the existence of chaotic attractors are studied. A hysteresis based system with a maximum chaotic stability margin is designed.

Second, systematic methods for generating 1D n-scroll chaotic attractors in the directions of the state variables and 2D $n\times m$-grid scroll chaotic attractors in the phase plane via continuous-time linear unstable second-order systems with a feedback of hysteresis function series are proposed. Furthermore, systematic methods for generating 1D n-scroll, 2D $n\times m$-grid scroll and 3D $n\times m\times l$-space scroll chaotic attractors via continuous-time linear unstable third-order systems using hysteresis function series feedback are also presented in this thesis. Simulation results are presented to demonstrate effectiveness of the schemes. It is shown that the multi-scroll chaos generation systems can be represented in Lur'e form, and as a result it may be used within synchronization schemes for secure communication.

Third, the limit cycle that bounds the basin of attraction in the multi-scroll chaos generation with second-order systems case is studied. The relationship of the size of the basin of attraction with the numbers of hysteresis function series is studied. The multi-scroll chaos generation mechanism is then further explored by analyzing the system trajectories; the switching boundaries, switching rules and the trajectories on each subspace. The chaotic behaviours are confirmed theoretically and it is proved that a non-ordinary attractor exists in the multi-scroll chaotic attractor of the second-order systems case. The abundant dynamical behaviour of the multi-scroll chaos generation systems using different hysteresis feedback are demonstrated.

A double-hysteresis function, which is the superimposition of two basic hysteresis functions, is proposed for the implementation of the hysteresis based chaotic system. In this

design, the double-hysteresis block and its series are constructed via a systematic method. The ideal hysteresis function series can be implemented easily with the proposed double-hysteresis function. The number of scroll attractors can be designed arbitrarily, and the multi-scroll chaotic attractors can be located anywhere and cover any chosen area of the phase plane. The circuitry implementation for generating 1D n–scroll, 2D $n\times m$–grid scroll chaotic attractors with linear second-order systems and hysteresis function series is given. And the oscilloscope illustrated waveforms which included as many as $9\times9=81$ scrolls chaotic attractor are presented.

The experimental results confirmed the theoretical analysis very well and validated the effectiveness as well as the feasibility of the proposed multi-scroll chaos generation schemes. This research may find potential engineering applications in areas such as digital coding and image processing, etc.

Chapter 1

Introduction

1.1 Motivation

Chaos is generally defined as a state that exists between definite and random states. Chaos is a very interesting nonlinear phenomenon and has been intensively studied during the last four decades. Chaos theory, as a branch of the theory of nonlinear dynamical systems, has brought to our attention a somewhat surprising fact: low-dimensional dynamical systems are capable of complex and unpredictable behaviour. One of the characteristics of chaotic systems is sensitivity to initial conditions; i.e. trajectories from two relatively close initial values will diverge as the systems evolve, or a very small difference in the starting values of the function will, after the function has been iterated many times, lead to a great difference in the produced behaviours. The characteristics of chaotic systems mentioned above, can be used in many practical applications, such as secure communication, chemistry, biology, and so on.

Chaos generation was first introduced by researchers with mathematical background rather than circuit-design background. Some circuit design implementations can not match up with the mathematical equations due to technical problems. In 1984, Matsumoto published the first paper about Chua's Circuit — a simple autonomous circuit with a chaotic attractor [1]. The chaos generated from Chua's circuit was then experimentally confirmed by Zhong in 1985 [2]. The double-scroll chaotic attractor and its family were reported later [3, 4], which became the focus of study of chaos phenomena in electronic engineering. For the past few decades, more and more publications have dealt with electronic circuits exhibiting chaotic behaviour.

Recently, there has been an increasing interest in exploiting chaotic dynamics in order to create or suppress chaos for engineering applications. One of the reasons for such an interest is that control promises both a better understanding of chaotic behaviour and the means of influencing and modifying it. Various applications were reported, such as increasing the reaction rate in chemical technologies, avoiding fatal voltage collapse in power networks, providing secure communications by using chaotic carrier instead of periodic one, regulating

dynamical responses of mechanical and electronic devices (e.g., diodes, laser, and machine tools), and treating cardiac arrhythmia. It is expected that "Coping with chaos" would cause a kind of revolution in science and technology [5]!

Motivated by the need of real-world applications, this research will develop new mechanisms for generating multi-scroll chaos using simple system models — continuous-time linear systems with a feedback control of hysteresis function series. The proposed schemes may lead to potential engineering applications in digital coding and image processing.

1.2 A Brief Review of the History on Chaos Research

The concept of chaos has been introduced into science quite recently, in the seventies of the twentieth century. Chaotic systems provide researchers with a new tool for modeling the uncertainty which differs from the classical probabilistic way. Chaotic motions are modeled as the solutions of nonlinear differential or difference equations with "floating" frequency and amplitude [5].

Despite the fact that common phenomena observed daily in circuits and signal-processing systems can be explained only by nonlinear models, the study of nonlinear dynamics is still a great-uncharted territory in system analysis [6]. Over many decades, the need for models of oscillatory behaviours was met by linear and nonlinear dynamical models with limit cycles. It was commonly believed that no other kind of oscillatory behaviour could be observed in generally deterministic systems. It is surprising that such a prejudice was supported by mathematical results. A misconception was believed by many mathematicians and physicists that given precise knowledge of the initial conditions, it should be possible to predict the future of the universe.

Throughout the history of science, complex nonlinear phenomena have been observed experimentally but, more often than not, have been disregarded because the concepts for explaining them simply did not exist. A classic example of this is the driven neon bulb oscillator circuit examined by the eminent Dutch electrical engineer and physicist Van Der Pol. He reported his oscillator experiment in *Nature* magazine in 1927, noting that "often an irregular noise is heard" in the circuit. He dismissed this "noise" as "a subsidiary phenomenon", not worthy of further investigation. It is only in more recent times that the conditions under which such noise is generated are being understood [6, 7].

In the development of chaos theory, the first evidence of physical chaos is believed to be Edward Lorenz's discovery in 1963 [8]. As a meteorologist, Edward Lorenz published an

analysis of a simple system with a third-order differential equation that he had extracted from a model of atmospheric convection. In Lorenz's meteorological computer modeling, he discovered the underlying mechanism of deterministic chaos: simply-formulated systems with only a few variables can display highly complicated behaviour that is unpredictable. Using his digital computer, through the printed numbers and simple strip chart plots of the variables, he saw that slight differences in one variable had profound effects on the outcome of the whole system. This was one of the first clear demonstrations of sensitive dependence on initial conditions in chaotic systems. Equally important Lorenz showed that this occurred in a simple, but physically relevant model. He also appreciated that in real weather situations, this sensitivity could mean the development of a front or pressure-system where there never would have been one in previous models. In his famous paper in 1963, Lorenz picturesquely explained that a butterfly flapping its wings in Beijing could affect the weather thousands of miles away some days later. This sensitivity is now called the "butterfly effect". In the process, he sketched the outlines of one of the first recognized chaotic attractors as shown in Fig. 1.1.

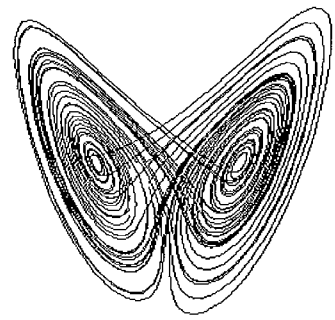

Fig. 1.1 Lorenz attractor — the first recognized chaotic attractor.

In the 1960s, the fractal structure had rarely been studied in the applied science. Perhaps because of this, chaotic attractors were first referred to as "strange attractors".

The first underlying mechanism within chaos was observed by Mitchell Feigenbaum, who in 1976 found that "when an ordered system begins to break down into chaos, a consistent pattern of rate doubling occurs" [8].

The first formal mathematical definition of chaos was given by Li and Yorke. Since then, there have several different but closely related definitions of chaos given in the literature [8].

While on a visit to Japan in 1983, having witnessed a futile attempt at producing chaos in an electrical analog of Lorenz's equations, Leon Chua was prompted to develop a chaotic electronic circuit. He realized that chaos could be produced in a piecewise-linear circuit if it possessed at least two unstable equilibrium points – one to provide stretching, and the other to fold trajectories. With this insight, he systematically identified those third-order piecewise-

linear circuits containing a single voltage-controlled nonlinear resistor that could produce chaos. Specifying that the driving-point characteristic of the voltage-controlled nonlinear resistor should be chosen to yield at least two unstable equilibrium points. He invented the Chua's circuit [7]. Chua's circuit became one of the simplest and most widely studied real nonlinear dynamical systems. That the circuit does exhibit chaos in the sense of Shilinikov was proved in 1986. Chua's circuit is the first physical system for which the presence of chaos has been established experimentally, confirmed numerically, proven mathematically and constructed by a Cellular Neural Network. This circuit is readily constructed at low cost using standard electronic components and exhibits a rich variety of bifurcation and chaos.

At the beginning of chaos research, the main research areas were the analysis and experimental confirmation of chaotic systems. Afterwards, other research areas in chaos were explored, such as control, synchronization, and anti-control of chaotic systems. In 1990, Ott, Grebogi, and Yorke (OGY) [9] introduced a linear feedback method for stabilizing unstable periodic orbits in chaotic systems, which did not require knowledge of the governing equations. The OGY method generated widespread interest, and various modifications of the scheme quickly followed. Methods for synchronizing chaotic systems were developed virtually simultaneously with the developments in chaos control. Pecora and Carroll first demonstrated how chaotic systems could be synchronized, using an electronic circuit coupled unidirectionally to a subsystem made up of components of the parent system [10, 11]. This innovation provided a new perspective on chaotic dynamics and inspired many studies on synchronizing chaotic systems. Cuomo and Oppenheim [12] further expanded the area by demonstrating how synchronized chaotic systems could be used in a scheme for secure communication.

Similar to the main stream research of controlling or suppressing chaos, the opposite direction of making a non-chaotic dynamical system chaotic or retaining the chaos of a chaotic system (called anti-control of chaos, or anti-chaos) [8] has also attracted increasing attention recently. Anti-controlling chaos has found some possible applications in the areas of secure communication, resonance prevention in mechanical systems, material damage control in lasers, fluid mixing, and nonlinear optics. In particular, within the biological context, anti-control of chaos has a great potential application in controlling drug-induced arrhythmias in irregular heartbeats.

It is important that we should understand the ideas of nonlinear dynamics at a deep level so that no naturally occurring phenomenon can be considered as strange. Even in this field, the steady-state behaviour of a chaotic system has been termed a "strange" attractor. We now

know that such attractors are not at all strange or unusual, but are ubiquitous throughout the natural and physical world [6].

1.3 Research Plan

This research will develop design schemes for generating complex chaos signals with simple systems. The schemes are accomplished by the continuous-time linear second-order or third-order systems with the help of hysteresis functions, which have simple system structures and are easy to implement.

This research work is a combination of theoretical development and engineering implementation. It includes the following aspects:

Theoretical Development

Theoretical studies on the design criteria of hysteresis based chaotic systems, the basin of attraction, analytic solutions on occurrence of chaos, and the mechanism of generating chaos via continuous-time linear second-order or third-order systems with hysteresis function series are presented. Mathematical models and proofs, analytic solutions are given.

Dynamics Analysis

Dynamical behaviours of corresponding chaotic systems are studied extensively. The Poincaré map is used to demonstrate these dynamical behaviours. Specific dynamical trajectories analysis, dynamical response on each subspace and switching rules are presented in order for chaotic behaviours to be confirmed theoretically. Various dynamical trajectories are demonstrated with different hysteresis feedbacks.

Numerical Simulations

Numerical simulations of the proposed schemes are programmed using Matlab. These simulations contain:

- Generating n-scroll chaotic attractors in the directions of the state variables, $n \times m$-grid scroll chaotic attractors in the phase plane via continuous-time linear second-order systems and hysteresis function series;
- Generating n-scroll, $n \times m$-grid scroll, and $n \times m \times l$-space scroll chaotic attractors via continuous-time linear third-order systems and hysteresis function series.

Circuitry Implementation

Some of the proposed multi-scroll chaotic attractors are implemented by electronic circuits. A double-hysteresis building block is proposed to provide ideal hysteresis function

series with simple circuitry implementation. Based on the double-hysteresis building block, the multi-scroll chaotic generators via linear second-order systems and hysteresis function series are designed and implemented.

1.4 The Organization of the Thesis

This thesis is organized as follows.

The present chapter proceeds with the motivation of this research, a brief review of the history on chaos research, research plan and the organization of this thesis.

In chapter two, a survey of fundamentals and advances in chaos and anti-control of chaos is conducted, particularly, hysteresis chaos generators are introduced in detail, and the engineering applications of chaos, especially in telecommunications are discussed.

Chapter three studies the design criteria for chaos generator via linear second-order systems and hysteresis functions. It includes:

- ♦ The preliminaries of hysteresis based systems, limit cycle, stability margin of chaotic attractors;
- ♦ The response property of hysteresis based systems. The Poincaré map is used to demonstrate the dynamical behaviours of the hysteresis based systems;
- ♦ The existence proof and calculation of the limit cycle, which defines the basin of chaotic attraction, are derived; The relationship between the system parameters and mechanisms of generating chaos is studied, and the analytic solutions are given;
- ♦ A hysteresis based chaotic system with maximum stability margin is designed.

Chapter four contains the mechanisms of generating multi-scroll chaos via continuous-time linear systems and hysteresis function series, it includes:

- ♦ The mathematical models of the linear systems and the hysteresis function series, Lur'e representation of the multi-scroll chaos generation system;
- ♦ Study of the limit cycle that bounds the basin of attraction of the multi-scroll chaotic attractors;
- ♦ Generation of 1D n-scroll chaotic attractors in the directions of state variables, and 2D $n \times m$-grid scroll chaotic attractors in the phase plane via continuous-time linear unstable second-order systems and hysteresis function series;

- Generation of 1D n-scroll chaotic attractors, 2D $n\times m$-grid scroll chaotic attractors and 3D $n\times m\times l$-space scroll chaotic attractors via continuous-time linear third-order systems and hysteresis function series;
- Numerical simulations to validate the schemes.

In chapter five, the dynamics of multi-scroll chaos generation systems are studied. It includes:

- The basic dynamical behaviours of 1D n-scroll chaotic attractors, 2D $n\times m$-grid scroll chaotic attractors via continuous-time linear second-order systems and hysteresis function series; The switching boundaries, switching rules and the trajectories on each subspace corresponding to n-scroll and $n\times m$-grid scroll chaotic attractors are studied, respectively;
- Two lemmas to show that a non-ordinary attractor exists in the n-scroll and $n\times m$-grid scroll chaotic attractor generated via the linear second-order systems and hysteresis function series;
- The dynamical behaviours of multi-scroll chaotic attractors via continuous-time linear third-order systems and hysteresis function series are studied. The switching planes, switching rules, the trajectories on each subspace, and grazing surfaces corresponding to n-scroll chaotic attractors are studied. The switching planes and switching rules corresponding to $n\times m$-grid scroll chaotic attractors are also demonstrated.
- The two-dimensional Poincaré return map is used to prove the n-scroll chaotic attractors in the third-order systems case;
- The dynamical behaviours with different hysteresis feedbacks is briefly demonstrated.

Chapter six presents the circuit implementation for the proposed chaos generation scheme via linear second-order systems and hysteresis function series. A design of double-hysteresis building block is proposed to implement the ideal hysteresis function series. It includes:

- The design and implementation of double-hysteresis building block;
- Implementation of ideal double-hysteresis series;
- Generating 1D n-scroll chaotic attractors, 2D $n\times m$-grid scroll chaotic attractors with continuous-time linear second-order systems and double-hysteresis series.

Finally, chapter seven concludes the thesis with a summary of this thesis and the research that will be done in the future.

Chapter 2

Fundamentals and Advances in Chaos and Anti-Control of Chaos

2.1 Introduction

Deterministic systems considered in classic textbooks on system dynamics and control display three types of behaviours in their solutions: to approach constant solutions, to converge toward periodic solutions or to converge toward quasi-periodic solutions. In the last decades, it has been confirmed that many physical systems can also display behaviours, which do not belong to any of the above three types. They become aperiodic (chaotic) if their parameters, internal variables, or external signals are chosen in a specific way. Unpredictable behavior of deterministic systems has been called chaos. Chaos is found in systems that are autonomous and non-autonomous, lossless or dissipative, discrete in time and of any dimension, or continuous in time and of dimension three or higher [13]. The feature of chaos is in its apparently random like behaviour which is also deterministic in nature.

In order to investigate hysteresis based chaotic systems in this thesis, some basic concepts of chaos are introduced in this chapter. Anti-control of chaos, hysteresis based chaos generation and some applications of chaos are also introduced here.

This chapter is organized as follows: Chaos and the basic analysis methods are introduced in section 2.2. Anti-control of chaos is discussed in section 2.3, followed by section 2.4 which is about the applications of chaos. A summary is given in the last section.

2.2 Chaos and the Basic Analysis Methods

This section introduces some fundamentals of chaos.

2.2.1 Chaos and Bifurcation in Nonlinear Systems

Nonlinear systems have various complex behaviours that are not observed in linear systems. Chaos is just one of several closely related prominent complex behaviours of nonlinear

dynamical systems. Chaotic processes are not random; they follow rules, but even simple rules can produce extreme complexity.

The intuitive understanding of chaotic motion is that it is locally unstable and globally bounded. There is no universally agreed definition of chaos in current literature. Because chaos is the solitary topic in this research, a definition is introduced as follows.

Consider a vector function $\boldsymbol{x}$ with a value in $\boldsymbol{R}^n$ defined on $\boldsymbol{R}_+$ which are solutions of the stationary (autonomous) system of differential equations:

$$\dot{\boldsymbol{x}} = \boldsymbol{F}(\boldsymbol{x}), \quad \boldsymbol{x}(t) \in \boldsymbol{R}^n \tag{2.1}$$

Definition 2.1 [5] A set $\boldsymbol{B}_0$ is called the *attracting set* for the system (2.1) if there exists an open set $\boldsymbol{B}$, $\boldsymbol{B}_0 \subset \boldsymbol{B}$, such that

$$\lim_{t\to\infty} dist(\boldsymbol{x}(t), \boldsymbol{B}_0) = 0 \tag{2.2}$$

for any solution $\boldsymbol{x}(t)$ with $\boldsymbol{x}(0) \in \boldsymbol{B}$.

Definition 2.2 [5] A closed attracting set $\boldsymbol{B}_0$ is called the *attractor* if it is minimal, i.e. there is no smaller attracting set $\boldsymbol{B}_0$. The set of initial conditions $\boldsymbol{B}$ for which (2.2) holds is called *the basin of attraction*.

Definition 2.3 [5] The closed trajectory $\boldsymbol{L}$ of dynamical system (2.1) is called *limit cycle* if it has no other closed trajectories in its neighborhood.

Definition 2.4 [5] The set $\boldsymbol{D}$ is called *a strange attractor* if it is bounded and all solutions of (2.1) which start from $\boldsymbol{D}$ are Lyapunov unstable. The system is called *chaotic* if it has at least one strange attractor.

If the attractor is a fixed point, we say that the dimensionality is equal to 0; If the attractor is a line or a simple closed curve, we say that the dimensionality is equal to 1. Similarly, a surface has a dimensionality of 2, a solid volume a dimensionality of 3. If an attractor for a dissipative system has a noninteger dimension, then we say that the system has a *strange attractor* [14]. The attractors other than strange attractor are called ordinary attractor.

A strange attractor may be defined as any bounded attractor that stretches and folds the bundle of final steady-state trajectories, producing sensitive dependence on initial conditions and long-term unpredictability. Strange attractors are often used to characterize chaos. A chaotic system is often associated with a strange attractor, and its trajectory can be expanding in certain directions but shrinking (attracting) in some other directions. The overall phase

portrait of a chaotic orbit moves towards a certain point (or limit set, or region) for some period of time but then moves away from it for another period of time. A chaotic orbit repeats this process infinitely many times without really setting down anywhere. *The limit cycle* is an isolated closed orbit of a dynamical system. A strange attractor generally has infinitely many unstable limit cycles embedded in it [5].

Despite the difficulty in definitions, some concepts and properties of chaos are well accepted for engineering applications.

Chaos is characterized by a stretching and folding mechanism. Nearby trajectories of a deterministic dynamical system are pulled apart and folded back together repeatedly to produce complicated bounded non-periodic motion in a strange attractor. The exponential divergence of trajectories that underlines chaotic behaviour, and the resulting sensitivity to initial conditions, leads to long-term unpredictability which manifests itself as randomness in the time-domain and produces a broadband noise-like power spectrum [7].

A chaotic system is predictable in the short-term but unpredictable in the long-term due to their extremely sensitive dependence on initial conditions. The possibility of unpredictability for a deterministic system is the key point to distinguish chaotic systems from linear or regular deterministic nonlinear systems.

A dynamical system is informally called chaotic if it contains bounded behaviour exhibiting several fundamental features, three of which are as follows:

1) A basically continuous, and possibly banded, Fourier or power spectrum.
2) Nearby orbits that diverge exponentially fast, thus causing an extreme sensitivity to initial conditions.
3) Ergodicity and mixing of the orbits in the bounded portion $\boldsymbol{E}$ of the phase space where the orbits exist [13].

Typically, a dynamical system is a structurally stable or robust system which retains its qualitative properties under small perturbations. However, the majority of chaotic attractors are structurally unstable.

Definition 2.5 [8] *Bifurcation* is a typical phenomenon of nonlinear systems that a quantitative change of system parameters leads to a qualitative change of system properties such as the number and the stability of equilibrium points.

A convenient way of studying bifurcation is through a bifurcation diagram. In such a graphical representation, a parameter is varied and plotted along the x-axis. On the y-axis, the asymptotic behaviour of a sampled state variable is plotted as discrete points. If the system

operates in period-1 (period equal to the sampling interval) for some parameter value, there will be only one point corresponding to that parameter value. If it is in period-2, there will be two points. If the system behaves chaotically, for some other parameter value, there will be a large (theoretically infinite) number of points corresponding to that parameter value.

2.2.2 Some Useful Tools

Differential equations are usually used to describe a dynamical system. The analytic formulation of a dynamical system is important as it shows the behaviour of the trajectories of the dynamical system. But in the study of bifurcation and chaos, it is rare that chaotic systems can be solved analytically. Usually, dynamical behaviour analysis is adopted in studying chaotic systems, especially, with high-order dimensions. In this subsection, some useful tools for analyzing chaotic systems are introduced.

1) Lyapunov Exponent

Among the main characteristics of chaos, the existence of one positive Lyapunov exponent is perhaps the most useful information about chaos to verify. Roughly speaking, Lyapunov exponents measure the rate of divergence of nearby orbits; in particular, the positive leading Lyapunov exponent is the time average logarithmic growth rate of the maximal distance between two nearby orbits.

To compute Lyapunov exponents, one can simply start with any two nearby points belonging to a system trajectory, and then evolve them in time, while measuring the growth rate of the distance between them. This is particularly useful when one has a time series rather than an analytic model. Another approach is to measure the growth rate of a vector tangent to the trajectory, which requires an accurate mathematical model for the dynamical system.

In the continuous-time system described by Eq. (2.1), the largest Lyapunov exponent is defined by:

$$\lambda(x_0) = \lim_{t\to\infty} \frac{1}{t} \ln\left\| z(t; x_0) \right\| \tag{2.3}$$

where $\|\cdot\|$ denotes the standard Euclidean norm of a finite-dimensional vector, and $z = z(t; x_0)$ is the solution of $\dot{z} = J(z)z$, $z(t_0) = x_0$, in which $J(\cdot) = \boldsymbol{F}'(\cdot)$ is the Jacobian matrix [8].

The total number of Lyapunov exponents is equal to the degree of freedom of the system. For a three-dimensional continuous-time system, the only possibility for chaos to exist is that the Lyapunov exponent of the systems are (+, 0, –) ($\lambda_1>0$, $\lambda_2=0$, $\lambda_3<0$), with the additional condition $\lambda_3<-\lambda_1$ (dissipative system), or $\lambda_3=-\lambda_1$ (conservative system). Intuitively, this

means that the trajectory of the system, in the phase plane, expands in a certain direction but shrinks in another direction, yields complex dynamical phenomena within a bounded region.

Lyapunov exponents provide a measure for the average convergence or divergence rate of the neighboring trajectories for a dynamical system. If the trajectories are bounded and have a positive Lyapunov exponent, the system would definitely exhibit chaotic behaviour. The larger the positive Lyapunov exponent, the shorter the time scale of the system predictability. However, the positive leading Lyapunov exponent alone is generally not sufficient to signify chaos since it may simply produce an unbounded system trajectory.

2) Poincaré Map

One of the ways to make a complex system easier to analyze is by reducing the system to a simple system that still captures the important features of the original system. This is achieved by a method invented by Henri Poincaré. It allows one to reduce the analysis of continuous motions in the n-dimensional space to a similar problem for discrete transformations (maps) in the $(n-1)$-dimensional space. It results in simplification of the initial problems and allows one to visually analyze the system behaviour for $n \leq 4$ [5].

In this method, one places a surface, called the Poincaré section, as shown in Fig. 2.1, at a suitable place in the state space. The Poincaré map is then the mapping of a point of intersection of a trajectory with the surface onto the subsequent intersection from the same side. In this way, the continuous-time evolution in state space is reduced to a map of Eq. (2.4) in a lower-dimensional space.

$$p_{n+1}=M(p_n) \tag{2.4}$$

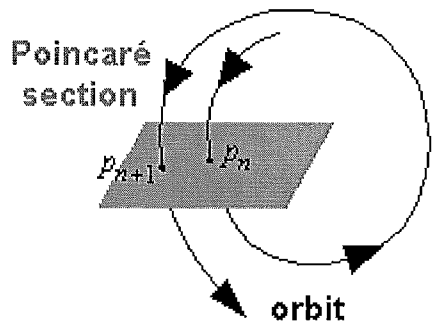

Fig. 2.1 The definition of Poincaré map.

If the continuous-time orbit is periodic, there are a finite number of points on the Poincaré section. In the case of quasi-periodic orbits, since the two frequencies are in commensurate, points in the sampled model will not fall on each other and will be arranged in a closed loop.

For a chaotic orbit, the asymptotic behaviour in discrete time shows an infinite number of points, contained within a finite volume, and distributed over a region of very intricate structure. This is the strange attractor in the discrete domain.

3) Smale Horseshoe Map

The Smale horseshoe map consists of a sequence of operations on the unit square. First, stretch in the y direction by more than a factor of two, then compress in the x direction by more than a factor of two. Finally, fold the resulting rectangle and fit it back onto the square, overlapping at the top and bottom, and not quite reaching the ends to the left and right (and with a gap in the middle), as illustrated in the Fig. 2.2. Repeating this generates the horseshoe attractor. The Smale horseshoe map is the set of basic topological operations for constructing an attractor consist of stretching (which gives sensitivity to initial conditions) and folding (which gives the attraction). Since trajectories in phase space cannot cross, the repeated stretching and folding operations result in an object of great topological complexity.

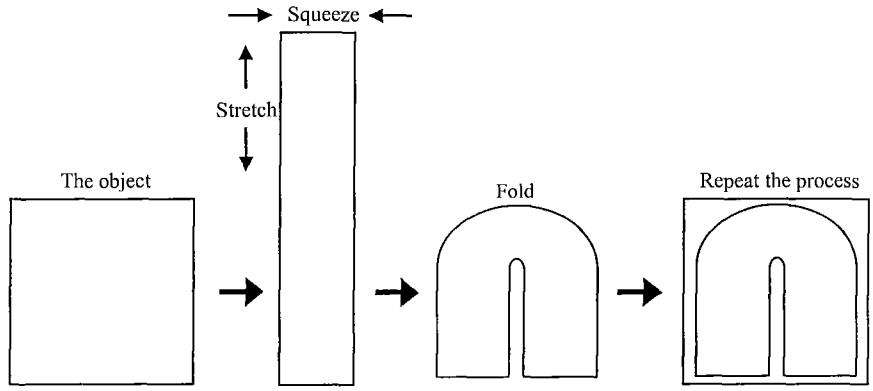

Fig. 2.2 Smale horseshoe map.

4) Li–Yorke Criterion

In 1975, Li and Yorke proved that any one-dimensional map which exhibits a regular cycle of period three will also display regular cycles of every other length as well as completely chaotic cycles. The Li–Yorke criterion is:

If $\boldsymbol{F}$ is a continuous function, and $\boldsymbol{F}$ has a periodic point of order 3, then $\boldsymbol{F}$ has a periodic point of all orders [15].

2.3 Anti-Control of Chaos

In a broader sense, controlling or ordering chaos can be understood as a process or mechanism which enhances the existing chaos or creates chaos in a dynamical system when it

is useful or beneficial, and suppresses it when it is harmful. In contrast to ordering or suppressing chaos, the need for intentionally making a non-chaotic dynamical system chaotic, or retaining the chaos of a chaotic system, is known as anti-control of chaos.

There is a growing interest in using the richness of chaos and purposely generating chaotic dynamics in engineering. Yet, anti-control of chaos – one of the unique features of chaos control – has begun to emerge as a theoretically attractive and potentially useful new concept in control systems theory and in some time-critical or energy-critical control applications. Broadly speaking, anti-control of chaos can be divided into two categories: to use chaos or to suppress it [8].

2.3.1 Anti-Control of Chaos and Chaos Generators

It is known that chaos can be generated from various systems via different methods. In this subsection, some works related to engineering anti-control of chaos are introduced.

1) Chua's Circuit — The first electronic circuit that generates chaos

Chua, the creator of the chaos circuit, first implemented chaos with electric circuits. Chua's circuit is a simple third-order nonlinear electronic circuit with a rich variety of dynamical behaviour including chaos. Shilnikov theorem was used to prove the existence of chaos in the double-scroll of Chua's circuit [4]. The main idea is: if ζ is a continuous piecewise-linear vector field associated with a third-order autonomous system, assume the origin is an equilibrium point with a pair of complex eigenvalues $\sigma \pm j\omega$ ($\sigma < 0$, $\omega \neq 0$) and a real eigenvalue $\gamma > 0$ satisfying $|\sigma| < \gamma$. If in addition, ζ has a homoclinic orbit through the origin, then ζ can be infinitesimally perturbed into a nearby vector field ζ with a countable set of horseshoes. Horseshoes give rise to extremely complicated behaviour typically observed in chaotic systems [4].

The importance of Chua's circuit is that it can exhibit every type of bifurcation and attractor in third-order continuous-time dynamical systems. While exhibiting a rich variety of complex dynamical behaviours, the circuit is simple enough to be constructed and modeled by using standard electronic parts and simulators [7]. A huge body of literature focuses on the double-scroll chaos based on the Chua's circuit in the recent two decades. Chip of Chua's circuit was designed [16], and the CNN (Cellular Neural Network) design was reported [17].

2) Works of Elwakil, Kennedy and their group

Followed the invention of Chua's circuit, Elwakil, Kennedy and their colleagues studied Chua's circuit extensively [18-20], and reported their study results on chaos

generators [21-30], most of which were in view of engineering design and implementation. Due to the nature of the nonlinearity in Chua's circuit, which is active and piecewise, designing such a nonlinear circuit is not straightforward. Attracted by the possible chaotic nature of conventional sinusoidal oscillators, they designed a current mode chaos generator [21, 22] that is more advantageous in terms of accuracy, bandwidth and noise immunity; and designed a high frequency RC chaos generator in which the signal frequency is beyond 1 MHz [23]; They also designed a Wien-type chaotic oscillator [24] and a Colpitts oscillator which exhibits radio-frequency chaotic signals. The frequency can vary from a few hertz up to the microwave region [25]. Chaotic oscillators are based on sinusoidal circuits. Starting with a sinusoidal that is later modified for chaos allows obtaining attractive features via linear design techniques, which transforms it into the nonlinear domain [23]. In fact, in most sinusoidal configurations, the oscillation condition coincides with the Hope bifurcation condition; that is, usually a supercritical bifurcation for which an equilibrium point loses its stability and a stable limit cycle is generated. By moving the control parameters away from the oscillation condition, many different kinds of complex behaviour may arise. These include chaotic behaviour or even more complex situations associated with co-existing attractors [25]. Some further work was also reported on producing chaos from sinusoidal oscillators by employing passive-only nonlinear devices [26] and a double-scroll-like chaos generator in CMOS chip [27]. By modifying sinusoidal oscillators using hysteresis nonlinear resistors, hysteresis chaotic oscillators were designed [28, 29].

Emphasis on the design process for chaotic oscillators relies primarily on techniques, which are well established based on linear circuit theory and which requires minimum knowledge of nonlinear dynamics. It was found that Chua's circuit, Saito's double-scroll hysteresis oscillator, Rossler's system as well as Lorenz system are all built upon a core sinusoidal oscillator and that the active-type of nonlinearity is not essential for generating chaos. Large collections of chaotic oscillators have been classified based on oscillator-nonlinear composite architecture. The simplest possible chaotic dynamics are most likely exhibited in a third-order continuous-time chaotic oscillator where any of these oscillators can be identified as being responsible for stretching the trajectories and where the switching action of a passive device is responsible for folding [30].

The design of Kennedy's chaos generator stressed more of the circuit-design background than the mathematical background. In some sense, their design lacks sufficient mathematical conditions for chaos generation.

3) Yalçin, Suykens and Vandewalle's contributions

There has been much interest recently in obtaining complex dynamical behaviours from simple systems by simple control or design techniques. The basic idea of generating chaos with piecewise linear (PWL) nonlinearities, such as Chua's circuit, is to introduce additional breakpoints in the nonlinearity. These breakpoints create equilibrium points which are located on a line in state space. By modifying the nonlinear characteristic of Chua's circuit with additional breakpoints, n double-scroll chaotic attractors were generated [31]. In [32], a simple model was suggested for generating even more complicated n-scroll chaotic attractors.

Yalçin, Suykens and Vandewalle also presented an experimental confirmation of 3- and 5-scroll chaotic attractors from a generalized Chua's circuit [33], and generating a family of scroll grid attractors, which the equilibrium points lie on a 2-dimensional plane or in 3-dimensional space, with stair function by systematically increasing the complexity of behaviour while keeping the system as a simple circuit implementation [34]. In [31-34], the chaotic attractors were only verified by using computer simulation and circuit implementation. However theoretical analysis and rigorous mathematical proofs are not provided.

4) Chen's attractor

Chen's attractor that exhibits more complicated chaotic scroll was reported [35], and its bifurcation analysis was studied in detail [36] so as to confirm the generation of chaos. The unstable periodic orbits detection and control of Chen's attractor were studied [37, 38]. Chen's attractor, which is topologically more complex than the Lorenz's attractor, belongs to another canonical family of chaotic systems. The circuitry implementation and synchronization of Chen's system was also reported [39]. Lü proposed a new attractor that bridges the gap between Lorenz's attractor and Chen's attractor [40, 41], and the dynamical behaviour was analyzed [42], and the attractor was experimentally confirmed [43]. The parameter identification and backstepping control of the uncertain Lü system was shown in [44]. In addition, Lü and his colleagues have also produced a chaotic generator with multiple merged basins of attraction [45] via a switching type of piecewise-linear controller. The controller can create chaos from a 3-D linear autonomous system within a wide range of parameters values. More ideas were reported for chaos generation from a mathematical perspective [46-48].

Along the same line, Tang and his colleagues also designed some simple sine-function circuits to generate multi-scroll chaotic attractors, with a circuit implementation that can physically produce up to nine scrolls visible on the oscilloscope [49, 50]. Zhong etc. proposed a systematic approach for generating n-scroll attractors based on Chua's circuit [51]. The

basic building blocks were employed in their design, so that the slopes and break points of multi-segment nonlinear resistor can be tuned independently. Distinct attractors with n-scroll (up to 10) were shown which were observed via simple tuning in their experimental setup.

Other works in the field of anti-control of chaos includes making a stable nonlinear autonomous system chaotic or enhancing the existing chaos of an originally chaotic system by using a small-amplitude feedback controller [52], and a systematic design approach based on time-delay feedback in a continuous-time system [53].

2.3.2 Hysteresis Based Chaos Generators

Complex chaos can be generated by simple systems. Chaos generators based on linear systems and a piecewise linear feedback block or switching element have received great attention due to the low cost of implementation and its simple structure, allowing the use of less complex tools for its analysis [54].

The hysteresis function as a nonlinear switching function depends on both the present and the past values of the input. The principal feature of electrical hysteresis element is a rapid switching between states. This generates a sort of Schmitt-trigger cycle by resorting to the "jumping phenomena", inherent noise immunity and memory of the input. Consequently, these elements have become indispensable building blocks in a variety of noise rejection and oscillator circuits [55]. Follows are the work on hysteresis based chaos generators.

1) Newcomb — The pioneer of hysteresis based chaos generator

Newcomb first proposed the idea to generate chaos with a modified second-order Lienard system whose nonlinearity is bent hysteresis in 1983 [56]. Motivated by studies on fibrillation of the heart, he studied the binary hysteresis chaos generator of a second-order system, in which the trajectories between two planes are determined by the two branches of binary hysteresis, and the chaos was assured by designing the system so that the first return map has a period three point. In order to obtain chaotic behaviour, which in essence should be able to represent fibrillations, the parameters in the second-order system were switched at various points on the trajectory. It was pointed that the conditions of Li & Yorke are satisfied for the generation of chaos [57, 58]. They also pointed out an open question that the presence of a discontinuity in their system does not seem to affect the presence or absence of chaos. But they chose parameters to obtain the continuity used in the theorem cited.

2) Saito and his group's contribution

Nearly at the same time, Saito reported generating chaotic scroll attractors by a third-order

piecewise linear differential equation with a small parameter ϵ. In the case $\epsilon \approx 0$, it is proved that the Poincaré map possesses the unique absolutely continuous invariant measure on some parameter region [59]. The hysteresis chaos family was reported [60], in which hysteresis chaos in 3- and 4-dimensional cases were studied by the Poincaré map and two-dimensional Poincaré map. Hyperchaos, usually defined as a chaotic attractor with more than one positive Lyapunov exponent, is a higher dimensional chaos. Saito reported an approach for constructing higher dimensional hysteresis chaos generators [61]. The two-dimensional Poincaré map was rigorously derived and its Lyapunov exponents verified the generation of hyperchaos and related phenomena. For a certain class of four-dimensional hysteresis circuits, rigorous evidence for chaos was presented [62], and a four-dimensional chaos generator with hysteresis, which exhibits a torus-doubling route to chaos and then to hyperchaos, was reported [63]. The basic bifurcations of a four-dimensional autonomous circuit, which includes one hysteresis element, were studied [64]. In [65], a simple piecewise linear hysteresis circuit was studied. A sufficient condition for chaos generation and a rigorous analysis of bifurcation phenomena were presented. The one-dimensional return map was defined, and the analytic formula was derived. Using a return map, a sufficient condition for chaos generation was given, where chaos is characterized by ergodicity and a positive Lyapunov exponent. In the phase space, their chaotic attractor exhibits a single or a double-screw form. Using an analytic equation, the parameter sets for tangent bifurcation, period-doubling bifurcation and crisis were given. A further step towards the engineering application of their work was control of chaos from a piecewise linear hysteresis circuit [66]. A chaos generator including two capacitors, two resistors, one linear voltage controlled current source (VCCS) and a hysteresis VCCS was reported [67], and control of a simple design of a hysteresis chaos generator was presented [68]. A 4-D chaotic oscillator based on a differential hysteresis comparator was discussed [69]. Furthermore, a two-port chaotic oscillator generating 2×2 scroll chaotic attractor were reported [70]. The chaotic behaviour in this paper was guaranteed theoretically using a piecewise exact solution. Some of their theoretical results were verified by experiments.

3) Parodi, Storace and their colleagues' works

Parodi etc. reported a lumped circuit exhibiting static hysteretic behaviour [71]. In their paper, the piecewise linear equations yield a very simple formulation of some important features concerning the hysteresis phenomena, such as the physical limits on the rate-independent behaviour, the energy loss evaluation, and the local and non-local memories.

Some results on the hysteresis based chaotic circuit were reported [72-76]. The dynamic features, such as the trajectories residing in the saturation region, ascending branch, descending branch and hysteresis for sinusoidal input in a PWL circuit were studied in detail [72]. It was shown that the control of the frequency behaviour could be achieved by a simple adjustment of the linear resistance of the ladder circuit. Motivated by the applications of hysteresis chaotic circuit, the dynamical behaviour of the circuit was studied by numerical simulations [73]. The use of the circuit was discussed as a basic element of a transmitter-receiver system for secure communication. Some implementations of a hysteresis chaos generator were also proposed [74, 75]. And the bifurcation analysis of a PWL hysteresis based chaotic circuit was studied through a one-dimensional map. According to the local memory property of the hysteresis cycle, the mathematical model is given by:

$$\begin{cases} \dot{x} = y \\ \dot{y} = 2\delta - x + (x \pm 1)\dfrac{p}{q} \end{cases} \tag{2.5}$$

The geometrical meaning of hysteresis cycles requires positive parameters p and q; $1/q$ is the slope of the ascending and descending branches of the hysteresis cycles, and $1/p$ is the slope of equilibrium points lying on each subplane. $\delta \in (0, 1)$ was assumed in their study, positive δ can guarantee the unstable foci. It was summarized that switching between different pieces of flow occurs when the trajectories cross particular lines at the intersection between boundary surfaces; Because of these switches, the resulting flow turns out to be non-smooth, non-invertible and even discontinuous for most parameter values, as a function of the initial conditions. When p changes in Eq. (2.5), the global dynamics were studied in detail [76].

4) Other relevent research

Elwakil and Kennedy reported the hysteresis chaotic oscillator [28, 29] by modifying sinusoidal oscillators using hysteresis nonlinear resistors. The chaotic oscillator based on a differential hysteresis comparator was reported in [77], which used a finite response time to increase the order of the differential hysteresis comparators. However, it is difficult to implement more hysteresis in their design due to some technical problems, only triple-scroll chaotic attractor can be demonstrated experimentally. More recently, the analysis of piecewise-linear oscillators with hysteresis was reported [54]. The point transformation method of Andronov was used to analyze the different kinds of oscillation that may occur in piecewise-linear systems, of the first, second, and third order, when a relay with hysteresis is used in the feedback loop. In [54], the dynamical system given by:

$$\begin{cases} \dot{x} = \boldsymbol{A}x + \boldsymbol{B}u \\ y = \boldsymbol{C}x \\ u = \boldsymbol{N}(y) \end{cases} \tag{2.6}$$

where $x \in \boldsymbol{R}^n$ is the state variable vector, $y \in \boldsymbol{R}$ is the system output, $u \in \boldsymbol{R}$ is the output of the feedback block. $\boldsymbol{A}$, $\boldsymbol{B}$, and $\boldsymbol{C}$ are matrices of compatible dimensions, and $\boldsymbol{N}(y)$ represents a piecewise-linear operator. $\boldsymbol{A}$ is supposed to be nonsingular. When analyzing the second-order system described by:

$$\begin{cases} \dot{x}_1 = x_2 \\ \dot{x}_2 = -x_1 + 2\alpha x_2 + \boldsymbol{N}(x_1) \end{cases} \tag{2.7}$$

which, in the general form given by Eq. (2.6), corresponds to:

$$\boldsymbol{A} = \begin{bmatrix} 0 & 1 \\ -1 & 2\alpha \end{bmatrix}, \qquad \boldsymbol{B} = \begin{bmatrix} 0 \\ 1 \end{bmatrix}, \qquad \boldsymbol{C} = [1 \quad 0].$$

$\boldsymbol{N}(x_1)$ represents the effect of the relay with hysteresis shown in Fig. 2.3.

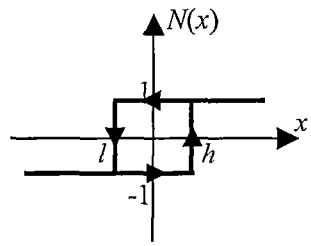

Fig. 2.3 Relay with hysteresis.

It is found that in the second-order system, the presence of hysteresis can produce limit cycle and chaotic attractor. The basin of attraction for the attractor is delimited by the limit cycle. The presence of chaotic oscillation is explained by $\alpha \in (0, \alpha_{max})$ the trajectories remain bounded inside the attractor by the limit cycle.

More scrolls mean more complicated dynamical behaviours and more stability margins for the chaotic attractor. Unfortunately, the experimental results only show the limited chaotic scroll via linear second-order systems and hysteresis for the technical problem. Producing multiple chaotic attractors or multi-scroll chaotic attractors by simple circuitry design remains a great technical challenge.

2.4 Applications of Chaos

Chaos is all around us and is found in many disciplines. For example, chaotic phenomena are found in lasers, electronic circuits, chemical systems, brains and hearts. Since the pioneer

works of synchronizing the chaotic systems [9-12], over the last decade, knowing that chaos can actually be useful and can be well controlled, the intensive study of chaotic dynamics has evolved from the traditional trend of understanding and analyzing chaos to the new attempt of controlling and utilizing it [8]. Some of the applications of chaos are introduced as follows.

2.4.1 Telecommunications

Chaotic signals appear noise-like, and are complex in structure and impossible to predict over long time. The most popular applications lie in the field of secure communications.

1) Cryptography

Chaotic cryptography systems are schemes that combine the classical cryptography techniques and chaotic synchronization to enhance the degree of security. By appropriate choices of nonlinear dynamics for the oscillators and the signal generators, it is possible to have a more secure and reliable cryptosystem capable of transmitting information securely and accurately.

The earliest applications of chaotic systems in cryptography were connected with encrypting a message with modulation of trajectories of continuous dynamic systems. These methods are strongly related to the concepts of the synchronization of two chaotic systems and controlling chaos. Different methods of message encoding and decoding in chaotic communications have been proposed, which can be classified into three main categories: chaos masking, chaos shift keying, and chaos modulation. In chaotic masking, the encoder consists of an autonomous chaotic system whose output signal is added to the information signal. This sum is transmitted over the channel. The decoder uses the transmission signal to synchronize. In chaos shift keying, the encoder consists of two or more autonomous chaotic systems with different parameters. According to the discrete information signal, one of them is selected whose output signal is transmitted over the cannel. In the decoder, the same number of chaotic systems tries to synchronize with their encoder counterparts. In chaotic modulation or inverse system, the encoder is a nonautonomous chaotic system whose state is influenced by the information signal. The decoder synchronizes with the encoder via reconstruction of its state using the transmission signal. The information signal is recovered by applying the inverse encoder operation to the reconstructed state and the transmission signal. All of these schemes have been investigated analytically and experimentally in continuous-time as well as in discrete-time applications [78]. Yang etc. proposed a cryptography based on a chaotic system, instead of encoding the message signal in a chaotic system directly. They used two chaotic signals, one to synchronize the chaotic encrypter and

the chaotic decrypter, the other to encrypt the plain signal by using a multishift cipher [79]. An adaptive chaotic encoder combined a chaotic encoder with an adaptive filter, producing a more complex encryption system and encoder was reported [80]. Inverse systems were also discussed in their study. A scheme proposed in [81] which increases the parameter sensitivity of chaotic self- synchronization systems is analogous to the concept of a magnifying glass and enhances the security level of a chaotic based cryptosystem.

2) Secure Communication

Among the chaos-based communication schemes that have been published, two basic configurations can be identified: (a) an approach consisting of the addition of the message signal to the chaotic carrier (transmitted signal) that is sent to the receiver. That is, the master system comprises the full-state model whereas the slave system is composed of a reduced model; (b) another transmitter/receiver design is based on the full-state model of the driving and response system. That is, both drive and response systems are represented by dynamical systems of the same order. Early studies in chaos-based communication showed the message signal can be recovered only under ideal conditions (with a high SNRs). The recent publications in this area include constructing an augmented dynamical system from the synchronization error system, and dynamical output feedback being applied to perform synchronization in spite of transmitter /receiver mismatches [82]. In this way, the transmitted message (which can be analog or digital) can be recovered.

Because of the continuous broadband, chaotic signals are useful for encoding information in spread spectrum communication. When a narrowband signal is spread over a much wider bandwidth, the average power spectral density (psd) becomes lower. As a sequence, the signal psd becomes comparable with the background noise. Thus, without prior knowledge of the transmission system, it is not easy to detect the presence of the signal, even if an unintended user detects the presence of the signal. In the case where coherent detection is required, it is very difficult to decode the data without prior knowledge of the encoding scheme [83]. Genetic programming can be particularly useful in the specific application of inverse problems such as finding an optimal mathematical expression that fits certain criteria. In spread-spectrum systems for multi-user access, a chaotic spreading code was generated using Genetic programming, the piecewise maps considering the channel SNR levels were designed [84]. The design of the mean-value demodulator is based on the ergodic property of the chaotic signal for information signal recovery at the receiver was reported [85].

In a digital communications system, data is transmitted from one location to another by

mapping bit sequence to symbols, and symbols to sample function of analog waveforms. The analog waveform passes through a bandlimited (possible time-varying) analog channel, where the signal is distorted and noise is added. In a conventional system, the analog sample function sent through the channel is weighted sums of one or more sinusoids. In a chaotic communication system, the sample function is segments of chaotic waveforms. At the receiver, the symbol may be recovered by means of coherent detection, where all possible sample functions are known, or by noncoherent detection, where one or more characteristics of the sample function are estimated. In a coherent receiver, synchronization is the most commonly used technique for recovering the sample functions from the received waveform. These sample functions are then used as reference signals for a correlator. The objective of the synchronization process is to recover basis functions from the noisy received signal in order to maximize the probability of correctly identifying the transmitted symbols. Synchronization-based receivers have advantages over noncoherent ones in terms of noise performance and bandwidth efficiency. These advantages are lost if synchronization cannot be maintained, for example, under poor propagation conditions. In these circumstances, communication without synchronization may be preferable. The main advantage of synchronization is that it makes the implementation of coherent receivers possible. However, there are significant costs associated with synchronization, in terms of synchronization time, circuit complexity, and severe penalties associated with the loss of synchronization [86]. The series tutorial [86, 87, 88] surveyed the theory and operation of conventional communication systems and identified the possible fields of application for chaotic communication [86]; The theory of conventional telecommunications is then extended to cover chaotic communication. Chaotic modulation techniques and receiver configurations are surveyed, and chaotic synchronization schemes are described [87]; Examples are given of chaotic communications schemes with and without synchronization, and the performance of the correlator-based system is evaluated in the context of noise and bandlimited channels [88].

While chaos masking and chaos shift keying both have limitations in maintaining perfect synchronization during message transmission, chaos modulation has been shown to be able to provide perfect synchronization in the presence of message variations. Since optical communication systems are of great advantage in pushing the bit rate into the Gb/s region, chaos modulation has also recently been implemented in chaotic optical communication using optoelectronic feedback systems with chaotic wavelength fluctuation [89]. An approach to calculating the approximate theoretical bit-error rate of a coherent chaos-shift-keying digital communication system under an additive white Gaussian noise environment was reported

in [90]. Impulsive control of a chaotic system is ideal for designing digital control schemes where the control systems are generated by digital devices. A promising application of impulsive synchronization of chaotic systems to secure communication was proposed [91]. Recent investigations show that wireless communication systems are also a very promising application area for chaotic dynamics. A high rate wireless communications scheme based on a wideband and an ultra-wideband chaotic carrier, generated directly in the microwave frequency band was proposed [92, 93].

2.4.2 Other Applications and the IC Implementation of Chaos Chip

Chaos and synchronization applications are also explored extensively in the electrical and electronic engineering areas. Some successful experiments with the control of chaotic oscillations in lasers, such as CO_2 lasers, solid-state lasers and semiconductor lasers were reported in [5]. It is reported that chaos exists for certain loading conditions in a simple power system [94]. Modern electrical power systems become heavily loaded and spread out over large areas. Possible sudden faults such as lighting, equipment failure, etc. may result in instability for the whole system. Stabilization of power system operations is one of the most important problems in power system control. When an electric power system operates near its stability limit, a voltage collapse may occur at a saddle node bifurcation of equilibrium points was proposed [95]. Cellular neural networks (CNN) are complex nonlinear dynamical systems. Applications of CNN can be found in image processing, forecasting, and optimization. Bifurcation and chaos of CNN were reported [96-98]. In the area of power electronics, the synchronization of Ćuk converters [99], and the bifurcation and chaos of a permanent magnet synchronous motor [100] were also reported.

In the areas of chemistry and chemical engineering, creating oscillations and chaos are very important. An important point is that in chemical applications there are not as many variables available for control as compared with electronic applications. For example some of the available variables are the concentrations of some species, the input flow rates or the overall temperature. Fluid mixing is a typical example in which chaos is not only useful but also very important [101]. Chaotic mixing is much faster and more efficient than diffusion. From a kinematic point of view, fluid mixing requires efficient stretching and folding of material lines and surfaces. Chaos is very desirable in these kinds of applications where two or more fluids are to be thoroughly mixed and the required energy is to be minimized. Chaotic mixing is also desirable in applications involving heating, such as plasma heating for a nuclear fusion reactor into which heat waves are injected. For this application, the best result

is obtained when the heat convection within the reactor is chaotic [102]. In combustion applications, chaos is also desirable because it enhances the mixing of air and fuel, and hence leads to better performance.

Other chaos applications are found in mechanics and mechanical engineering. One example is suppressing vibrations in ships. Due to the nonlinear dynamics of the ship, the ship rolling motion can exhibit chaos even for purely periodic waves. Thus, the problem is to decrease the amplitude of chaotic oscillation under disturbance. Techniques of creating chaos can be applied to washing machines. It is known that washing may be accelerated when the angular velocity of the rotor is oscillating. Moreover, chaotic oscillations are more desirable due to the fact that chaotic changes in the rotor speed better mix the laundry and better dissolve the detergent [5]. Other examples such as swinging one degree-of-freedom (pendulum-like) systems to achieve a desired value of angular velocity or energy; and the brachiate robot – a kind of mobile robot that moves using its arms like a gibbon moving from branch to branch [5].

Another possible applications are in biology and biochemistry, such as controlling the populations of two competitive species (prey and predators) [5], treating cardiac arrhythmias [103, 104] and pathological brain activities [105, 106]. Reference [106] presents evidence for confirming the existence of chaotic dynamics in a biologically realistic model of brain electrical activity. Oscillations and even chaos in fact occur at every level of a biological organization.

Quite recently interest in models of nonlinear dynamics and chaos have arisen in financial studies. By means of rescale-range analysis, it has been shown that the dynamics of many financial time series are better described by chaotic models than by conventional ones. Some publications devoted to nonlinear dynamics and chaos [107, 108] in economics and finance. The solution of the Metzler business-cycles model may exhibit chaotic behaviour, so predictions of the evolution of business-cycles are not possible [109]. However, it is *forecasted that the control of oscillations and chaos will have an increasing significance in the* fields of economics and finance [5].

IC designs for chaotic attractors are another hot topic. The main feature for IC designs is that the key parameters governing the bifurcation and natural frequency of the circuit can be adjusted electronically. The IC chips of Chua's circuit [16] and some other chaotic attractors have been produced. A chaos oscillator suitable for low voltage, high frequency and IC implementation was reported in [110].

Recently, Munakata and his colleagues reported the basic principles for implementing the

most fundamental computing functions using chaotic elements. The logic AND, OR, NOT, XOR and NAND operations and bit-by-bit arithmetic operations can be realized by employing single chaotic elements which may be particularly suited for the simulation of chaotic phenomena such as weather forecasting or biomedical problems and the analysis of the brain and heart, etc. They believe that harnessing some of the abundant chaotic phenomena in engineered and natural systems for the development of a simple, fast and cost-effective chaotic computer will be an exciting endeavor [111].

2.4.3 The future of Chaos: Skepticism and Optimism

The understanding of chaotic phenomena is only a recent advancement in science. Before this time the idea of chaos was basically unknown. For example it was only within the last three decades that the notion that chaotic motion is in general neither predictable not controllable has gained acceptance by the scientific community. This is relatively a short time in the history of science. Much progress has been made in recent times that have provided some understanding of many concepts related to chaos.

Although there are technical difficulties in some application areas of chaos, the significance of future applications drive scientific research to persevere in understanding chaos. Much has been accomplished in the past three decades, yet much more remains a challenge for the future [8]. Perhaps within a short time, a chaotic secure communication system, a chaotic computer and many other chaos applications will be put into practical use.

2.5 Summary

In this chapter, some basic knowledge and advances in the study of chaos have been introduced. Anti-control of chaos, especially hysteresis based chaos generation has been surveyed in detail.

The applications of chaos, particularly in secure communication are very appealing. One major problem for the future applications of chaos-based systems is the hardware implementation for the generation of various chaotic signals. This stimulates research on generating complex attractors by using electronic devices with simple and lower-order systems. Nowadays, generating multi-scroll chaotic attractors is not a very difficult task. But hysteresis based chaotic systems promise to be able to generate more complex dynamical behaviours. In the following chapters, we will study this class of systems and their practical implementations.

Chapter 3

Design of Hysteresis Based Chaos Generators

3.1 Introduction

The need for systematic methods for the design of chaos generators has increased due to the many practical applications of chaos.

Hysteresis based systems for generating chaotic attractors have been studied by Newcomb [56–58], Saito's group [59–70], and Storace's group [71–76] for more than twenty years. Basically, the circuits for generating chaotic attractors are constructed based on the dynamics described by two linear two-dimensional equations coupled together by hysteresis switchings. The chaotic behaviours were studied in [57] and [65], respectively. Further study on this topic was conducted by Moreno and his colleagues, and they suggested that the unstable periodic orbit that was obtained corresponds to the limit cycle which bounds the domain of attraction for the chaotic attractor [54].

This chapter studies the design criteria for chaos generation via linear second-order systems with a hysteresis function. Based on the study in [54], the specific design conditions for guaranteeing chaos generation is proposed. And a hysteresis based system which achieving a maximum chaotic stability margin is designed. The Poincaré map is used to demonstrate the dynamical behaviour of hysteresis based systems. The analytic solution of the limit cycle, which defines the basin of attraction, is derived. The relationship between the system parameters and the mechanism for generating chaos is studied. Conditions are derived for the existence of chaotic behaviour in the hysteresis based system.

This chapter is organized as follows: Section 3.2 introduces the preliminaries of this chapter. Section 3.3 demonstrates some properties of the hysteresis based systems. Section 3.4 contains the existence and the calculation of the boundaries of the chaotic attractors. Section 3.5 studies the conditions for the occurrence of chaos. A summary of this chapter is presented in section 3.6.

3.2 Preliminaries

The linear second-order system used to generate chaos in this thesis is described as:

$$\begin{cases} \dot{x} = y \\ \dot{y} = -ax + by \end{cases} \tag{3.1}$$

where x and y are two state variables; a and b are two positive numbers.

For a constant k, the hysteresis function is described as:

$$h(z) = \begin{cases} 0 & z < k \\ 1 & z > 0 \end{cases} \tag{3.2}$$

where $h(z)$ is switched from 1 to 0 if z hits the threshold 0 from above, and is switched from 0 to 1 if z hits k from below, as shown in Fig. 3.1.

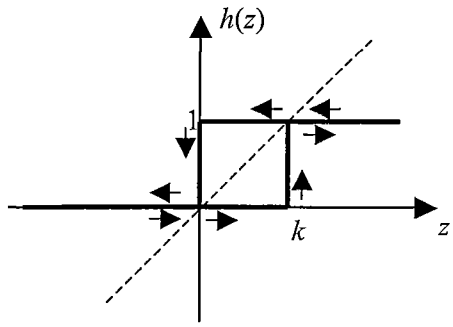

Fig. 3.1 Hysteresis function.

Definition 3.1: If the state variable x of system (3.1) is input to the hysteresis function in Eq. (3.2), and a controller of hysteresis function $h(x)$ is added to system (3.1), the controlled system is called *hysteresis based system* which is described as:

$$\begin{pmatrix} \dot{X} \\ \dot{Y} \end{pmatrix} = \begin{pmatrix} 0 & 1 \\ -a & b \end{pmatrix} \begin{pmatrix} X \\ Y \end{pmatrix} + \begin{pmatrix} 0 \\ h(x) \end{pmatrix} \tag{3.3}$$

where $(X, Y)^T=(x, y)^T$, for $x \in V_1$; $(X, Y)^T=(x-1, y)^T$, for $x \in V_2$.

The two subspaces V_1 and V_2 are defined as respectively:

$$V_1=\{x, y: h(x)=0\},\ V_2=\{x, y: h(x)=1\}.$$

The equilibrium points of the system (3.3) are $(0, 0) \in V_1$, $(1, 0) \in V_2$. On each subspace, the exact solution of the system (3.3) is given by:

$$\begin{cases} X(t) = e^{\alpha t}\{X(0)\cos(\beta t) + \dfrac{1}{\beta}[Y(0) - \alpha X(0)]\sin(\beta t)\} \\ Y(t) = e^{\alpha t}\{Y(0)\cos(\beta t) + \dfrac{\alpha}{\beta}[Y(0) - \dfrac{\alpha^2 + \beta^2}{\alpha} X(0)]\sin(\beta t)\} \end{cases} \tag{3.4}$$

where $X(0)$, $Y(0)$ are the initial conditions, and $\alpha = b/2$, $\beta = \sqrt{4a - b^2}/2$.

Definition 3.2: With a constant k, the closed trajectory $\boldsymbol{L}$ of the hysteresis based system (3.3) shown in Fig. 3.2 is called *limit cycle*.

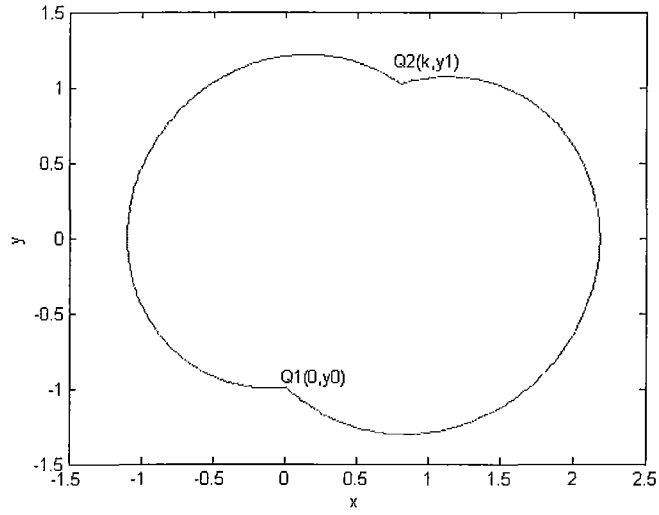

(a)

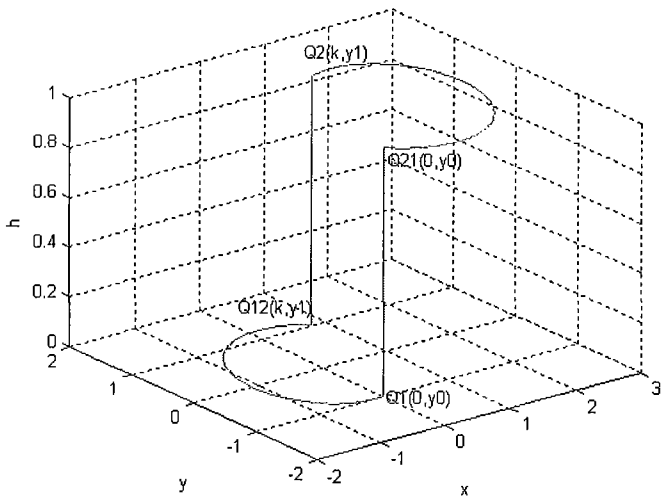

(b)

Fig. 3.2 Trajectory of limit cycle. (a) x-y plane. (b) x-y-h space.

The limit cycle trajectory in Fig. 3.2 starts from (x_0, y_0) on V_1 (or V_2), and runs outgoing exponentially to (k, y_1) (or $(0, y_0)$), switched by the hysteresis value k (or 0). It jumps instantaneously to another subspace V_2 (or V_1), and keeps the x, y coordinate unchanged. It then runs outgoing exponentially, switched by another hysteresis value 0 (or k), then comes back to its start point (x_0, y_0).

Definition 3.3: *The chaos stability margin* means the range of variations in which the design parameters can be taken before the underlying nonlinear system changes from chaotic motion to either unstable or asymptotically stable motion.

3.3 Some Properties of the Hysteresis Based Systems

This section will discuss some properties of the hysteresis based system (3.3) for chaos generation.

3.3.1 Basic Conditions for the Second-Order Systems

To generate chaos, the dynamical behaviour of the hysteresis based system (3.3) should possess the typical chaotic stretching and folding property. So the linear second-order autonomous system (3.1) must have a divergently spiralling trajectory, and its characteristic equation must have a pair of conjugate complex eigenvalues with positive real parts. This requires that:

$$\begin{cases} b>0 \\ b^2-4a<0 \end{cases}$$

so the basic conditions for chaos generation in the hysteresis based system (3.3) are:

$$\begin{cases} b>0 \\ a>\dfrac{b^2}{4} \end{cases} \tag{3.5}$$

3.3.2 The Poincaré Map

The Poincaré map is a useful tool for analysing the dynamical characteristics of chaotic systems. It is used to discuss the dynamical behaviour of hysteresis based system (3.3).

The positive x-axis in the phase plane 0-xy is chosen as the Poincaré section. The Poincaré map is defined as:

$$P_1=M(P_0) \tag{3.6}$$

where P_0 and P_1 are the x coordinates of the system in the Poincaré section. Eq. (3.6) means that if the system starts from position P_0 in the Poincaré section, the next position hitting the Poincaré section again, P_1, can be calculated using Eq. (3.6).

When a=1, b=0.125 in Eq. (3.1), with two different hysteresis switching values k=1.0 and 1.4, the Poincaré map of system (3.3) is shown in Fig. 3.3 (a) and (b), respectively. Note that, in the two figures, the 45° line (P_1=P_0) is used to help analyse the dynamical behaviour of the Poincaré map.

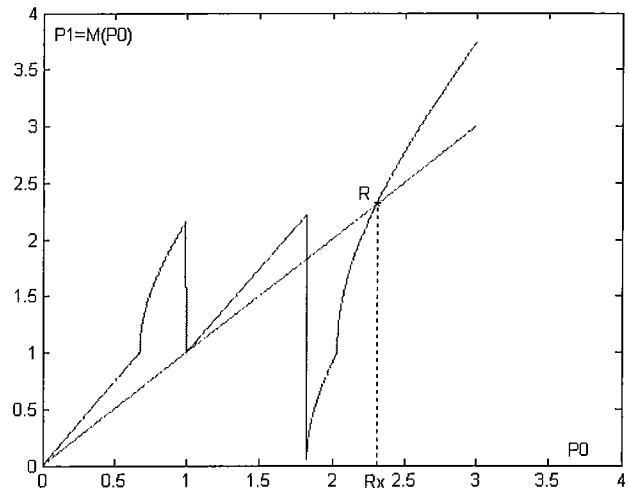

(a)

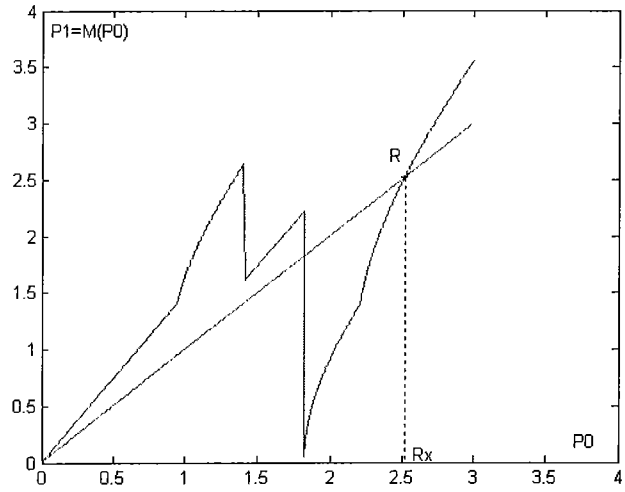

(b)

Fig. 3.3 Poincaré maps of system (3.3) when a=1, b=0.125. (a) k=1.0. (b) k=1.4.

From Fig. 3.3, one can find that there are two peaks in the Poincaré map. The points R are the intersections between the Poincaré map and the 45° line (P_1=P_0). R corresponds to the

unstable limit cycle trajectory discussed in [54].

Remark 3.1. In Fig. 3.1, two values falling down from two peaks correspond to the two switching points of hysteresis function (3.2), k and 0, respectively. Fig. 3.3 (a) corresponds to the possible chaotic response of system (3.3) with suitable initial values. Fig. 3.3 (b) corresponds to the unbounded trajectories of system (3.3). Furthermore, from the Poincaré map shown in Fig. 3.3, it is observed that if $x(0) > R_x$, the response of system (3.3) is unbounded for both k =1.0 and 1.4.

If both peaks are lower than point R in the Poincaré map, and the initial values are within the basin of attraction $\boldsymbol{L}$, the system (3.3) is bounded (chaotic). But if either peak is higher than the vertical coordinate R in Poincaré map, the trajectories are unbounded. That is, in this case, even though the initial values are within the basin of attraction $\boldsymbol{L}$, the trajectories of the system (3.3) could go outside the basin of $\boldsymbol{L}$ and lead to unboundedness. In the case of the unbounded trajectories, the stretching of the spirally divergent response of system (3.1) cannot be folded properly by the hysteresis function (3.2). Therefore, once the trajectories are outside the $\boldsymbol{L}$, the hysteresis based system is unbounded. The limit cycle $\boldsymbol{L}$ is the boundary of the basin of attraction; Inside $\boldsymbol{L}$ is the basin of chaotic attraction.

3.3.3 Chaotic Behaviours of the Hysteresis Based Systems

The limit cycle $\boldsymbol{L}$ is the boundary of the basin of attraction for chaotic attractors. The area inside the limit cycle is the basin of attraction. In [54], it is reported that if the existence of an attractor and that the exponential divergence of the trajectories are inside the attractor, and that the trajectories remain bounded inside the attractor, then the presence of a chaotic oscillation is guaranteed. Therefore, if Eq. (3.5) holds, and both peaks are lower than point R in the Poincaré map, and the initial values are within basin of attraction, then the trajectories of the system will always stay within $\boldsymbol{L}$, and the trajectories of the system (3.3) will always stay within the bounded region so that the chaotic response will be seen. The trajectory covered area of the chaotic response is defined as $\boldsymbol{C}$.

It shows that as time proceeds, the trajectories of system (3.3) will spirally diverge on subspace V_1 (or V_2). When reaching the hysteresis switching points, the trajectories will be switched to another subspace V_2 (or V_1) instantaneously holding (x, y) constant, and then repeat the spirally divergent trajectories. As $t \to \infty$, the trajectories of system (3.3) are repeatedly stretched and folded in the state space infinitely many times via hysteresis switchings, leading to the appearance of bifurcations and chaos. The unstable divergent spirals realize a "stretching

mechanism", by using hysteresis switching, divergence is suppressed and a "folding mechanism" is realized. Therefore, if the trajectories of the system (3.3) always stay within the region ***L***, a chaotic response will appear.

3.4 Derivation of the Boundaries of Chaotic Attractors

This section discusses the existence and calculation of the limit cycle in the hysteresis based system (3.3). Based on the assumption that condition (3.5) holds for second-order systems, the describing function is used to show the existence of a limit cycle in the hysteresis based system (3.3). Then the analytic solution of the limit cycle can be derived.

3.4.1 Existence of the Boundaries of the Attractors

The describing function is adopted to show the existence of a limit cycle in system (3.3). A linear coordinate transformation, $x'=x-k/2$, is made in order to make the hysteresis function symmetric. The block diagram of the transformed system is shown in Fig. 3.4.

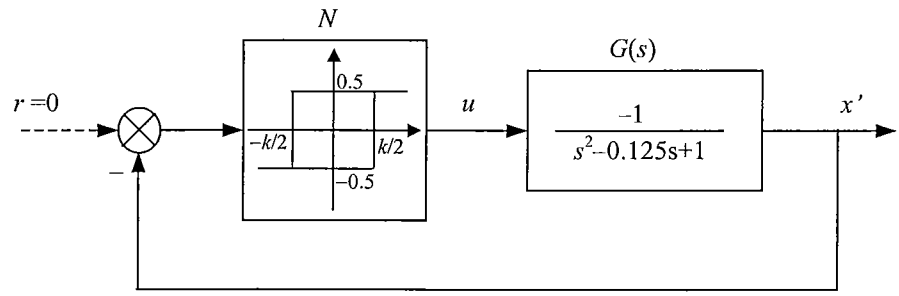

Fig. 3.4 Block diagram for the existence of limit cycles.

When $a=1$, $b=0.125$, the transfer function for the linear second-order system in Fig. 3.4 is:

$$G(s)=\frac{-1}{s^2-0.125s+1}$$

and the describing function of the hysteresis function is:

$$N(A)=\frac{2}{\pi A}\sqrt{1-\left(\frac{k}{2A}\right)^2}-j\frac{k}{\pi A^2} \qquad A\geq\frac{k}{2}$$

where A is the amplitude of the input to the hysteresis function, and ω is the frequency of $-x'(t)$, that is, it is assumed $-x'(t)=A\sin(\omega t)$.

The characteristic equation of the system shown in Fig.3.4 is:

$$1+N(A)\,G(j\omega)=0$$

If the above characteristic equation is satisfied, a limit cycle exists. The existence of a limit cycle can be demonstrated graphically by finding the intersection of the two loci in the complex plane. Fig. 3.5 shows the trajectories of $-1/N(A)$ and $G(j\omega)$ of the hysteresis based system (3.3). While the switching value k of the hysteresis function varies, the trajectories of $-1/N(A)$ are lines parallel to the real axis. These parallel lines will intersect the trajectory of $G(j\omega)$. The conclusions are:

1) The limit cycles exist for different k;
2) The limit cycles are unstable.

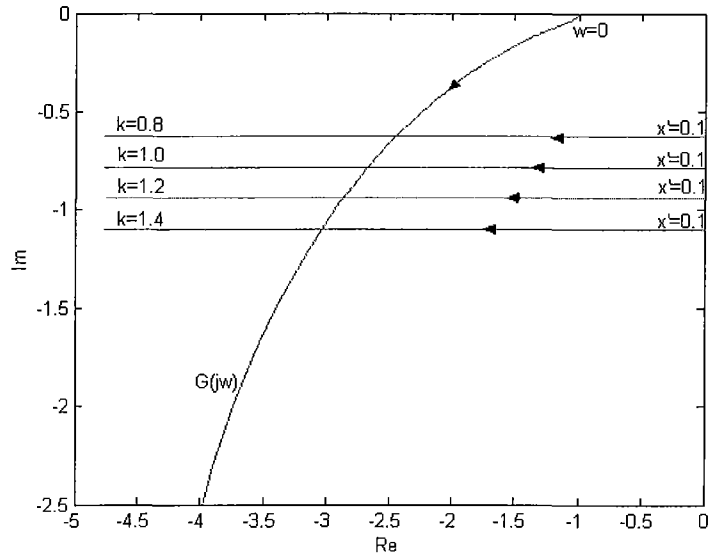

Fig. 3.5 Trajectories of $-1/N(A)$ and $G(j\omega)$ of the hysteresis based system (3.3).

3.4.2 Calculation of the Boundaries of the Attractors

According to the analysis in subsection 3.4.1, an unstable limit cycle always exists in system (3.3) for a particular k. Fig. 3.2 shows a typical limit cycle in the 0-xy plane and the 0-xyh space, respectively. Denote $Q(x, y)$ as a point in the state space. As shown in Fig. 3.2 (b), when the system starts from an initial position on the subspace V_1 (h=0), $Q_1(0, y_0)$ at $t = 0$, it will spiral divergently on the subspace V_1 first. When reaching the hysteresis switching point k at $t=t_1$, the coordinate is $Q_{12}(k, y_1)$, then the trajectory will be switched to Q_2 on subspace V_2 (h=1) instantaneously while (k, y_1) becomes a new initial condition. Then, the trajectory continuously diverges to reach $Q_{21}(0, y_0)$ at $t=T=t_1+t_2$, before being switched to subspace V_1 at Q_1. This completes one period of the limit cycle.

The following can be derived from Eq. (3.4):

$$\begin{cases} e^{\alpha t_1}\dfrac{1}{\beta}y_0\sin(\beta t_1)=k \\ e^{\alpha t_1}\dfrac{1}{\beta}y_0\left(\beta\cos(\beta t_1)+\alpha\sin(\beta t_1)\right)=y_1 \end{cases}, \quad \text{for } (x,y)\in V_1 \tag{3.7}$$

From Eq. (3.7), it is seen that:

$$\tan(\beta t_1)=\frac{k\beta}{y_1-k\alpha}$$

and

$$\beta t_1=\pi+\arctan\frac{k\beta}{y_1-k\alpha}$$

so time t_1 can be calculated by:

$$t_1=\frac{1}{\beta}\left(\pi+\arctan\frac{k\beta}{y_1-k\alpha}\right). \tag{3.8}$$

From Eq. (3.7), another expression of t_1 can be obtained:

$$e^{\alpha t_1}\frac{1}{\beta}y_0\frac{-k\beta}{\sqrt{(k\beta)^2+(y_1-k\alpha)^2}}=k$$

and time t_1 can be obtained by:

$$t_1=\frac{1}{\alpha}\ln\frac{\sqrt{(k\beta)^2+(y_1-k\alpha)^2}}{-y_0}. \tag{3.9}$$

Combining Eqs. (3.8) and (3.9) gives:

$$\frac{1}{\alpha}\ln\frac{\sqrt{(k\beta)^2+(y_1-k\alpha)^2}}{-y_0}=\frac{1}{\beta}\left(\pi+\arctan\frac{k\beta}{y_1-k\alpha}\right).$$

In order to solve the above equation, define the following function:

$$f_1(y_0,y_1)=\frac{1}{\alpha}\ln\frac{\sqrt{(k\beta)^2+(y_1-k\alpha)^2}}{-y_0}-\frac{1}{\beta}\left(\pi+\arctan\frac{k\beta}{y_1-k\alpha}\right)=0. \tag{3.10}$$

For the special case k=1, because of symmetry with the hysteresis based system (3.3), y_1=$-y_0$, the existence condition of limit cycle (3.10) becomes:

$$f(y_0)=\frac{1}{\alpha}\ln\frac{\sqrt{\beta^2+(-y_0-\alpha)^2}}{-y_0}-\frac{1}{\beta}\left(\pi+\arctan\frac{\beta}{-y_0-\alpha}\right)=0. \tag{3.11}$$

For the running time t_2, from Eq. (3.4), one has:

$$\begin{cases} 1+e^{\alpha t_2}\left((k-1)\cos(\beta t_2)+\dfrac{1}{\beta}(y_1-\alpha(k-1))\sin(\beta t_2)\right)=0 \\ e^{\alpha t_2}\left(y_1\cos(\beta t_2)+\dfrac{\alpha}{\beta}\left(y_1-\dfrac{\alpha^2+\beta^2}{\alpha}(k-1)\right)\sin(\beta t_2)\right)=y_2 \end{cases}, \quad \text{for } (x,y)\in V_2. \tag{3.12}$$

From Eq. (3.12),

$$\frac{y_1\cos(\beta t_2)+\dfrac{\alpha}{\beta}\left(y_1-\dfrac{\alpha^2+\beta^2}{\alpha}(k-1)\right)\sin(\beta t_2)}{(k-1)\cos(\beta t_2)+\dfrac{1}{\beta}(y_1-\alpha(k-1))\sin(\beta t_2)}=-y_2$$

then,

$$y_1+\frac{\alpha}{\beta}\left(y_1-\frac{\alpha^2+\beta^2}{\alpha}(k-1)\right)\tan(\beta t_2)=-y_2(k-1)-\frac{1}{\beta}(y_1-\alpha(k-1))y_2\tan(\beta t_2)$$

and

$$\tan(\beta t_2)=\frac{\beta(y_2(1-k)-y_1)}{(\alpha+y_2)y_1+(\alpha y_2+\alpha^2+\beta^2)(1-k)}$$

so,

$$\beta t_2=\pi+\arctan\frac{\beta(y_2(1-k)-y_1)}{(\alpha+y_2)y_1+(\alpha y_2+\alpha^2+\beta^2)(1-k)}.$$

Therefore time t_2 can be obtained as:

$$t_2=\frac{1}{\beta}\left(\pi+\arctan\frac{\beta(y_2(1-k)-y_1)}{(\alpha+y_2)y_1+(\alpha y_2+\alpha^2+\beta^2)(1-k)}\right). \tag{3.13}$$

From Eq. (3.12):

$$e^{-\alpha t_2}=\left((1-k)\cos(\beta t_2)+\frac{1}{\beta}(\alpha(1-k)-y_1)\sin(\beta t_2)\right).$$

Another expression for time t_2 is:

$$t_2=-\frac{1}{\alpha}\ln\left((1-k)\cos(\beta t_2)+\frac{1}{\beta}(\alpha(1-k)-y_1)\sin(\beta t_2)\right). \tag{3.14}$$

Combining Eqs. (3.13) and (3.14), yields:

$$\pi+\arctan\frac{\beta(y_2(1-k)-y_1)}{(\alpha+y_2)y_1+(\alpha y_2+\alpha^2+\beta^2)(1-k)}=-\frac{\beta}{\alpha}\ln\left((1-k)\cos(\beta t_2)+\frac{1}{\beta}(\alpha(1-k)-y_1)\sin(\beta t_2)\right).$$

For the limit cycle trajectory, $y_2=y_0$, the following function can be obtained:

$$\begin{aligned}f_2(y_0,y_1)=\pi+\arctan\frac{\beta(y_0(1-k)-y_1)}{(\alpha+y_0)y_1+(\alpha y_0+\alpha^2+\beta^2)(1-k)}\\+\frac{\beta}{\alpha}\ln\left((1-k)\cos(\beta t_2)+\frac{1}{\beta}(\alpha(1-k)-y_1)\sin(\beta t_2)\right)=0\end{aligned}. \tag{3.15}$$

Combining Eqs. (3.10) and (3.15) gives the formula for calculating the limit cycle:

$$\begin{cases}f_1(y_0,y_1)=0\\f_2(y_0,y_1)=0\end{cases}. \tag{3.16}$$

There are four parameters for tuning the limit cycle, y_0, y_1, t_1 and t_2. Once the parameters a, b of system (3.1) and k of hysteresis function (3.2) are determined, the parameters, y_0 and y_1 can be calculated by using Eq. (3.16). Then, the run times t_1 and t_2 on two sections of the limit cycle can be calculated by using Eqs. (3.8) and (3.13), or Eqs. (3.9) and (3.14).

When k=1, y_0=$-y_1$. Because of the symmetry of the limit cycle in Fig. 3.2, the running time on both parts is equal, that is:

$$t_1 = t_2. \tag{3.17}$$

In this case, the analytical solution for determining the parameters of the limit cycle, y_0, is given by Eq. (3.11).

The limit cycle parameters with several different k for system (3.3) are shown in Tab. 3.1. x_{max} is the positive x-coordinate while y=0. y_0 is the y-coordinate when x=0 in Fig. 3.2, and y_1 is the y-coordinate when x=k.

Tab. 3.1 Limit cycle parameters with different k.

k	0.8	0.869	0.9	1.0	1.1	1.2	1.226	1.3
y_0	-0.9865	-1.0526	-1.0812	-1.1690	-1.2511	-1.3284	-1.3477	-1.4015
t_1	3.850	3.870	3.875	3.880	3.907	3.933	3.950	3.970
y_1	1.0170	1.0748	1.0989	1.1690	1.2287	1.2793	1.2909	1.3215
t_2	4.165	4.043	4.000	3.880	3.767	3.659	3.623	3.560
x_{max}	2.1756	2.2174	2.2361	2.2949	2.3517	2.4067	2.4205	2.4599
property	divergent	critical	chaotic	chaotic	chaotic	chaotic	critical	divergent

From Tab. 3.1, it can be seen that:

1) If $k<1$, the running time t_1 on the subspace V_1 is less than the time t_2 running on the subspace V_2, that is, $t_1 < t_2$.
2) If $k>1$, the running time t_1 on the subspace V_1 is greater than the time t_2 running on the subspace V_2, that is, $t_1 > t_2$.

It should be noted that the parameter b has more influence on the divergent spirals than a in system (3.1).

3.5 Occurrence of Chaos

In this section, the conditions guaranteeing that the trajectories are within the basin of attraction are further discussed. Then the analytic solutions for occurrence of chaos are presented.

Based on condition (3.5), the hysteresis function must switch the outgoing spirals trajectory at a suitable time in order to realize the folding so that system (3.3) exhibits chaotic behaviour. Fig. 3.3 (b) shows one peak is higher than point R in the Poincaré map, indicating that the trajectory will run out of the limit cycle. On the other hand, even though the two peaks are lower than point R in the Poincaré map, improper initial conditions would make the trajectories unbounded.

In order to guarantee that the trajectories stay within the basin of attraction, two necessary conditions must be satisfied, which are studied in the following section.

3.5.1 Trajectories within the Basin of Attraction on Subspace V_1

The limiting (extreme) case is that the trajectory starts from the equilibrium point $(k, 0)$, which is critical for identifying bounded (but chaotic) or unbounded trajectories. When the trajectory runs 90° clockwise and exponentially divergence on V_1 for time t_{10}, it arrives at the negative y-axis, as shown in Fig. 3.6. If the y coordinate travels out of the limit cycle, then the trajectory is unbounded. The initial and final values are $[x(0), y(0)] = (k, 0)$ and $[x(t_{10}), y(t_{10})] = (0, y_{10})$ on V_1. From Eq. (3.4), one has:

$$\begin{cases} x(t_{10}) = e^{\alpha t_{10}}\left(k\cos(\beta t_{10}) - \dfrac{\alpha k}{\beta}\sin(\beta t_{10})\right) = 0 \\ y(t_{10}) = -e^{\alpha t_{10}}\dfrac{\alpha^2+\beta^2}{\beta}k\sin(\beta t_{10}) = y_{10} \end{cases}.$$

From above equations:

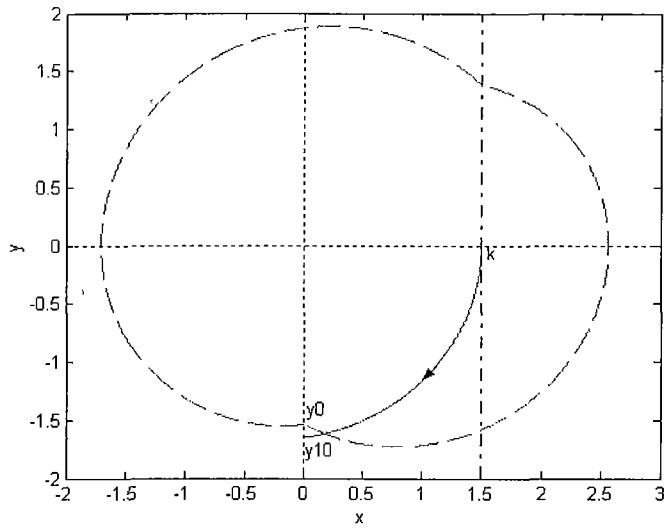

Fig. 3.6 Trajectory running out of the limit cycle on V_1.

$$\tan(\beta t_{10}) = \frac{\beta}{\alpha}$$

so that time t_{10} can be calculated by:

$$t_{10} = \frac{1}{\beta}\arctan\frac{\beta}{\alpha} \tag{3.18}$$

and y_{10} can be calculated by:

$$y_{10} = -e^{\frac{\alpha}{\beta}\arctan\frac{\beta}{\alpha}} k\sqrt{\alpha^2+\beta^2} \tag{3.19}$$

if

$$y_{10} < y_0 \tag{3.20}$$

then the system becomes divergent.

From Eq. (3.19), it can be found that when the parameters of system (3.1) are determined, y_{10} is in direct ratio to $-k$. This means y_{10} is linearly decreasing with the increase of k.

3.5.2 Trajectories within the Basin of Attraction on Subspace V_2

For easy comparison with conditions in the last subsection, the extreme case considered is when the system trajectory starts from (0, 0) on subspace V_2, runs clockwise and exponentially divergent around the equilibrium point (k, 0) on V_2 for time t_2. When the trajectory arrives at the negative y-axis, as shown in Fig. 3.7. Since the trajectories have already run out of the limit cycle, the system must be unbounded. The initial and finial values are $[x(0), y(0)] = (0, 0)$ and $[x(t_{20}), y(t_{20})] = (0, y_{20})$ on V_2. From Eq. (3.4):

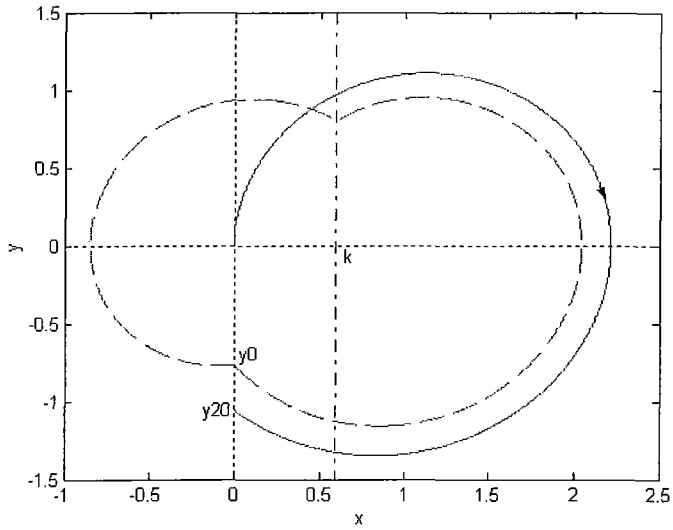

Fig. 3.7 Trajectory running out of the limit cycle on V_2.

$$\begin{cases} x(t_{20}) = 1 + e^{\alpha t_{20}}\left(-\cos(\beta t_{20}) + \dfrac{\alpha}{\beta}\sin(\beta t_{20})\right) = 0 \\ y(t_{20}) = e^{\alpha t_{20}}\dfrac{\alpha^2+\beta^2}{\beta}\sin(\beta t_{20}) = y_{20} \end{cases}.$$

and from above equations, one has:

$$\tan(\beta t_{20}) = \frac{y_{20}}{\dfrac{\alpha^2+\beta^2}{\beta} + \dfrac{\alpha}{\beta}y_{20}} = \frac{\beta y_{20}}{\alpha^2+\beta^2+\alpha y_{20}}$$

and

$$\beta t_{20} = 2\pi + \arctan\frac{\beta y_{20}}{\alpha^2+\beta^2+\alpha y_{20}}$$

so the time t_{20} can be calculated by:

$$t_{20} = \frac{1}{\beta}\left(2\pi + \arctan\frac{\beta y_{20}}{\alpha^2+\beta^2+\alpha y_{20}}\right) \tag{3.21}$$

and y_{20} can be calculated by:

$$y_{20} = e^{\alpha t_{20}}\frac{\alpha^2+\beta^2}{\beta}\sin(\beta t_{20}). \tag{3.22}$$

If

$$y_{20} < y_0 \tag{3.23}$$

then the response is unbounded.

Eq. (3.22) cannot been written in as simple a form as Eq. (3.19). However, it can be solved by numerical calculation. But it can be found that once the parameters of the unstable second-order system (3.1) are given and y_{20} is determined, it is independent of the hysteresis switching value k.

When solving Eqs. (3.19), (3.20), (3.22) and (3.23), y_0 can be obtained by solving Eq. (3.16).

3.5.3 Hysteresis Switching Ranges for Guaranteeing the Chaotic Behaviours

Once the parameters of the second-order system and the hysteresis function are given, the limit cycle can be determined by solving Eq. (3.16). By calculating the two cases with Eqs. (3.19)~(3.23), one can judge if the response is bounded (chaotic) or unbounded. Note that, if either Eq. (3.20) or Eq. (3.23) is satisfied, the system (3.3) will be unbounded. Tab. 3.2 shows some calculation results of y_0, y_{10}, y_{20} with different k. The response property of system (3.3) can be judged by comparing the relationship of y_{10}, y_{20} with y_0.

Tab. 3.2 Response property with different k.

k	0.8	0.869	0.9	1.0	1.1	1.2	1.226	1.3
y_{10}	-0.8792	-0.9550	-0.9891	-1.0990	-1.2089	-1.3188	-1.3474	-1.4287
y_{20}	-1.0525	-1.0525	-1.0525	-1.0525	-1.0525	-1.0525	-1.0525	-1.0525
y_0	-0.9865	-1.0526	-1.0812	-1.1690	-1.2511	-1.3284	-1.3477	-1.4015
Result	$y_{20}<y_0$	$y_{20}\approx y_0$	$y_{10}>y_0$ $y_{20}>y_0$	$y_{10}>y_0$ $y_{20}>y_0$	$y_{10}>y_0$ $y_{20}>y_0$	$y_{10}>y_0$ $y_{20}>y_0$	$y_{10}\approx y_0$	$y_{10}<y_0$
Property	divergent	critical	chaotic	chaotic	chaotic	chaotic	critical	divergent

From Tab. 3.2, one can find that:

1) With small k, the outgoing trajectory of system (3.3) cannot be switched properly on the subspace V_2 and Eq. (3.23) holds. The left peak is higher than point R in the Poincaré map. System (3.3) is unbounded.

2) With the increase of k, the trajectory will enter the basin of attraction for the chaotic attractors. With suitable initial values, the chaotic trajectory appears.

3) If k is further increased, the outgoing trajectory of system (3.3) cannot be switched properly on subspace V_1 and Eq. (3.20) holds. The right peak is higher than point R in the Poincaré map. System (3.3) is unbounded.

Fig. 3.8 shows the relationship y_0, y_{10}, y_{20} versus the hysteresis switching value k. From

Fig. 3.8, it can be found that the range of k that guarantees the existence of chaos is:

$$k_1 \leq k \leq k_2 \tag{3.24}$$

where k_1 is the intersect point of y_{20} and y_0, and k_2 is the intersect point of y_{10} and y_0.

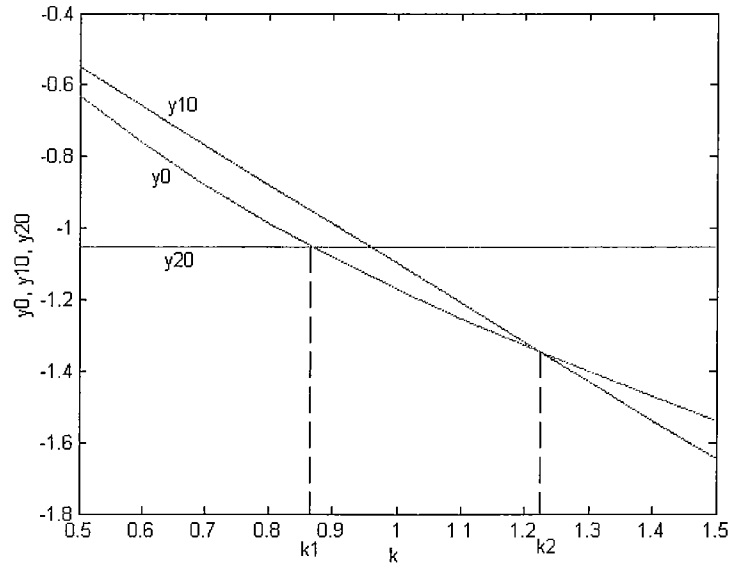

Fig. 3.8 Variation of y_0, y_{10}, y_{20} with respect to k.

For example, when a=1, b=0.125 in system (3.3), the range is

$$0.869 \leq k \leq 1.226.$$

This area can also be obtained by solving Eqs. (3.10), (3.15), (3.19) and (3.22), which can be used as a design criterion for choosing the appropriate hysteresis switching value thus guaranteeing chaos generation in the hysteresis based system.

Remark 3.2. When designing a chaotic hysteresis based system, if neither Eq. (3.20) nor (3.23) is satisfied, and Eq. (3.5) holds, the system is chaotic. When chaotic behaviour appears, the trajectory $\boldsymbol{C}$ is within $\boldsymbol{L}$. The further the distance of the outer boundary of $\boldsymbol{C}$ to $\boldsymbol{L}$, the greater the stability margin the system has.

Remark 3.3. For given parameters a and b, the desired value of k for chaos generation is around $(k_2 - k_1)/2$, which appears to have the maximum chaos stability margin.

When a=1, b=0.125 in Eq. (3.3), the desired k=$(k_2 - k_1)/2$=1.048. The Poincaré map and the trajectory of double-scroll chaos are shown in Fig. 3.9 and Fig. 3.10, respectively.

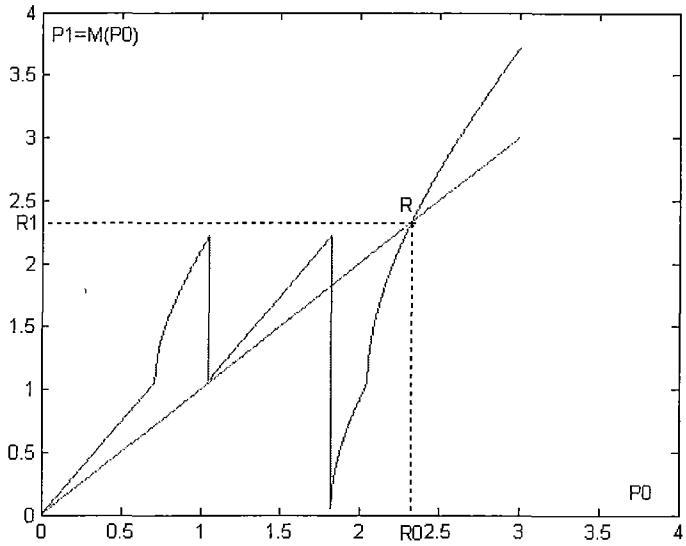

Fig. 3.9 Poincaré map when a=1, b=0.125, k=1.048.

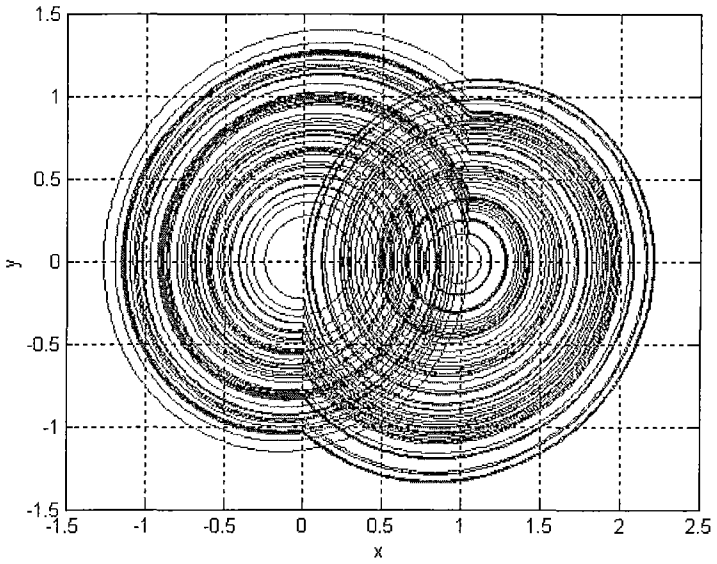

Fig. 3.10 Double-scroll chaotic attractor with maximum stability margin.

Compared to other k, this designed hysteresis based chaotic system has the maximum chaos stability margin. As shown in Fig. 3.9, both peaks in Poincaré map have the same height in this case. Compared with the other design, the ranges of variation that the system parameters can have before the system becomes divergent are maximized.

3.6 Summary

In this chapter, hysteresis based chaos generation using second-order linear systems with a

feedback of hysteresis function have been studied and the following results have been obtained:

1) The trajectories of this class of system can be unstable or stable (but chaotic) according to the system parameters and the initial values. The limit cycle which bounds the basin of chaotic attraction can be calculated mathematically.

2) The dynamical behaviour has been revealed by a Poincaré map with derived conditions for guaranteeing chaotic behaviour. It was observed that when chaos appears, the actual trajectory is within the limit cycle. The further the distance from the limit cycle, the greater the stability margin the system has.

3) The concept of chaos stability margin has been proposed, which can be used as guide for designing chaos generators.

In the following chapters, we will deal with generation of multi-scroll chaotic attractors.

Chapter 4

Multi-Scroll Chaotic Attractors via Linear Systems

4.1 Introduction

Chaos can be generated by simple systems. Hysteresis based chaos has been studied extensively [54-77]. Unfortunately, only limited scroll numbers of chaotic attractors were generated via linear second-order systems and a hysteresis function. In this chapter, methods for generating multi-scroll chaotic attractors via continuous-time linear second-order or third-order systems and hysteresis function series are proposed. The basic idea of generating chaos here is creating unstable equilibrium points and setting the system to wander (be stretched and folded) over the unstable equilibrium points. Furthermore, the simple equations of the multi-scroll chaos generation system allow one to establish some algebraic relationships, leading to a topological analysis of the phase space without making use of more sophisticated concepts and tools.

It is shown that 1D n-scroll chaotic attractors can be generated in the directions of the state variables, 2D $n\times m$-grid scroll chaotic attractors can be generated in the phase plane via linear second-order systems with a feedback control of the hysteresis function series. Furthermore, 1D n-scroll chaotic attractors, 2D $n\times m$-grid scroll chaotic attractors as well as 3D $n\times m\times l$-space scroll chaotic attractors can be generated via linear third-order systems with a feedback control using the hysteresis function series. Computer simulation results verify the proposed new multi-scroll chaos generation scheme.

This chapter is organized as follows. Section 4.2 introduces the preliminaries of this chapter, in which the mathematical models and the Lur'e representation of the multi-scroll chaos generation scheme both the second-order and the third-order systems models are included. Section 4.3 presents the multi-scroll chaotic attractor generation via a linear second-order system and a hysteresis function series. Section 4.4 demonstrates the multi-scroll

chaotic attractor generation via a linear third-order system and a hysteresis function series. Summary of this chapter comes in section 4.5.

4.2 Preliminaries

Consider a simple continuous-time linear system with a feedback control:

$$\dot{\boldsymbol{X}} = \boldsymbol{AX} + \boldsymbol{BU}(\boldsymbol{CX}) \tag{4.1}$$

where $\boldsymbol{X} \in R^n$ (n=2 or 3) is the state variable vector;

$\boldsymbol{A}$, $\boldsymbol{B}$ and $\boldsymbol{C}$ are matrices of compatible dimensions;

$\boldsymbol{U} \in R^m$ (m=1, 2, or 3) is a feedback controller.

Hysteresis function series $h(x, p, q)$ is depicted in Fig. 4.1, and can be described as:

$$h(x,p,q) = \sum_{i=1}^{p} h_i(x) + \sum_{i=1}^{q} h_{-i}(x) \tag{4.2}$$

where p and q are positive integers, and

$$h_i(x) = \begin{cases} 1 & for\ x > i-1 \\ 0 & for\ x < i \end{cases}, \quad h_{-i}(x) = \begin{cases} 0 & for\ x > -i \\ -1 & for\ x < -i+1 \end{cases}$$

$h_1(x)$ is the hysteresis function defined in Eq. (3.2).

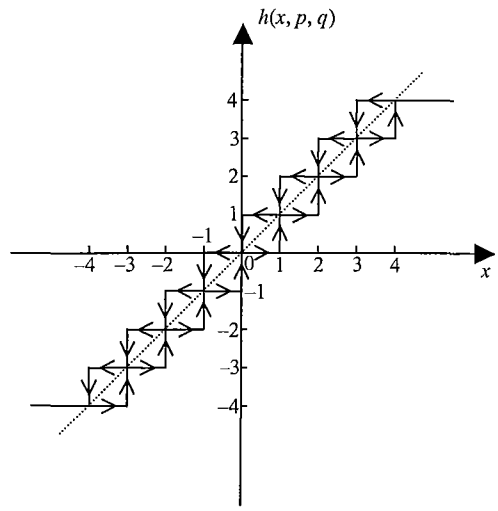

Fig. 4.1 Hysteresis function series.

The system (4.1) can be represented as a hybrid Lur'e system, which is regarded as a linear system with hysteresis feedback nonlinearity. The second-order and the third-order systems cases are discussed in the following.

4.2.1 Second-Order Systems Case

If $\boldsymbol{X}=(x, y)^T$ is the state vector of the linear second-order system, the feedback controller is $\boldsymbol{U}=(u, v)^T$, and

$$\boldsymbol{A}=\begin{pmatrix} 0 & 1 \\ -a & b \end{pmatrix},\ \boldsymbol{B}=\begin{pmatrix} 0 & -k_v \\ k_h a & -k_v b \end{pmatrix},\ \boldsymbol{C}=\begin{pmatrix} k_h & 0 \\ 0 & k_v \end{pmatrix} \tag{4.3}$$

thus, there are three different sub-cases as follows:

1) Generation of 1D horizontal n-scroll chaotic attractor. If $k_h=1$, $k_v=0$, then

$$\boldsymbol{U}(\cdot)=\begin{pmatrix} h(x,p,q) \\ 0 \end{pmatrix}.$$

System (4.1) can generate a 1D horizontal n-scroll chaotic attractor whose equilibrium points are located on the x-axis as shown in Fig. 4.2 (a).

2) Generation of 1D vertical n-scroll chaotic attractor. If $k_h=0$, $k_v=1$, then

$$\boldsymbol{U}(\cdot)=\begin{pmatrix} 0 \\ h(y,p,q) \end{pmatrix}.$$

System (4.1) can generate a 1D vertical n-scroll chaotic attractor whose equilibrium points are located on the y-axis as shown in Fig. 4.2 (b).

3) Generation of 2D $n\times m$-grid scroll chaotic attractor. If $k_h=1$, $k_v=1$, then

$$\boldsymbol{U}(\cdot)=\begin{pmatrix} h(x,p_1,q_1) \\ h(y,p_2,q_2) \end{pmatrix}.$$

System (4.1) can generate a 2D $n\times m$-grid scroll chaotic attractor whose equilibrium points are integer points on the xy-plane as shown in Fig. 4.2 (c).

4.2.2 Third-Order Systems Case

If $\boldsymbol{X}=(x, y, z)^T$ is the state vector of the linear third-order system, the feedback controller is $\boldsymbol{U}=(u, v, w)^T$, and

$$\boldsymbol{A}=\begin{pmatrix} 0 & 1 & 0 \\ 0 & 0 & 1 \\ -a & -b & -c \end{pmatrix},\ \boldsymbol{B}=\begin{pmatrix} 0 & -k_2 & 0 \\ 0 & 0 & -k_3 \\ k_1 a & k_2 b & k_3 c \end{pmatrix},\ \boldsymbol{C}=\begin{pmatrix} k_1 & 0 & 0 \\ 0 & k_2 & 0 \\ 0 & 0 & k_3 \end{pmatrix} \tag{4.4}$$

thus, one has three different sub-cases as follows:

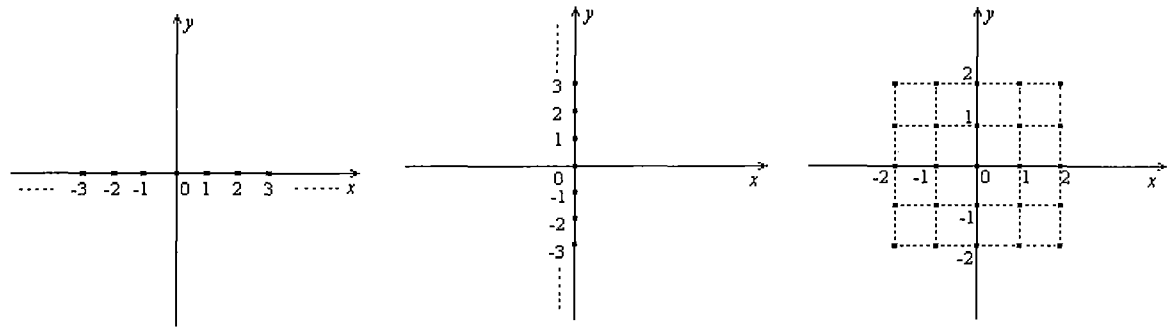

(a) (b) (c)

Fig. 4.2 Equilibrium points for system (4.1), (4.3).

(a) 1D horizontal n-scroll; (b) 1D vertical n-scroll; (c) 2D $n\times m$-grid scroll.

1) Generation of 1D n-scroll chaotic attractor. If $k_1=1$, $k_2=k_3=0$, then

$$\boldsymbol{U}(\cdot)=\begin{pmatrix} h(x,p_1,q_1) \\ 0 \\ 0 \end{pmatrix}.$$

System (4.1) can generate a 1D n-scroll chaotic attractor whose equilibrium points are located on the x-axis as shown in Fig. 4.3 (a).

2) Generation of 2D $n\times m$-grid scroll chaotic attractor. If $k_1=k_2=1$, $k_3=0$, then

$$\boldsymbol{U}(\cdot)=\begin{pmatrix} h(x,p_1,q_1) \\ h(y,p_2,q_2) \\ 0 \end{pmatrix}.$$

System (4.1) can generate a 2D $n\times m$-grid scroll chaotic attractor whose equilibrium points are integer points on the xy-plane as shown in Fig. 4.3 (b).

3) Generation of 3D $n\times m\times l$-space scroll chaotic attractor. If $k_1=k_2=k_3=1$, then

$$\boldsymbol{U}(\cdot)=\begin{pmatrix} h(x,p_1,q_1) \\ h(y,p_2,q_2) \\ h(z,p_3,q_3) \end{pmatrix}.$$

System (4.1) can generate a 3D $n\times m\times l$-space scroll chaotic attractor whose equilibrium points are integer points on the xyz-space as displayed in Fig. 4.3 (c).

Thus, the multi-scroll chaos generation systems can be represented in Lur'e form, and as a result they may be used within synchronization schemes for secure communication.

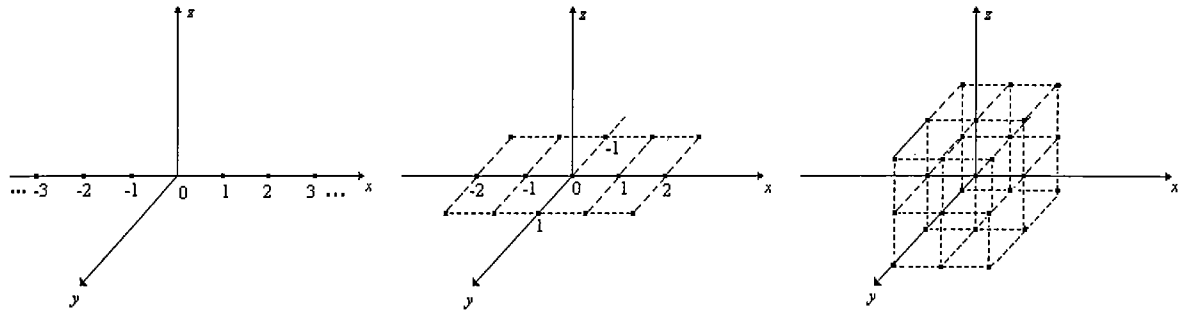

(a) (b) (c)

Fig. 4.3 Equilibrium points for system (4.1), (4.4).

(a) 1D n-scroll; (b) 2D $n\times m$-grid scroll; (c) 3D $n\times m\times l$-space scroll.

4.3 Multi-Scroll Chaotic Attractors via Second-Order Systems

In this section, generating multi-scroll chaotic attractors via linear second-order systems and a hysteresis function series are studied. It includes generating 1D n-scroll chaotic attractors in the directions of state variables, and 2D $n\times m$-grid scroll chaotic attractors in the phase plane.

4.3.1 Generating Horizontal N-Scroll Chaotic Attractors

Consider a linear second-order system, if the state variable x is input to the hysteresis function series (4.2), then by feeding back the output of the hysteresis function series to system (4.1), the equations become:

$$\begin{cases} \dot{x} = y \\ \dot{y} = -ax + by + au \\ u = h(x, p, q) \end{cases} \tag{4.5}$$

which corresponds to $k_h=1$, $k_v=0$ in (4.3).

It can easily be verified that if $a>0$ and $b>0$, then the trajectory of the system (4.5) will be spirally divergent with a positive damping ratio. With the use of the hysteresis function series (4.2), system (4.5) is able to generate n-scroll chaotic attractors.

The equilibrium points of system (4.5) are located on x-axis, which are given by

$$O_x = [-p, -p+1, \ldots, -1, 0, 1, \ldots, q-1, q].$$

System (4.5) can generate a $(p+q+1)$-scroll chaotic attractor in the direction of the state variable x for some suitable parameters a and b, which is called a 1D horizontal n-scroll chaotic attractor. When $a=1$, $b=0.125$, $p=q=3$, system (4.5) creates a horizontal $p+q+1=7$-scroll chaotic attractor, as shown in Fig. 4.4.

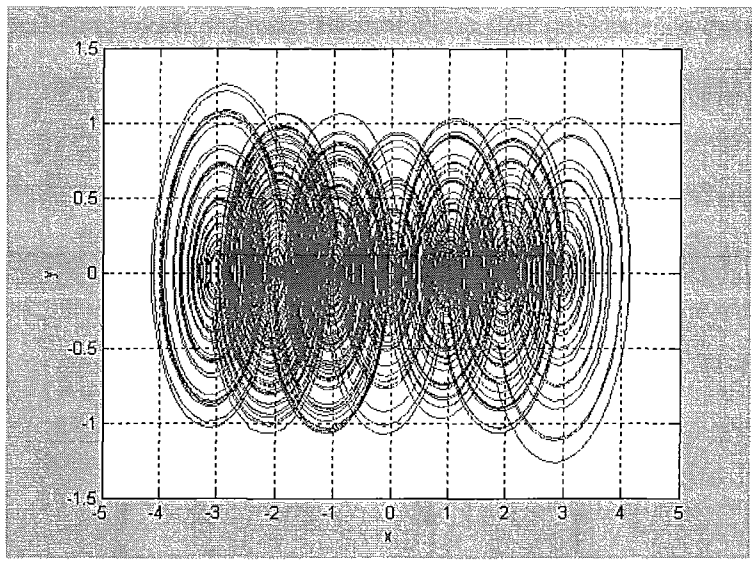

(a)

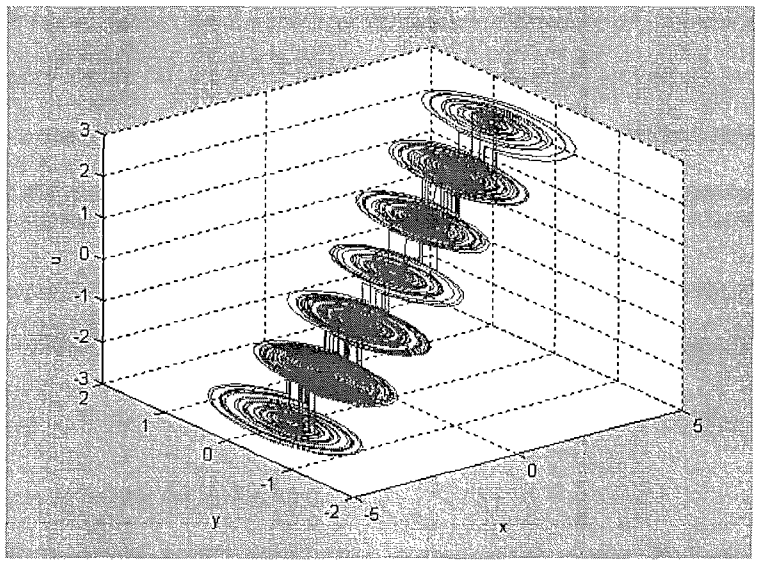

(b)

Fig. 4.4 The horizontal 7-scroll chaotic attractor of system (4.5).
(a) x-y phase trajectory; (b) x-y-u trajectory.

A closer look at the trajectories of system (4.5) reveals that it is a 3-dimensional system (x, y, u) and can be regarded as a configuration of the 2-dimensional linear system on (p+q+1) subspaces connecting with one another via switching of the hysteresis function series $h(x, p, q)$, where the subspaces are:

$$\begin{cases} V_{-p} = \{(x,y,u) \mid x < -p+1, u = -p\} \\ V_i = \{(x,y,u) \mid i-1 < x < i+1, u = i\} \quad -p+1 < i < q-1. \\ V_q = \{(x,y,u) \mid x > q-1, u = q\} \end{cases} \tag{4.6}$$

Note that each subspace V_i ($-p \le i \le q$) includes one and only one of the equilibrium points of system (4.5). System (4.5) is especially unstable in every subspace V_i, thus the system trajectories will not stay in any subspace forever. For a given initial value $(x_0, y_0, u_0) \in V_i$ as $t \to \infty$, the trajectory of system (4.5) spirally diverges around its equilibrium point in subspace V_i; when the trajectory reaches the boundaries of subspace V_i, it is switched to another neighboring subspace V_j ($j \neq i$), and so on. It is noticed that the trajectory will go through every subspace V_j ($-p \le j \le q$). After a long enough time, the trajectory definitely returns to the original subspace V_i, and then the motion will repeat infinitely many times. As $t \to \infty$, the system changes its dynamical behaviours (folding and stretching) repeatedly as the orbit goes through (p+q+1) regions alternatively and repeatedly, leading to very complex dynamics such as the appearance of chaos. It should be pointed that the switching of the hysteresis function series $h(x, p, q)$ plays a key role in generating chaos.

4.3.2 Generating Vertical *N*-Scroll Chaotic Attractors

Consider a second-order system, if the state variable y is input to the hysteresis function series (4.2), then by feeding back the output of the hysteresis function series to system (4.1), the equations become:

$$\begin{cases} \dot{x} = y - v \\ \dot{y} = -ax + by - bv \\ v = h(y, p, q) \end{cases} \tag{4.7}$$

which corresponds to k_h=0, k_v=1 in (4.3).

The equilibrium points of system (4.7) are located on the y-axis, and are given by:

$$O_y = [-p, -p+1, \ldots, -1, 0, 1, \ldots, q-1, q].$$

System (4.7) can generate a (p+q+1)-scroll chaotic attractors in the direction of the state variable y for some suitable parameters a and b, which is called a 1D vertical n-scroll chaotic attractor. When a=1, b=0.125, p=q=3, system (4.7) creates a vertical p+q+1=7-scroll chaotic attractor, as shown in Fig. 4.5.

A closer look at the trajectories of system (4.7) reveals that it is a 3-dimensional system (x, y, v) and can be regarded as a configuration of 2-dimensional linear system on (p+q+1) subspaces connecting to one another via the switching of the hysteresis function series $h(y, p, q)$, where the subspaces are:

$$\begin{cases} V_{-p} = \{(x,y,v) \mid y < -p+1, v = -p\} \\ V_j = \{(x,y,v) \mid j-1 < y < j+1, v = j\} \quad -p+1 < j < q-1. \\ V_q = \{(x;y,v) \mid y > q-1, v = q\} \end{cases} \tag{4.8}$$

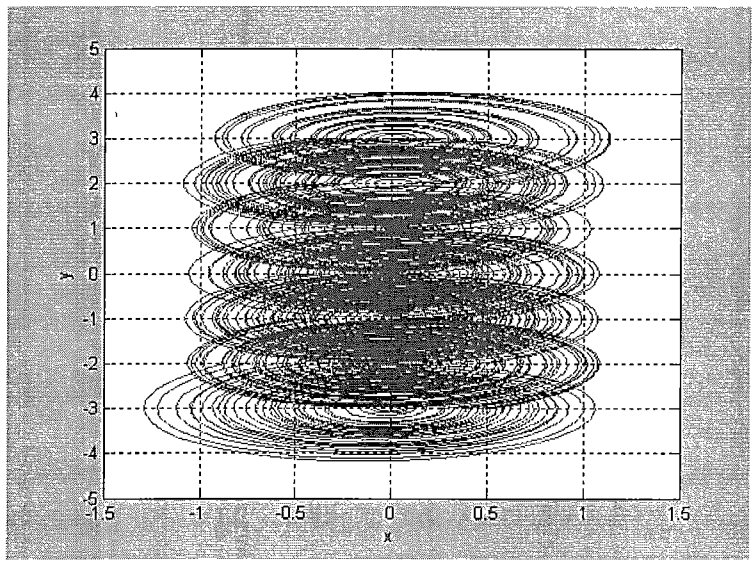

(a)

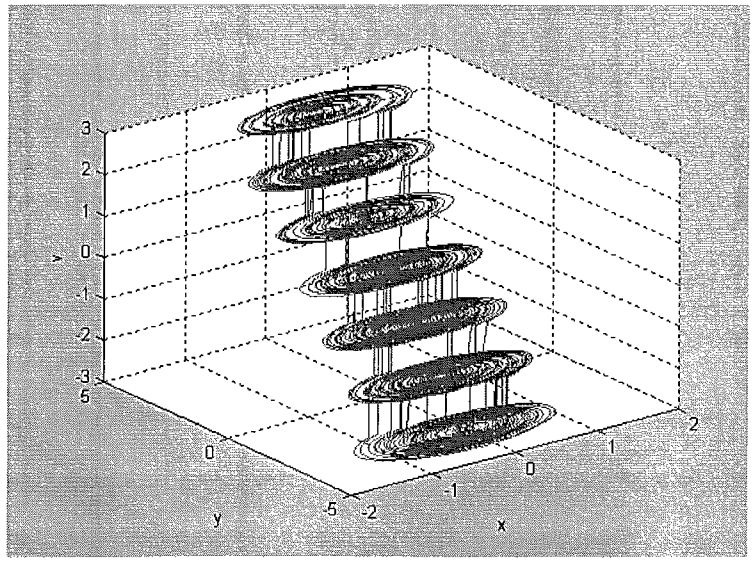

(b)

Fig. 4.5 The vertical 7-scroll chaotic attractor of system (4.7).
(a) x-y phase trajectory; (b) x-y-v trajectory.

Note that each subspace V_j ($-p \leq j \leq q$) includes one and only one of the equilibrium points of system (4.7). System (4.7) is especially unstable in every subspace V_j, thus the system trajectories will not stay in any subspace forever. Multiple scroll chaotic attractors are generated in exactly the same way as in the horizontal direction discussed in 4.3.1.

4.3.3 Generating $N\times M$-Grid Scroll Chaotic Attractors

If both state variables x and y of a second-order system are input to the hysteresis function series (4.2), then by feeding back the outputs of the hysteresis function series to the system (4.1), one has:

$$\begin{cases} \dot{x} = y - v \\ \dot{y} = -ax + by + au - bv \\ u = h(x, p_1, q_1) \\ v = h(y, p_2, q_2) \end{cases} \tag{4.9}$$

corresponds to $k_h=1$, $k_v=1$ in (4.3), the equilibrium points satisfy the following equation:

$$\begin{cases} x = u \\ y = v \end{cases}.$$

Therefore, system (4.9) has $(p_1+q_1+1)\times(p_2+q_2+1)$ equilibrium points, which are given by:

$$O_{xy} = [(i,j)|\ i = -p_1, -p_1+1, \ldots, q_1\ ; j = -p_2, -p_2+1, \ldots, q_2].$$

Thus, system (4.9) can generate an $n\times m$-grid scroll chaotic attractor in the phase plane for some suitable parameters a and b, called a 2D $n\times m$-grid scroll chaotic attractor, where $n = p_1+q_1+1$ and $m = p_2+q_2+1$. When $a=1$, $b=0.125$, $p_1=q_1=3$, $p_2=q_2=2$, system (4.9) can generate a 7×5-grid scroll chaotic attractor, as shown in Fig. 4.6. The x-y phase trajectory of system (4.9) is shown in Fig. 4.6 (a). If the item bv in the second equation of system (4.9) is omitted, only the positions of the equilibrium points are affected. The simulation result is shown in Fig. 4.6 (b), in which the equilibrium points are a little inclined. The trajectories of x-y-u and x-y-v for system (4.9) are shown in Fig. 4.7 (a) and (b), respectively.

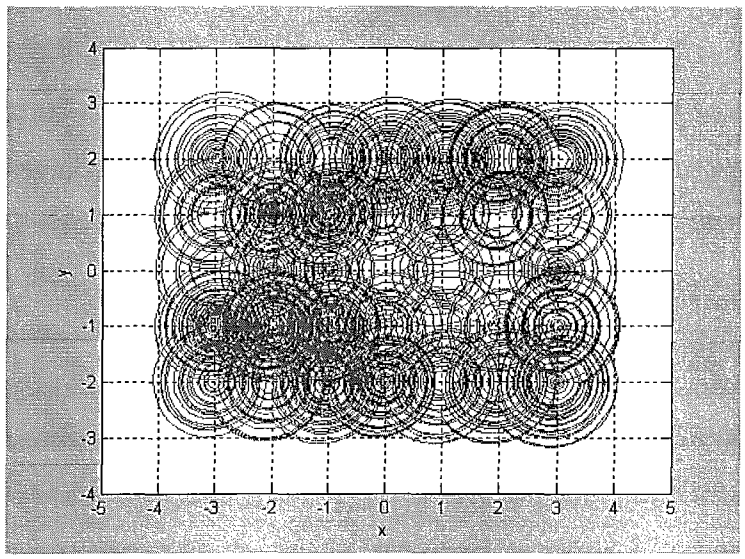

(a)

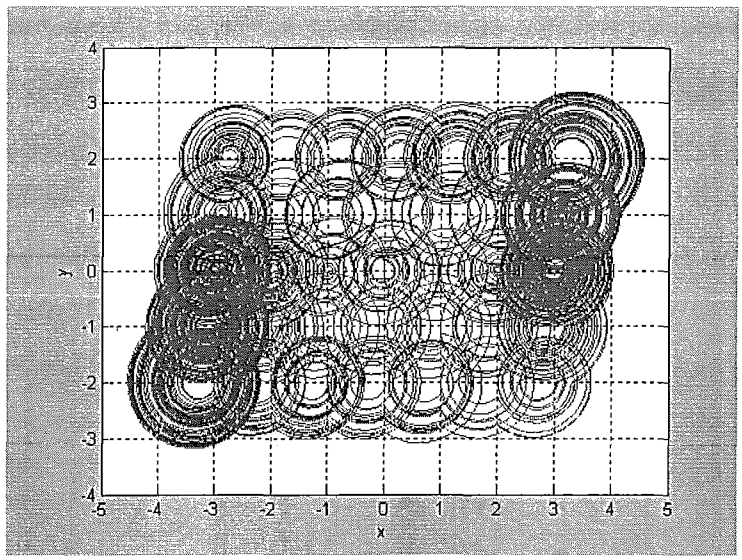

(b)

Fig. 4.6 Phase trajectories of 7×5-scroll chaotic attractor of system (4.9).
(a) x-y phase trajectory; (b) x-y phase trajectory with equilibrium point inclined.

A closer look at the trajectories of system (4.9) reveals that it is a 4-dimensional system (x, y, u, v) and can be regarded as a configuration of a 2-dimensional linear system on $(p_1+q_1+1)\times(p_2+q_2+1)$ subspaces connecting one another via switching of the hysteresis function series $h(x, p_1, q_1)$ and $h(y, p_2, q_2)$, where the $n\times m$ subspaces are:

$$\begin{cases} R_{-p_1} = \{(x,y,u) \mid x < -p_1 + 1, u = -p_1\} \\ R_i = \{(x,y,u) \mid i-1 < x < i+1, u = i\} & -p_1 + 1 < i < q_1 - 1 \\ R_{q_1} = \{(x,y,u) \mid x > q_1 - 1, u = q_1\} \end{cases}$$

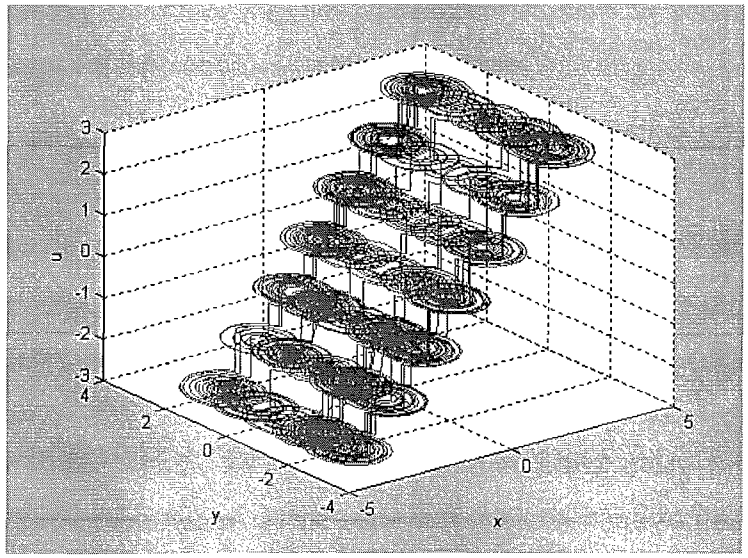

(a)

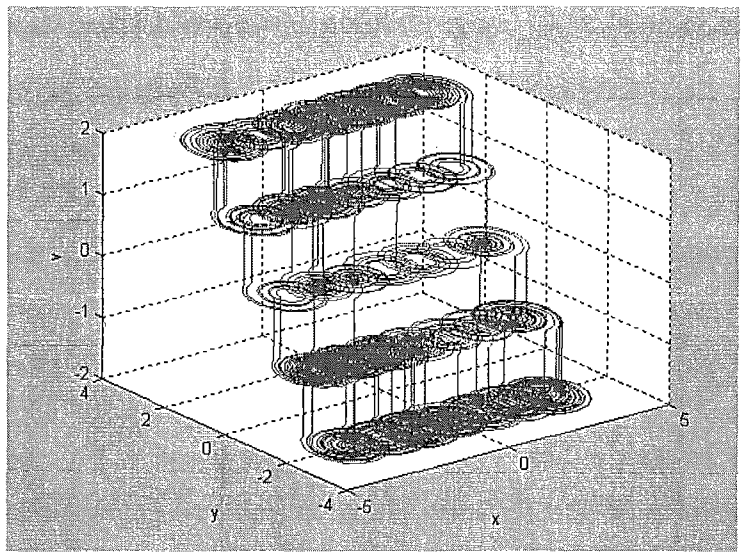

(b)

Fig. 4.7 Space trajectories of 7×5-scroll chaotic attractor of system (4.9).
(a) *x*-*y*-*u* trajectory; (b) *x*-*y*-*v* trajectory.

$$\begin{cases} S_{-p_2} = \{(x, y, v) \mid y < -p_2 + 1, v = -p_2\} \\ S_j = \{(x, y, v) \mid j - 1 < y < j + 1, v = j\} \quad -p_2 + 1 < j < q_2 - 1 \\ S_{q_2} = \{(x, y, v) \mid y > q_2 - 1, v = q_2\} \end{cases}$$

$$V_{(i,j)} = \{(x, y, u, v) \mid x \in R_i, y \in S_j, u = i, v = j\} (-p_1 + 1 \le i \le q_1 - 1, -p_2 + 1 \le j \le q_2 - 1) \quad (4.10)$$

Note that every subspace $V_{(i,j)}$ ($-p_1 \le i \le q_1$, $-p_2 \le j \le q_2$) includes one and only one of the equilibrium points of system (4.9). Since the system (4.9) is divergent in every subspace $V_{(i,j)}$, the system trajectories will not stay in any subspace forever. Multiple scroll chaotic attractors are generated in exactly the same way as both the horizontal and vertical cases studied in 4.3.1 and 4.3.2, except for the notion of system trajectories.

4.4 Multi-Scroll Chaotic Attractors via Third-Order Systems

In this section, it is shown that linear third-order systems and hysteresis function series can also generate multi-scroll chaotic attractors. How to generate a 1D *n*-scroll, a 2D *n*×*m*-grid scroll, and a 3D *n*×*m*×*l*-space scroll chaotic attractor are discussed respectively.

4.4.1 Generating *N*-Scroll Chaotic Attractors

Consider a linear third-order system, if the state variable *x* is input to the hysteresis function series (4.2), by feeding back the output of Eq. (4.2) to the system (4.1), the new system is:

$$\begin{cases} \dot{x} = y \\ \dot{y} = z \\ \dot{z} = -ax - by - cz + au \\ u = h(x, p, q) \end{cases} \tag{4.11}$$

which corresponds to $k_1=1$, $k_2=k_3=0$ in (4.4). The corresponding characteristic equation is:

$$\lambda^3 - c\lambda^2 - b\lambda + a = 0 . \tag{4.12}$$

Numerical simulations show that with the help of the hysteresis function series on system (4.11), if Eq. (4.12) has a negative eigenvalue and a pair of conjugate complex eigenvalues with positive real parts, then the multi-scroll chaotic attractors can be generated.

Let $\lambda=\Lambda-c/3$. Substituting it into Eq. (4.12), then

$$\Lambda^3 + (b - \frac{1}{3}c^2)\Lambda + \frac{2}{27}c^3 - \frac{1}{3}bc + a = 0 \tag{4.13}$$

Denoting

$$r = b - \frac{1}{3}c^2 ,$$

$$s = \frac{2}{27}c^3 - \frac{1}{3}bc + a ,$$

$$\Delta = \frac{1}{27}ac^3 - \frac{1}{108}b^2c^2 - \frac{1}{6}abc + \frac{1}{27}b^3 + \frac{1}{4}a^2 .$$

and solving (4.13) yields:

$$\begin{cases} \lambda_1 = \Lambda_1 - \frac{1}{3}c = -\frac{1}{3}c + \sqrt[3]{-\frac{s}{2} + \sqrt{\Delta}} + \sqrt[3]{-\frac{s}{2} - \sqrt{\Delta}} \\ \lambda_{2,3} = \Lambda_{2,3} - \frac{1}{3}c \\ \quad = -\frac{1}{3}c - \frac{1}{2}(\sqrt[3]{-\frac{s}{2} + \sqrt{\Delta}} + \sqrt[3]{-\frac{s}{2} - \sqrt{\Delta}}) + j\frac{\sqrt{3}}{2}(\sqrt[3]{-\frac{s}{2} + \sqrt{\Delta}} - \sqrt[3]{-\frac{s}{2} - \sqrt{\Delta}}) \\ \quad \equiv \alpha + j\beta \end{cases} . \tag{4.14}$$

Under the conditions $\lambda_1<0$, $\alpha>0$ and $\beta\neq0$, it is possible for system (4.11) to generate chaos.

The equilibrium points of system (4.11) are located on the x-axis, and are given by:

$$O_x = [-p, -p+1, \cdots, -1, 0, 1, \cdots, q-1, q].$$

System (4.11) can generate a $(p+q+1)$-scroll chaotic attractor for some suitable parameters a, b, and c. Fig. 4.8 shows a 7-scroll chaotic attractor where $a=0.8$, $b=0.72$, $c=0.6$, $p=q=3$.

It is noted that system (4.11) is a 4-dimensional system of $\overline{X} = (x, y, z, u)$ and can be regarded as a configuration of a 3-dimensional linear system on (p+q+1) subspaces connecting to one another via switching of the hysteresis function series $h(x, p, q)$. The subspaces are:

$$\begin{cases} W_{-p} = \{\overline{X} \mid x < -p+1, u = -p\} \\ W_i = \{\overline{X} \mid i-1 < x < i+1, u = i\} \quad -p+1 < i < q-1 \\ W_q = \{\overline{X} \mid x > q-1, u = q\} \end{cases} \tag{4.15}$$

where $\overline{X} = (x, y, z, u)$.

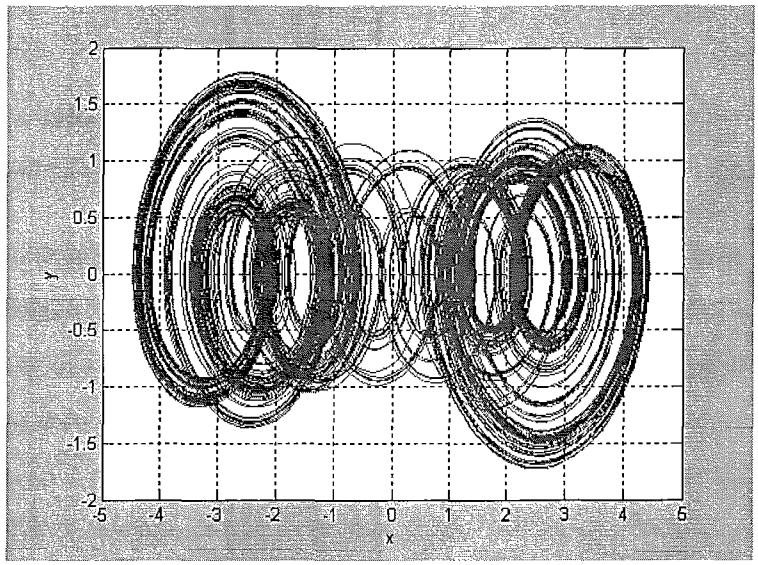

(a)

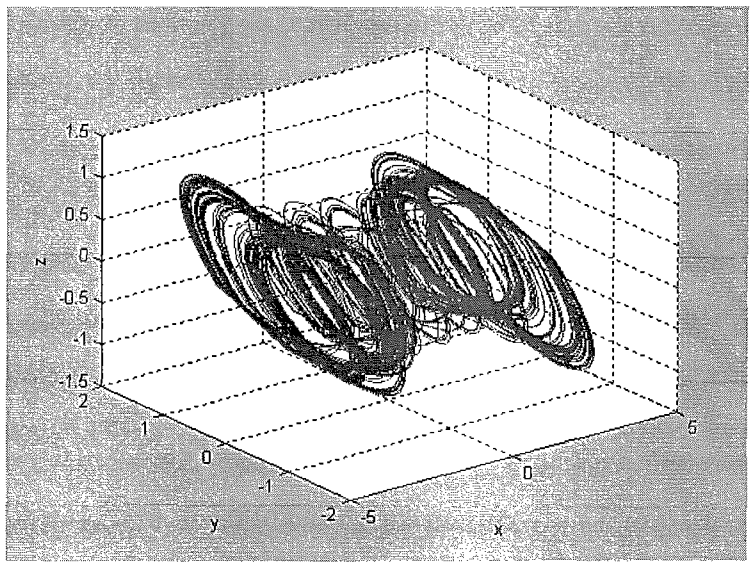

(b)

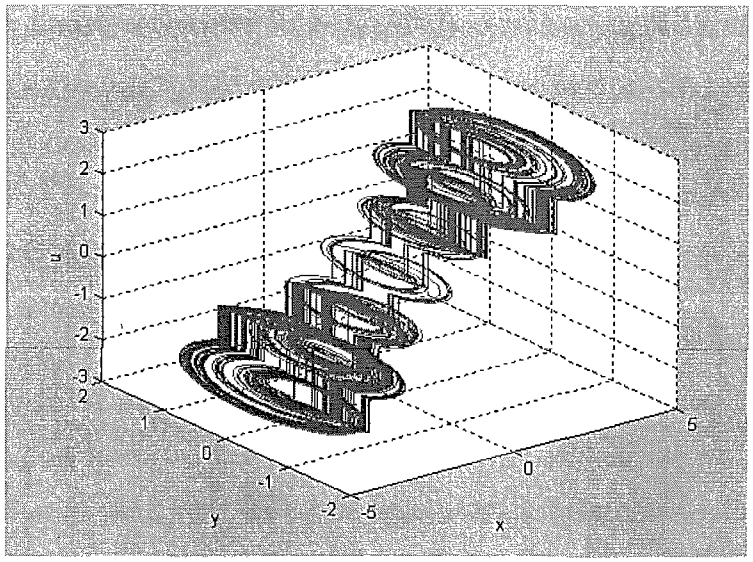

(c)

Fig. 4.8 The 7-scroll chaotic attractor of system (4.11).
(a) x-y plane;(b) x-y-z space; (c) x-y-u space.

It is very clear that there exists one and only one of the equilibrium points O_x in every subspace W_i ($-p \le i \le q$); and every equilibrium point corresponds to one scroll of the chaotic attractor. Moreover, the system (4.11) is divergent in each subspace W_i, thus the system trajectories will not stay in any subspace forever.

For a given initial value $(x_0, y_0, z_0, u_0) \in W_i$, as $t \to \infty$ the trajectory of system (4.11) spirally diverges around its equilibrium point in subspace W_i. When the trajectory reaches the boundaries of W_i, it jumps onto another neighbouring subspace W_j ($j \neq i$) holding (x, y, z) constant, and then continuously to do so. Here, the switching boundaries are planes rather than lines as the second-order systems case. Note that the trajectory will go through every subspace $W_j(-p \le j \le q)$. After a long enough time, the trajectory definitely returns to the original subspace W_i, and then repeats a similar motion infinitely many times. As $t \to \infty$ the system changes its dynamical behaviour (stretching and folding) repeatedly as the trajectory goes through the $(p+q+1)$ regions alternately and repeatedly, leading to very complex dynamics such as the appearance of chaos. Here, the switching of the hysteresis function series $h(x, p, q)$ play a key role in generating chaos. Also, it is clear that the switching mechanics of system (4.11) are more complex than that of second-order systems case.

4.4.2 Generating $N \times M$-Grid Scroll Chaotic Attractors

If both state variables x and y of a linear third-order system are input to the hysteresis function

series (4.2), and feeding back the outputs of Eq. (4.2) to the system (4.1), the new system is:

$$\begin{cases} \dot{x} = y - v \\ \dot{y} = z \\ \dot{z} = -ax - by - cz + au + bv \\ u = h(x, p_1, q_1) \\ v = h(y, p_2, q_2) \end{cases} \tag{4.16}$$

which corresponds to $k_1 = k_2 = 1$, $k_3 = 0$ in (4.4).

System (4.16) has $(p_1+q_1+1) \times (p_2+q_2+1)$ equilibrium points, which are given by:

$$O_{xy} = [(i, j) | -p_1 \le i \le q_1, -p_2 \le j \le q_2]$$

Thus, for some suitable parameters a, b, and c, system (4.16) can generate a $(p_1+q_1+1)\times(p_2+q_2+1)$-grid scroll chaotic attractor. Fig. 4.9 shows a 5×7-scroll chaotic attractor, where a=0.8, b=0.7, c=0.6, $p_1=q_1=2$, $p_2=q_2=3$.

It should be noted that system (4.16) is a 5-dimensional system of $\overline{X} = (x, y, z, u, v)$, and can be regarded as a configuration of a 3-dimensional linear system on $(p_1+q_1+1)\times(p_2+q_2+1)$ subspaces connecting to one another via switching of the hysteresis function series $h(x, p_1, q_1)$ and $h(y, p_2, q_2)$. Denote:

$$\begin{cases} R_{-p_1} = \{\overline{X} \mid x < -p_1 + 1\} \\ R_i = \{\overline{X} \mid i - 1 < x < i + 1\} \quad -p_1 + 1 < i < q_1 - 1 \\ R_{q_1} = \{\overline{X} \mid x > q_1 - 1\} \end{cases}$$

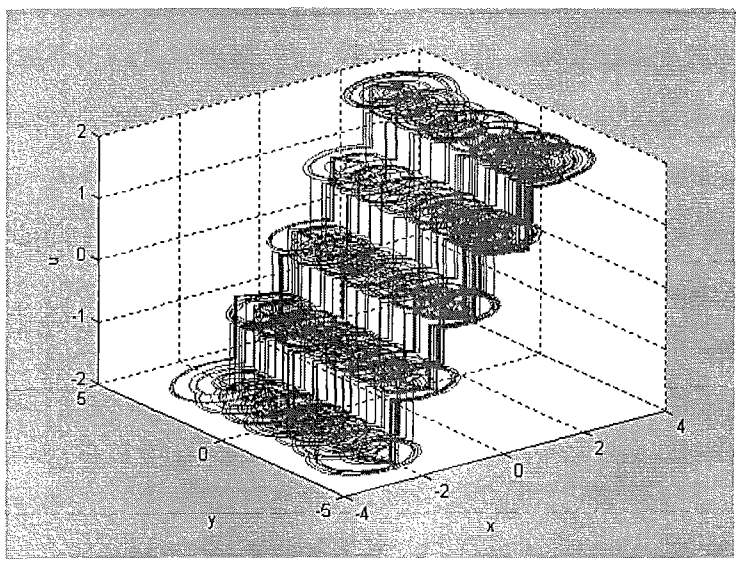

(a)

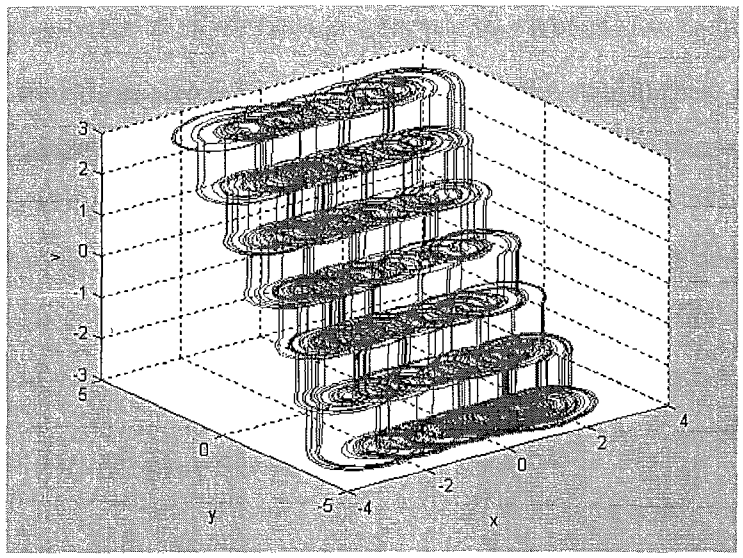

(b)

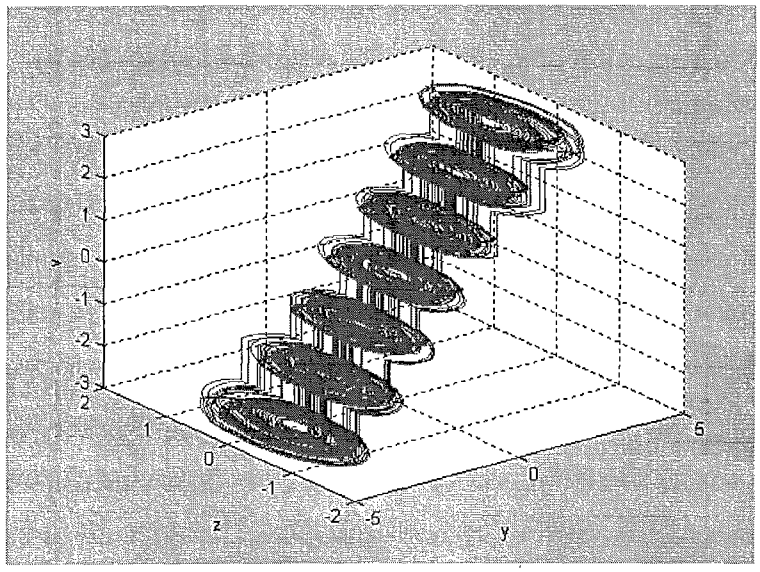

(c)

Fig. 4.9 The 5×7-scroll chaotic attractor of system (4.16).
(a) *x*-*y*-*u* space; (b) *x*-*y*-*v* space; (c) *y*-*z*-*v* space.

$$\begin{cases} S_{-p_2} = \{\overline{X} \mid y < -p_2 + 1\} \\ S_i = \{\overline{X} \mid j-1 < y < j+1\} \quad -p_2 + 1 < j < q_2 - 1. \\ S_{q_2} = \{\overline{X} \mid y > q_2 - 1\} \end{cases}$$

Thus, the subspaces are:

$$W_{(i,j)} = \{\overline{X} \mid x \in R_i, y \in S_j, u = i, v = j\} \ (-p_1+1 \le i \le q_1-1, -p_2+1 \le j \le q_2-1) \qquad (4.17)$$

where $\overline{X} = (x, y, z, u, v)$.

It is very clear that there exists one and only one of the equilibrium points O_{xy} in every subspace $W_{(i,j)}$ ($-p_1 \le i \le q_1$, $-p_2 \le j \le q_2$). Moreover, the system trajectories will not stay in any subspace forever since the system (4.16) is divergent in every subspace $W_{(i,j)}$. Note that the 2D $n\times m$-grid scroll chaotic attractor is generated in exactly the same way as the 1D case discussed in 4.4.1, except for the notion of the system trajectories. Similarly, one can easily design a 2D $n\times m$-grid scroll chaotic attractor in the x-z or y-z directions.

4.4.3 Generating $N\times M\times L$-Space Scroll Chaotic Attractors

In the following, three state variables x, y, and z of a third-order system are input to the hysteresis function series (4.2) for generating a 3D $n\times m\times l$-space scroll chaotic attractor. By feeding back the outputs of Eq. (4.2) to the third-order system, the new system is:

$$\begin{cases} \dot{x} = y - v \\ \dot{y} = z - w \\ \dot{z} = -ax - by - cz + au + bv + cw \\ u = h(x, p_1, q_1) \\ v = h(y, p_2, q_2) \\ w = h(z, p_3, q_3) \end{cases} \tag{4.18}$$

which corresponds to $k_1 = k_2 = k_3 = 1$ in (4.4).

System (4.18) has $(p_1+q_1+1)\times(p_2+q_2+1)\times(p_3+q_3+1)$ equilibrium points, which are given by:

$$O_{xyz} = [(i, j, k) | -p_1 \le i \le q_1, -p_2 \le j \le q_2, -p_3 \le k \le q_3)]$$

Thus, for some suitable parameters a, b, and c, system (4.18) can generate a $(p_1+q_1+1)\times(p_2+q_2+1)\times(p_3+q_3+1)$-space scroll chaotic attractors. Fig. 4.10 shows a 5×8×3-scroll chaotic attractors, where a=0.8, b=0.72, c=0.66, p_1=q_1=2, p_2=3, q_2=4, p_3=q_3=1. It is clear that there are 5 scrolls in the x-direction, 8 scrolls in the y-direction and 3 scrolls in the z-direction in Fig. 4.10.

It is observed that system (4.18) is a 6-dimensional system of $\overline{X} = (x, y, z, u, v, w)$, and can be regarded as a configuration of a 3-dimensional linear system on $(p_1+q_1+1)\times(p_2+q_2+1)\times(p_3+q_3+1)$ subspaces connecting to one another via switching of the hysteresis function series $h(x, p_1, q_1)$, $h(y, p_2, q_2)$ and $h(z, p_3, q_3)$. Denote:

$$\begin{cases} R_{-p_1} = \{\overline{X} \mid x < -p_1 + 1\} \\ R_i = \{\overline{X} \mid i-1 < x < i+1\} \quad -p_1 + 1 < i < q_1 - 1 \\ R_{q_1} = \{\overline{X} \mid x > q_1 - 1\} \end{cases}$$

$$\begin{cases} S_{-p_2} = \{\overline{X} \mid y < -p_2 + 1\} \\ S_i = \{\overline{X} \mid j-1 < y < j+1\} \quad -p_2 + 1 < j < q_2 - 1 \\ S_{q_2} = \{\overline{X} \mid y > q_2 - 1\} \end{cases}$$

and

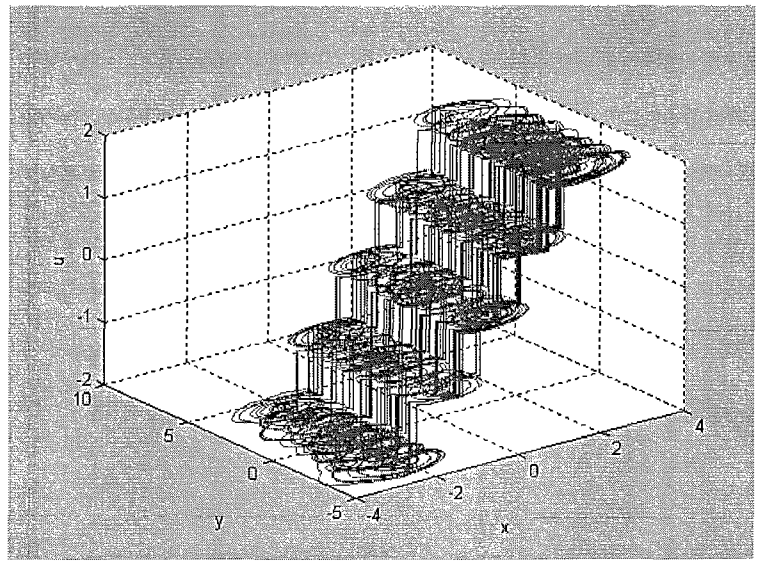

(a)

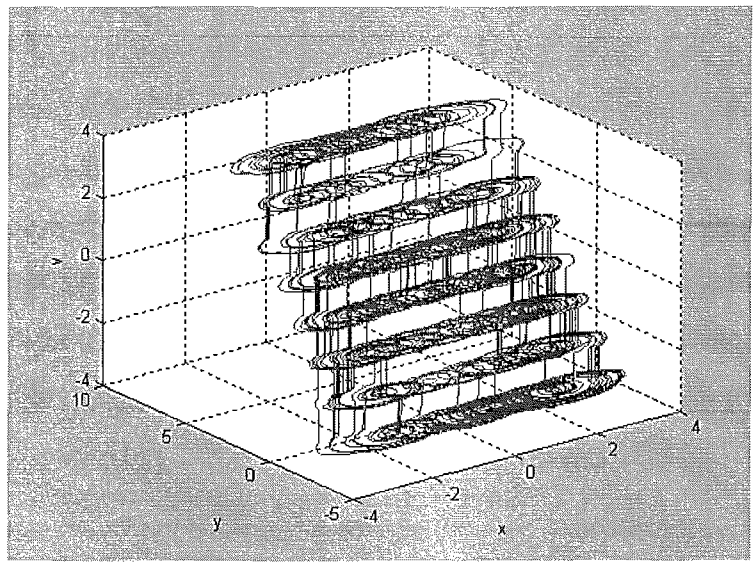

(b)

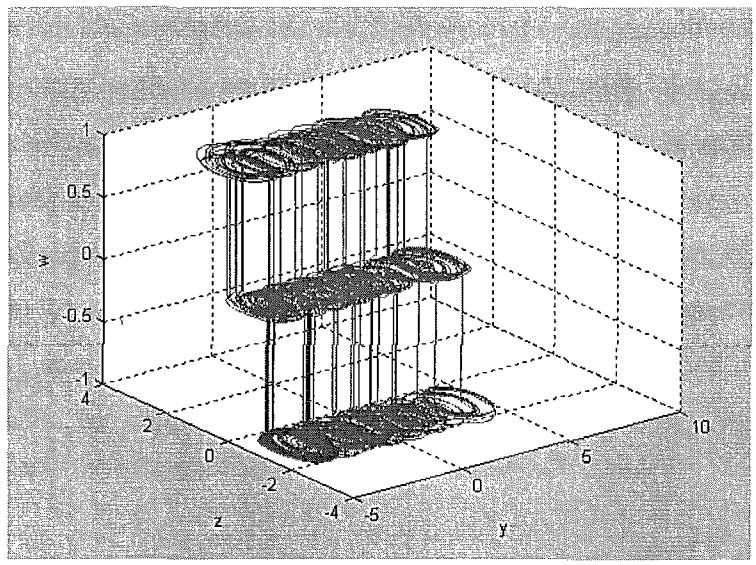

(c)

Fig. 4.10 The 5×8×3-scroll chaotic attractor of system (4.18).
(a) *x*-*y*-*u* space; (b) *x*-*y*-*v* space; (c) *y*-*z*-*w* space.

$$\begin{cases} T_{-p_3} = \{\overline{X} \mid z < -p_3 + 1\} \\ T_i = \{\overline{X} \mid k-1 < z < k+1\} \quad -p_3 + 1 < k < q_3 - 1. \\ T_{q_3} = \{\overline{X} \mid z > q_3 - 1\} \end{cases}$$

Thus, the subspaces are:

$$W_{(i,j,k)} = \{\overline{X} \mid x \in R_i, y \in S_j, z \in T_k, u=i, v=j, w=k\} \ (-p_1+1 \le i \le q_1-1, -p_2+1 \le j \le q_2-1, -p_3+1 \le k \le q_3-1) \tag{4.19}$$

where $\overline{X} = (x, y, z, u, v, w)$.

Note that there exists one and only one of the equilibrium points O_{xyz} in every subspace $W_{(i,j,k)}$ ($-p_1 \le i \le q_1$, $-p_2 \le j \le q_2$, $-p_3 \le k \le q_3$). Moreover, the system trajectories will not stay in any subspace forever since the system (4.18) is divergent in every subspace $W_{(i,j,k)}$. Note that 3D $n \times m \times l$-space scroll chaotic attractors are generated exactly in the same way as the 1D and 2D cases discussed in 4.4.1 and 4.4.2, except for the notion of the system trajectories.

4.5 Summary

A systematic method for generating multi-scroll chaotic attractors via linear systems using a feedback control of the hysteresis function series has been presented in this chapter. It has been shown that the 1D *n*-scroll chaotic attractors in the directions of the state variables and

the 2D $n \times m$-grid scroll chaotic attractors in the phase plane can be generated via continuous-time linear second-order systems and a hysteresis function series. Also the 1D n-scroll, 2D $n \times m$-grid scroll and 3D $n \times m \times l$-space scroll chaotic attractors can be generated via continuous-time linear third-order systems and the hysteresis function series.

The multi-scroll chaos generation systems can be represented as hybrid Lur'e systems, and as a result they may be used within synchronization schemes for secure communication. The desired number of scrolls and their space positions can be obtained using a developed methodology intended for engineering applications. This methodology will be shown in the following chapters.

Chapter 5

Dynamics of the Multi-Scroll Chaotic Attractors

5.1 Introduction

In the last chapter, a multi-scroll chaotic attractor was developed using a continuous-time linear second-order or third-order system with a hysteresis function series. The dynamical behaviours of multi-scroll chaotic attractors are further investigated in this chapter in order to study the chaos generation mechanism and confirm the chaotic behaviour theoretically.

The basin of attraction and the stability margin of the 1D multi-scroll chaotic attractor in the second-order system case are studied. The switching boundaries, switching rules and the trajectories on each subspace are investigated in detail. The dynamical behaviours of the chaotic systems with different hysteresis feedback are demonstrated.

This chapter is organized as follows. Section 5.2 contains the basin of attraction and the stability margin for the chaotic attractor. Section 5.3 studies the dynamical behaviour of the multi-scroll chaotic attractor. Dynamical behaviour analysis with a different hysteresis controller is studied in section 5.4. Section 5.5 summaries this chapter.

5.2 Basin of Attraction and Stability Margin of the Chaotic Attractor

In this section, the basin of attraction for the multi-scroll chaotic attractor proposed in chapter 4 is investigated. The stability margin of the chaotic attractor is proposed.

5.2.1 Basin of Attraction of the Chaotic Attractor

For simplicity, suppose a=1, b=2α, p=n, q=0, and the 1D horizontal n-scroll chaotic attractor generation equations (4.5) can be written as:

$$\begin{cases} \dot{x} = y \\ \dot{y} = -x + 2\alpha y + h(x, n, 0) \end{cases}. \tag{5.1}$$

According to the analysis given in Chapter 3, there is an unstable limit cycle in the hysteresis based system (3.3). There still is an unstable limit cycle ***L*** in system (5.1) even when the scroll number is increased. This limit cycle ***L*** bounds the basin of attraction for the chaotic attractor. For example, when n=2 and 5, the 3- and 6-scroll chaotic attractor generated by system (5.1) and the trajectories of ***L*** are shown in Fig. 5.1, where ***C*** stands for the area covered by the chaotic trajectory.

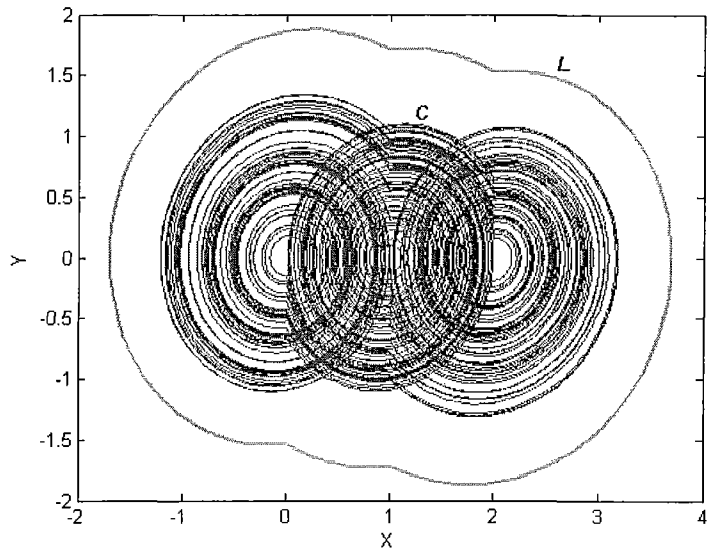

(a)

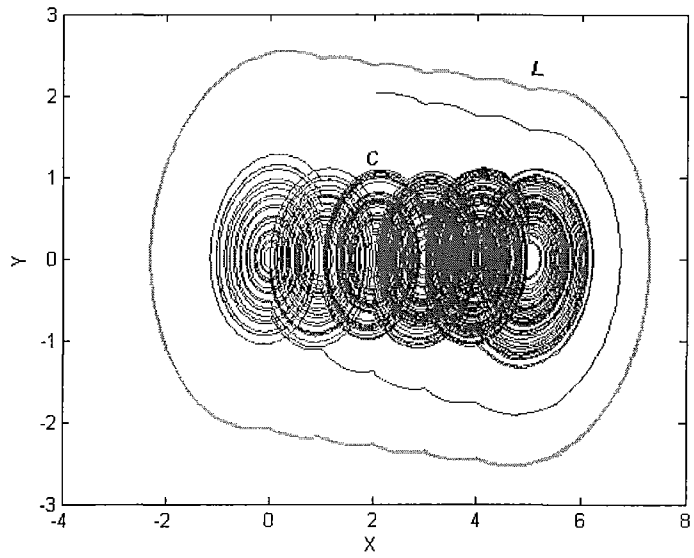

(b)

Fig. 5.1 Limit cycle and the chaotic trajectories when α=0.0625. (a) 3-scroll; (b) 6-scroll.

Fig. 5.1 shows that both the horizontal and vertical coordinates of $\boldsymbol{L}$ increase with an increase in the scroll number. The initial values for Fig. 5.1 (b) are (2.0528, 2.02), which results in an unbounded trajectory when n=2 and a bounded trajectory when n=5. This occurs eventhough it is outside the chaotic trajectory region $\boldsymbol{C}$ (but within the basin of attraction $\boldsymbol{L}$).

The positive x-axis in Fig. 5.1 is chosen as the Poincaré section. When n=2, the Poincaré map with three different parameters of system (5.1) are shown in Fig. 5.2.

From Fig. 5.2, it can be seen that:

1) Point L in Fig. 5.2 corresponds to the unstable limit cycle that bounds the basin of attraction. When α increases, its horizontal coordinate $L0$ decreases.

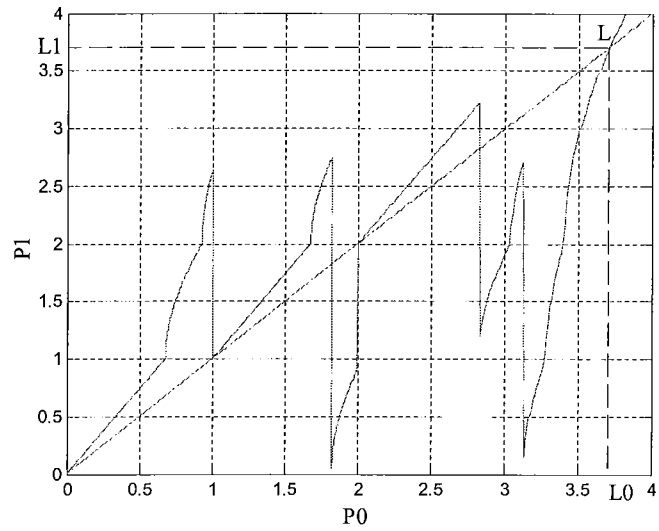

(a)

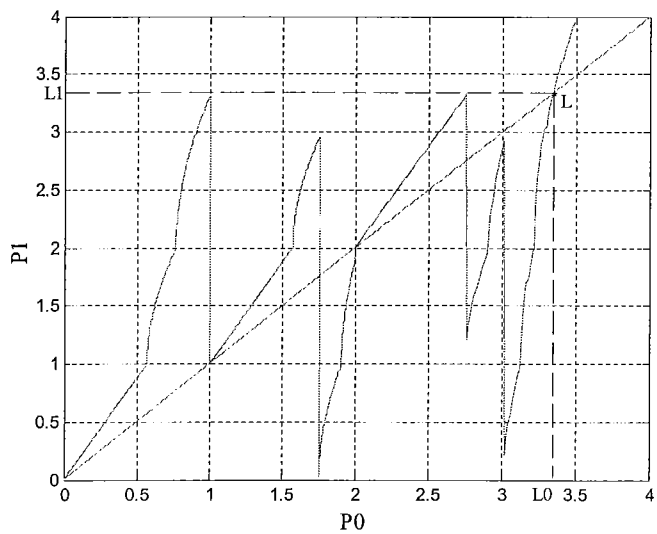

(b)

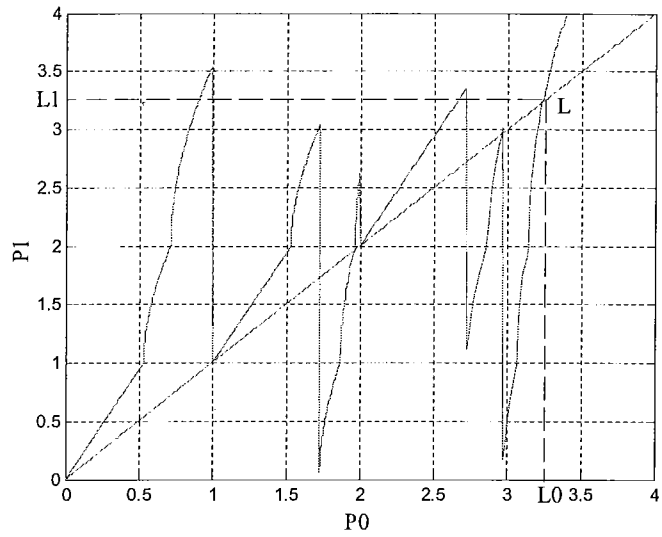

(c)

Fig. 5.2 Poincaré map of system (5.1) when n=2. (a) α=0.0625; (b) α=0.0896; (c) α=0.1.

2) If the maximum vertical coordinate of the Poincaré map is smaller than $L1$ (the vertical coordinate of point L), as shown in Fig. 5.2 (a) when α=0.0625, all trajectories will stay within the basin of attraction when the initial conditions are within the basin.

3) Fig. 5.2 (b) shows the limiting case for the occurrence of chaos when $\alpha=\alpha_{max}$=0.0896. The maximum vertical coordinate of the Poincaré map equals to $L1$. In other words, the outer border of the chaotic trajectory covered by region ***C*** is the limit cycle.

4) Fig. 5.2 (c) shows that the maximum vertical coordinate of the Poincaré map is larger than $L1$, which means that the trajectories will run out of the basin of attraction even if the initial conditions are within it.

When α=0.1 as that in Fig. 5.2 (c), an unbounded trajectory is created when n=2 and chaos appears when n is increased to 4. The Poincaré map of a 5-scroll chaotic attractor is shown in Fig. 5.3, in which the maximum vertical coordinate is smaller than $L1$.

5.2.2 Stability Sensitivity Analysis

The stability of system (5.1) is dependent on the system parameter α and the number of hysteresis functions n. The Poincaré maps in Fig. 5.2 (c) and Fig. 5.3 show that when parameter α is unchanged, the unbounded trajectory may become bounded when n is increased, or the unstable trajectory may become stable (but chaotic). Fig. 5.4 shows the maximum value of α versus n for occurrence of chaos.

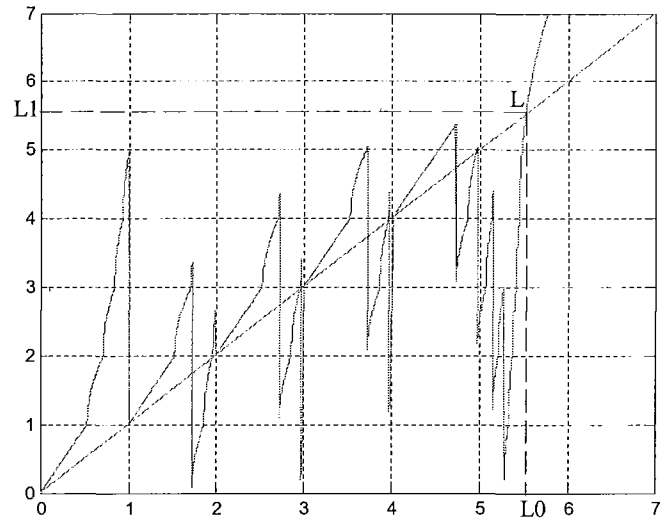

Fig. 5.3 Poincaré map of system (5.1) when n=4, α=0.1.

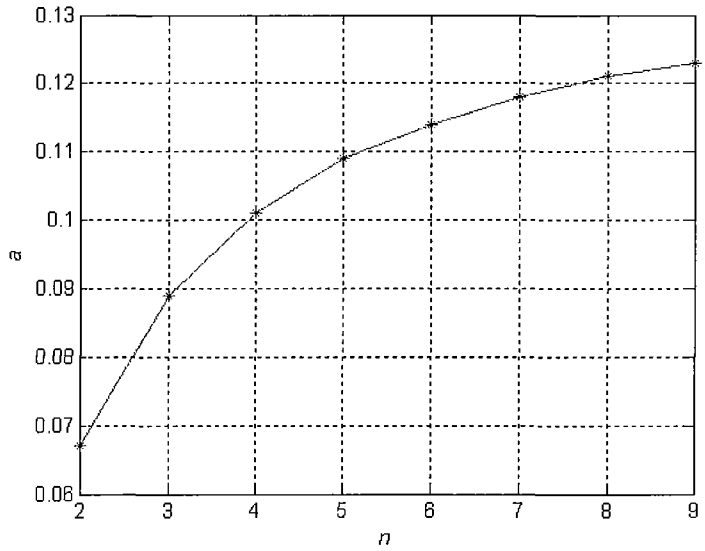

Fig. 5.4 The maximum value of α in system (5.1) versus n.

It can been seen in Fig. 5.4 that when n is increased, the maximum value of parameter α for the occurrence of chaos in system (5.1) also increases. The limit cycle is also dependent on α and n. The maximum x-coordinate of the limit cycle (when y=0) in the Poincaré map, $L0$, versus n while $\alpha=\alpha_{max}$ is shown in Fig. 5.5, which indicates that $L0$ increases linearly with respect to n.

The limit cycle trajectory is sensitive to the system parameter α. The relationship of $L0$ versus α when n=4 is shown in Fig. 5.6, where the maximum x-coordinate (when y=0) of limit cycle, $L0$, decreases when the system parameter α is increased and when n is fixed.

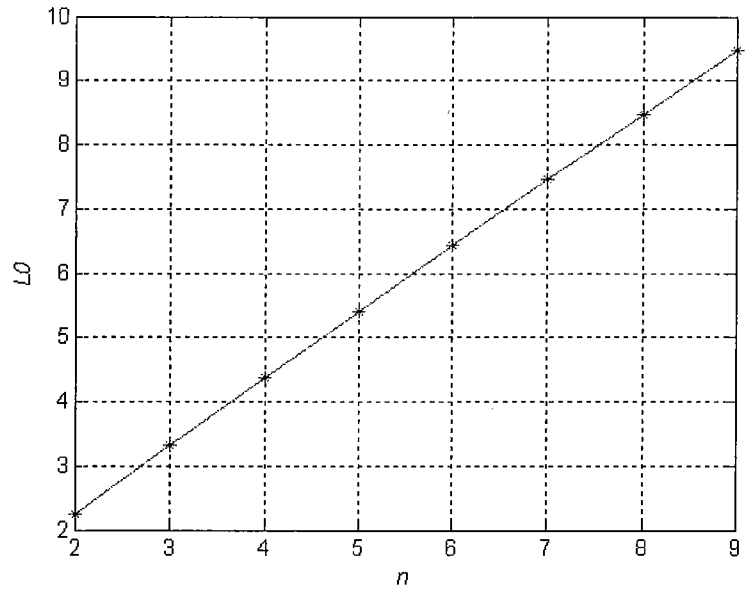

Fig. 5.5 $L0$ versus n while $\alpha = \alpha_{max}$.

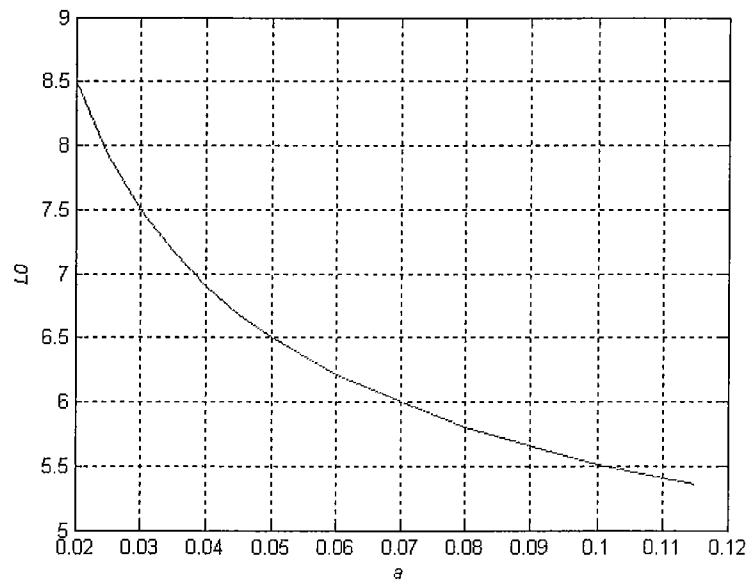

Fig. 5.6 $L0$ versus parameter α when n=4.

From the above analysis, it can be seen that there still exists an unstable limit cycle which bounds the basin of attraction $\boldsymbol{L}$ in the multi-scroll chaos generation system. The size of basin of attraction is dependent on the parameter of the second-order system and the number of the hysteresis function. If the system parameter is unchanged, the size of $\boldsymbol{L}$ increases when the hysteresis number increases. If the hysteresis number is unchanged, then the size of $\boldsymbol{L}$ decreases when the system parameter α increases.

5.3 Dynamical Behaviour Analysis of Multi-Scroll Chaotic Attractors

In this section the dynamical behaviour of the 1D horizontal n-scroll chaotic attractor and 2D $n\times m$-grid scroll chaotic attractor via second-order systems and hysteresis function series, and the dynamical behaviour of the 1D n-scroll, 2D $n\times m$-grid scroll as well as 3D $n\times m\times l$-space scroll chaotic attractors are studied.

5.3.1 3-Scroll Chaotic Attractors via Second-Order Systems

If $p=q=1$, and $\alpha=0.0625$, system (5.1) has a 3-scroll chaotic attractor as shown in Fig. 5.7. It has three equilibrium points, located in three corresponding subspaces:

$$(1, 0, 1)\in V_1=\{(x, y, u)\,|\,x>0, u=1\};$$

$$(0, 0, 0)\in V_2=\{(x, y, u)\,|\,-1<x<1, u=0\};$$

$$(-1, 0, -1)\in V_3=\{(x, y, u)\,|\,x<0, u=-1\}.$$

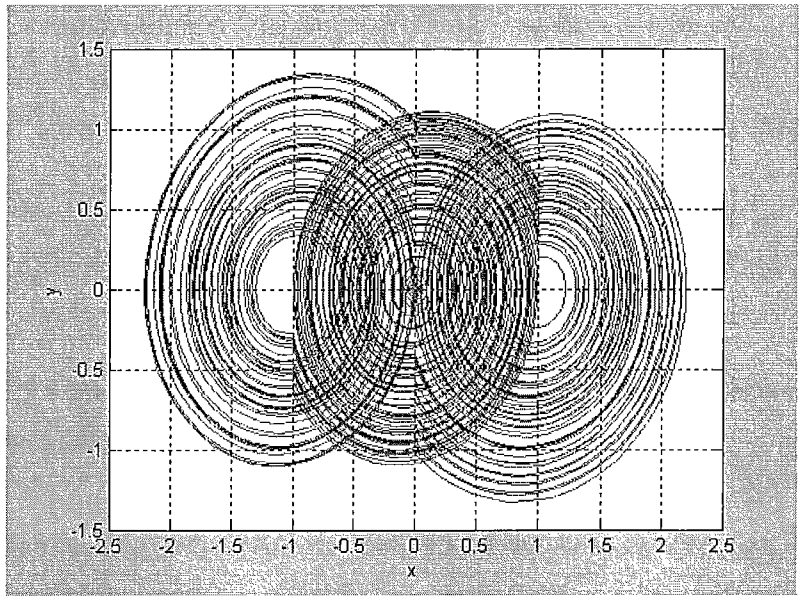

Fig. 5.7 Trajectory of a 3-scroll chaotic attractor of second-order systems case.

The boundaries for the above three subspaces V_1, V_2 and V_3 are defined as:

$$M_1\equiv\{(x, y, u)\,|\,x=0\}\cap V_1;$$

$$M_2\equiv\{(x, y, u)\,|\,x=1\}\cap V_2;$$

$$M_3\equiv\{(x, y, u)\,|\,x=-1\}\cap V_2;$$

$$M_4\equiv\{(x, y, u)\,|\,x=0\}\cap V_3.$$

Consider the trajectory on V_1. It rotates divergently around the equilibrium point (1,0,1), and hits the boundary M_1, then jumps onto V_2 with the same (x, y), that is, the switching rule is:

$$(x, y, u)(t^+)=(0, y, 0)\subset V_2 \text{ if } (x, y, u)(t)=(0, y, 1)\subset M_1;$$

Similarly, the other switching rules are described by:

$$(x, y, u)(t^+)=(1, y, 1)\subset V_1 \text{ if } (x, y, u)(t)=(1, y, 0)\subset M_2;$$

$$(x, y, u)(t^+)=(-1, y, -1)\subset V_3 \text{ if } (x, y, u)(t)=(-1, y, 0)\subset M_3;$$

$$(x, y, u)(t^+)=(0, y, 0)\subset V_2 \text{ if } (x, y, u)(t)=(0, y, -1)\subset M_4.$$

In the following, four specially grazing trajectories [70] are defined as shown in Fig. 5.8:

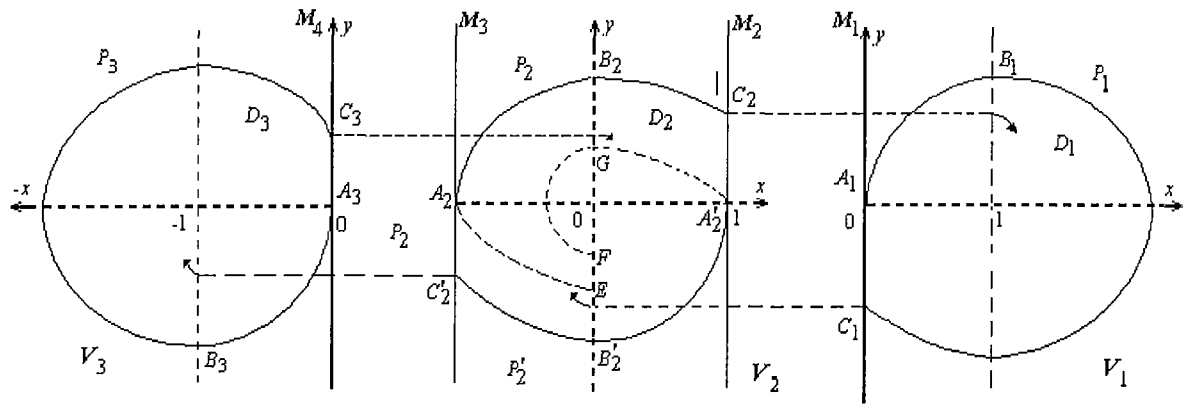

Fig. 5.8 Trajectories distribution of 3-scroll of second-order systems case.

1) $\boldsymbol{P}_1$ is a trajectory on V_1 that starts from A_1 (0,0,1) $\in M_1$ at $t = 0$, intersects B_1 $(1,b_1,1)$ $\in\{(x,y,1)\,|\,x=1, y>0\}\in V_1$ at $t = t_1$ and hits C_1 $(0,c_1,1)$ $\in M_1$ at $t = t_2$. Since the starting point A_1 lies in the line $\dot{x} = y = 0$, the trajectory $\boldsymbol{P}_1$ grazes M_1 at A_1.

2) $\boldsymbol{P}_2$ is a trajectory on V_2 that starts from A_2 $(-1,0,0)$ $\in M_3$ at $t = 0$, intersects B_2 $(0,b_2,0)$ $\in\{(x,y,0)\,|\,x=0, y>0\}\in V_2$ at $t = t_3$ and hits C_2 $(1,c_2,0)$ $\in M_2$ at $t = t_4$. Since the starting point A_2 lies in the line $\dot{x} = y = 0$, the trajectory $\boldsymbol{P}_2$ grazes M_3 at A_2. There exists a point $E(0,e,0)$ such that the trajectory starting from E passes through the point A_2 as shown in Fig. 5.8.

3) P_2' is a trajectory on V_2 that starts from $A_2'(1,0,0)\in M_2$ at $t = 0$, intersects $B_2'(0,b_2',0)$ $\in\{(x,y,0)\,|\,x=0, y<0\}\in V_2$ at $t = t_5$ and hits C_2' $(-1,c_2',0)$ $\in M_2$ at $t = t_6$. Since the

starting point A_2' lies in the line $\dot{x} = y = 0$, the trajectory P_2' grazes $\boldsymbol{M}_2$ at A_2'. There exists a point $F(0,f,0)$ ($f<0$) such that the trajectory starting from F passes through the point $G(0,g,0)$ ($g>0$) and hits A_2' as shown in Fig. 5.8.

4) $\boldsymbol{P}_3$ is a trajectory on $\boldsymbol{V}_3$ that starts from A_3 $(0,0,-1)\in\boldsymbol{M}_4$ at $t = 0$, intersects B_3 $(1,b_3,1)$ $\in\{(x,y,-1)\,|\,x=-1,\ y<0\}\in\boldsymbol{V}_3$ at $t = t_7$ and hits C_3 $(0,c_3,1)\in\boldsymbol{M}_4$ at $t = t_8$. Note that the trajectory $\boldsymbol{P}_3$ grazes $\boldsymbol{M}_4$ at A_3 since the starting point A_3 lies in the line $\dot{x} = y = 0$.

Now, define a special region of trajectories, based on the four grazing trajectories and the four boundaries of the three subspaces, by:

$$\boldsymbol{\Phi} = \boldsymbol{D}_1 \cup \boldsymbol{D}_2 \cup \boldsymbol{D}_3$$

where $\boldsymbol{D}_1$: a region on $\boldsymbol{V}_1$ surrounded by $\boldsymbol{P}_1$ and $\boldsymbol{M}_1$;

$\boldsymbol{D}_2$: a region on $\boldsymbol{V}_2$ surrounded by $\boldsymbol{P}_2$, $\boldsymbol{P}_2'$, $\boldsymbol{M}_2$ and $\boldsymbol{M}_3$;

$\boldsymbol{D}_3$: a region on $\boldsymbol{V}_3$ surrounded by $\boldsymbol{P}_3$ and $\boldsymbol{M}_4$.

It is noted that the parameters b_1, b_2, b_3, c_1, c_2, c_3, e, f, g can be regarded as functions of system parameter α, and can be exactly calculated by using the exact solution (3.4) and arriving time t_i. Especially note that, B_1 and B_3, C_1 and C_3, B_2 and B_2', C_2 and C_2' are symmetrical. Therefore, $b_3 = -b_1$, $c_3 = -c_1$, $b_2' = -b_2$, $c_2' = -c_2$, $e = -g$.

Lemma 5.1: $\boldsymbol{\Phi}$ is an invariant set and has a non-ordinary attractor if the parameter α of system (5.1) satisfy:

$$\begin{cases} c_1(\alpha) \geq b_2'(\alpha) \\ b_1(\alpha) \geq c_2(\alpha) \end{cases} \tag{5.2}$$

Proof: Suppose that condition (5.2) holds. Consider a trajectory starting from a point in $\boldsymbol{V}_1$. After a long enough time, it will reach the boundary $\boldsymbol{M}_1$ of $\boldsymbol{V}_1$. According to the switching rule, it jumps onto a segment $\{(0,\ y,\ 0)\,|\,c_1 \leq y \leq 0\}\in\boldsymbol{V}_2$. Since $c_1(\alpha) \geq b_2'(\alpha)$, the jumping point is in $\boldsymbol{D}_2$. After a long enough time, it will reach boundary $\boldsymbol{M}_2$ or $\boldsymbol{M}_3$ of $\boldsymbol{V}_2$. If it reaches $\boldsymbol{M}_2$, from the switching rule, it jumps onto a segment $\{(1,\ y,\ 1)\,|\,0 \leq y \leq b_1\}\in\boldsymbol{V}_1$. Since $b_1(\alpha)\geq c_2(\alpha)$, the jumping point is in $\boldsymbol{D}_1$. If the trajectory reaches $\boldsymbol{M}_3$, it jumps onto $\boldsymbol{V}_3$ from $c_2'(\alpha) = -c_2(\alpha) \geq -b_1(\alpha) = -b_3(\alpha)$.

Similarly, for a trajectory starting from a point in V_3, it will reach the boundary M_4 of V_3, and then jump onto V_2. Therefore, the trajectory starting from a point in Φ remains in Φ forever; that is, Φ is an invariant set.

It is clear that the three equilibrium points (1, 0, 1), (0, 0, 0), (−1, 0, −1) of Φ are unstable. The trajectory in regions D_1, D_2, D_3 are expanding at an exponential rate $e^{\alpha t}$. Moreover, the trajectory can not stay within any one subset D_i (i =1, 2, 3) forever. Thus, there is no stable equilibrium point or stable limit cycle in region Φ. Hence, there exists a non-ordinary attractor in Φ. The proof is thus completed.

5.3.2 3×3-Grid Scroll Chaotic Attractors via Second-Order Systems

Rewrite the 2D n×m-grid scroll chaotic attractor generation equations (4.9) as:

$$\begin{cases} \dot{x} = y - v \\ \dot{y} = -ax + by + au - bv \\ u = h(x, p_1, q_1) \\ v = h(y, p_2, q_2) \end{cases} \tag{5.3}$$

If p_1=q_1=1, p_2=q_2=1, and a=1, b=0.125, then system (5.3) has a 3×3-grid scroll chaotic attractor as shown in Fig. 5.9, which has nine equilibrium points, located in nine subspaces:

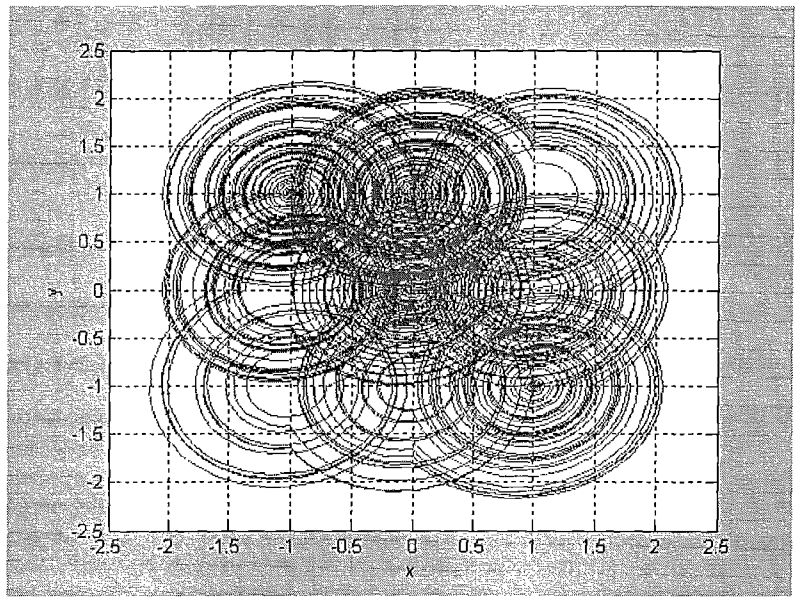

Fig. 5.9 Trajectory of a 3×3-grid scroll of second-order systems case.

$(1, 1, 1, 1) \in V_1 = \{(x, y, u, v) \mid x>0, y>0, u=1, v=1\}$;

$(0, 1, 0, 1) \in V_2 = \{(x, y, u, v) \mid -1<x<1, y>0, u=0, v=1\}$;

$(-1, 1, -1, 1)\in V_3=\{(x, y, u, v) \mid x<0, y>0, u=-1, v=1\}$;

$(1, 0, 1, 0)\in V_4=\{(x, y, u, v) \mid x>0, -1<y<1, u=1, v=0\}$;

$(0, 0, 0, 0)\in V_5=\{(x, y, u, v) \mid -1<x<1, -1<y<1, u=0, v=0\}$;

$(-1, 0, -1, 0)\in V_6=\{(x, y, u, v) \mid x<0, -1<y<1, u=-1, v=0\}$;

$(1, -1, 1, -1)\in V_7=\{(x, y, u, v) \mid x>0, y<0, u=1, v=-1\}$;

$(0, -1, 0, -1)\in V_8=\{(x, y, u, v) \mid -1<x<1, y<0, u=0, v=-1\}$;

$(-1,-1, -1,-1)\in V_9=\{(x, y, u, v) \mid x<0, y<0, u=-1, v=-1\}$.

One can get the exact solution (3.4) on each subspace of hysteresis system (5.3). Now, define boundaries for the nine subspaces $V_i (1\le i\le 9)$:

V_1: $M_1\equiv\{(0, y, 1, 1) \mid y\ge 0\}$, $N_1\equiv\{(x, 0, 1, 1) \mid x\ge 0\}$;

V_2: $M_2\equiv\{(1, y, 0, 1) \mid y\ge 0\}$, $N_2\equiv\{(-1, y, 0, 1) \mid y\ge 0\}$,

$P_2\equiv\{(x, 0, 0, 1) \mid -1\le x\le 1\}$;

V_3: $M_3\equiv\{(0, y, -1, 1) \mid y\ge 0\}$, $N_3\equiv\{(x, 0, -1, 1) \mid x\le 0\}$;

V_4: $M_4\equiv\{(0, y, 1, 0) \mid -1\le y\le 1\}$, $N_4\equiv\{(x, 1, 1, 0) \mid x\ge 0\}$,

$P_4\equiv\{(x, -1, 1, 0) \mid x\ge 0\}$;

V_5: $M_5\equiv\{(1, y, 0, 0) \mid -1\le y\le 1\}$, $N_5\equiv\{(-1, y, 0, 0) \mid -1\le y\le 1\}$,

$P_5\equiv\{(x, 1, 0, 0) \mid -1\le x\le 1\}$, $Q_5\equiv\{(x, -1, 0, 0) \mid -1\le x\le 1\}$;

V_6: $M_6\equiv\{(0, y, -1, 0) \mid -1\le y\le 1\}$, $N_6\equiv\{(x, 1, -1, 0) \mid x\le 0\}$,

$P_6\equiv\{(x, -1, -1, 0) \mid x\le 0\}$;

V_7: $M_7\equiv\{(0, y, 1, -1) \mid y\le 0\}$, $N_7\equiv\{(x, 0, 1, -1) \mid x\ge 0\}$,

V_8: $M_8\equiv\{(1, y, 0, -1) \mid y\le 0\}$, $N_8\equiv\{(-1, y, 0, -1) \mid y\le 0\}$;

$P_8\equiv\{(x, 0, 0, -1) \mid -1\le x\le 1\}$;

V_9: $M_9\equiv\{(0, y, -1, -1) \mid y\le 0\}$, $N_9\equiv\{(x, 0, -1,-1) \mid x\le 0\}$.

The switching rules are described by:

V_1: $\theta(t^+)=(0, y, 0, 1)\in V_2$ if $\theta(t)\in M_1$, $\theta(t^+)=(x, 0, 1, 0))\in V_3$ if $\theta(t)\in N_1$;

V_2: $\theta(t^+)=(1, y, 1, 1)\in V_1$ if $\theta(t)\in M_2$, $\theta(t^+)=(-1, y, -1, 1))\in V_3$ if $\theta(t)\in N_2$,

$\theta(t^+)=(x, 0, 0, 0)\in V_5$ if $\theta(t)\in \boldsymbol{P}_2$;

V_3: $\theta(t^+)=(0, y, 0, 1)\in V_2$ if $\theta(t)\in \boldsymbol{M}_3$, $\theta(t^+)=(x, 0, -1, 0))\in V_6$ if $\theta(t)\in \boldsymbol{N}_3$;

V_4: $\theta(t^+)=(0, y, 0, 0)\in V_5$ if $\theta(t)\in \boldsymbol{M}_4$, $\theta(t^+)=(x, 1, 1, 1))\in V_1$ if $\theta(t)\in \boldsymbol{N}_4$,

$\theta(t^+)=(x, -1, 1, -1)\in V_7$ if $\theta(t)\in \boldsymbol{P}_4$;

V_5: $\theta(t^+)=(1, y, 1, 0)\in V_4$ if $\theta(t)\in \boldsymbol{M}_5$, $\theta(t^+)=(-1, y, -1, 0)\in V_6$ if $\theta(t)\in \boldsymbol{N}_5$,

$\theta(t^+)=(x, 1, 0, 1)\in V_2$ if $\theta(t)\in \boldsymbol{P}_5$, $\theta(t^+)=(x, -1, 0, -1)\in V_8$ if $\theta(t)\in \boldsymbol{Q}_5$;

V_6: $\theta(t^+)=(0, y, 0, 0)\in V_5$ if $\theta(t)\in \boldsymbol{M}_6$, $\theta(t^+)=(x, 1, -1, 1)\in V_3$ if $\theta(t)\in \boldsymbol{N}_6$,

$\theta(t^+)=(x, -1, -1, -1)\in V_9$ if $\theta(t)\in \boldsymbol{P}_6$;

V_7: $\theta(t^+)=(0, y, 0, -1)\in V_8$ if $\theta(t)\in \boldsymbol{M}_7$, $\theta(t^+)=(x, 0, 1, 0)\in V_4$ if $\theta(t)\in \boldsymbol{N}_7$;

V_8: $\theta(t^+)=(1, y, 1, -1)\in V_7$ if $\theta(t)\in \boldsymbol{M}_8$, $\theta(t^+)=(-1, y, -1, -1)\in V_9$ if $\theta(t)\in \boldsymbol{N}_8$,

$\theta(t^+)=(x, 0, 0, 0)\in V_5$ if $\theta(t)\in \boldsymbol{P}_8$;

V_9: $\theta(t^+)=(0, y, 0, -1)\in V_8$ if $\theta(t)\in \boldsymbol{M}_9$, $\theta(t^+)=(x, 0, -1, 0)\in V_6$ if $\theta(t)\in \boldsymbol{N}_9$.

where $\theta=(x, y, u, v)$.

In the following, consider eight special trajectories as shown in Fig. 5.10.

1) $\overrightarrow{A_1B_1C_1}$ is a trajectory on V_1 that starts from $A_1(0,1,1,1)\in \boldsymbol{M}_1$ at $t = 0$, intersects $B_1(1,b_1,1,1) \in \{(1,y,1,1)| y > 0\}$ at $t = t_1$ and reaches $C_1(0,c_1,1,1)\in \boldsymbol{N}_1$ at $t = t_2$.
2) $\overrightarrow{A_2B_2C_2}$ is a trajectory on V_2 that starts from $A_2(-1,0,0,1)\in \boldsymbol{N}_2$ at $t = 0$, intersects $B_2(0,b_2,0,1)\in \{(0,y,0,1)| y >0\}$ at $t = t_3$ and reaches $C_2(1,c_2,0,1) \in \boldsymbol{M}_2$ at $t = t_4$.
3) $\overrightarrow{A_3B_3C_3}$ is a trajectory on V_3 that starts from $A_3(-1,0,-1,1) \in \boldsymbol{N}_3$ at $t = 0$, intersects $B_3(b_3,1,-1,1)\in \{(x,1,-1,1)| x<0\}$ at $t = t_5$ and reaches $C_3(0,c_3,-1,1)\in \boldsymbol{M}_3$ at $t = t_6$.
4) $\overrightarrow{A_4B_4C_4}$ is a trajectory on V_4 that starts from $A_4(1,1,1,0)\in \boldsymbol{N}_4$ at $t = 0$, intersects $B_4(b_4,0,1,0)\in \{(x,0,1,0)| x>0\}$ at $t = t_7$ and reaches $C_4(c_4,-1,1,0)\in \boldsymbol{P}_4$ at $t = t_8$.
5) $\overrightarrow{A_6B_6C_6}$ and $\overrightarrow{A_4B_4C_4}$, $\overrightarrow{A_7B_7C_7}$ and $\overrightarrow{A_3B_3C_3}$, $\overrightarrow{A_8B_8C_8}$ and $\overrightarrow{A_2B_2C_2}$, $\overrightarrow{A_9B_9C_9}$ and $\overrightarrow{A_1B_1C_1}$ are symmetrical.

Note that the parameters b_i, c_i ($1 \le i \le 4$) can be regarded as functions of a, b, and can be calculated exactly by using the solution (3.4) and the arriving time t_i.

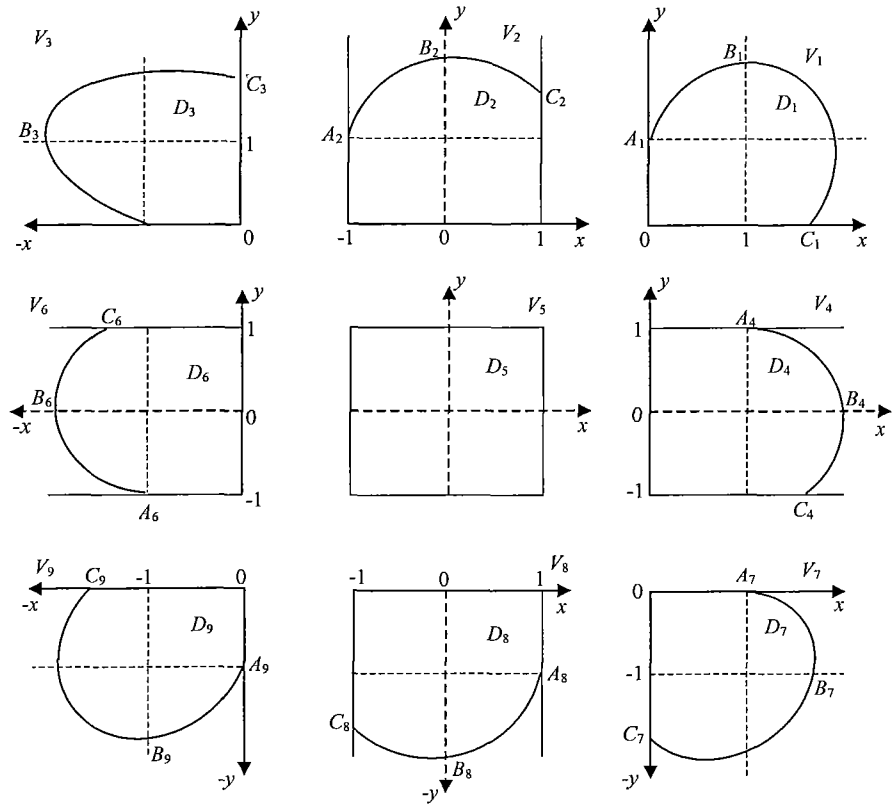

Fig. 5.10 Trajectories distribution of 3×3-scroll of second-order systems case.

Next, define a special region of trajectories, based on the 8 trajectories and the 24 boundaries of nine subspaces, by:

$$\Phi = \bigcup_{i=1}^{9} \boldsymbol{D}_i$$

where $\boldsymbol{D}_1$: a region on V_1 surrounded by $\overrightarrow{A_1B_1C_1}$, $\boldsymbol{M}_1$ and $\boldsymbol{N}_1$;

$\boldsymbol{D}_2$: a region on V_2 surrounded by $\overrightarrow{A_2B_2C_2}$, $\boldsymbol{M}_2$, $\boldsymbol{N}_2$ and $\boldsymbol{P}_2$;

$\boldsymbol{D}_3$: a region on V_3 surrounded by $\overrightarrow{A_3B_3C_3}$, $\boldsymbol{M}_3$ and $\boldsymbol{N}_3$;

$\boldsymbol{D}_4$: a region on V_4 surrounded by $\overrightarrow{A_4B_4C_4}$, $\boldsymbol{M}_4$, $\boldsymbol{N}_4$ and $\boldsymbol{P}_4$;

$\boldsymbol{D}_5$: a region on V_5 surrounded by $\boldsymbol{M}_5$, $\boldsymbol{N}_5$, $\boldsymbol{P}_5$ and $\boldsymbol{Q}_5$;

$\boldsymbol{D}_6$: a region on V_6 surrounded by $\overrightarrow{A_6B_6C_6}$, $\boldsymbol{M}_6$, $\boldsymbol{N}_6$ and $\boldsymbol{P}_6$;

$\boldsymbol{D}_7$: a region on V_7 surrounded by $\overrightarrow{A_7B_7C_7}$, $\boldsymbol{M}_7$ and $\boldsymbol{N}_7$;

$\boldsymbol{D}_8$: a region on $\boldsymbol{V}_8$ surrounded by $\overrightarrow{A_8B_8C_8}$, $\boldsymbol{M}_8$, $\boldsymbol{N}_8$ and $\boldsymbol{P}_8$;

$\boldsymbol{D}_9$: a region on $\boldsymbol{V}_9$ surrounded by $\overrightarrow{A_9B_9C_9}$, $\boldsymbol{M}_9$ and $\boldsymbol{N}_9$.

Lemma 5.2: Φ is an invariant set and has a non-ordinary attractor if the parameters a, b of system (5.3) satisfy:

$$\begin{cases} b_1(a,b) \geq c_2(a,b) \\ b_2(a,b) \geq c_3(a,b) \\ b_3(a,b) \leq c_4(a,b) \\ b_4(a,b) \geq c_1(a,b) \end{cases} \tag{5.4}$$

Since the proof of Lemma 5.2 is similar to that of Lemma 5.1, it is omitted here. Similarly, one can derive a condition for chaos generation with an $n \times m$-grid (n, m>3) scroll chaotic attractor for system (5.3).

5.3.3 3-Scroll Chaotic Attractors Via Third-Order Systems

Rewrite the 1D n-scroll chaotic attractors generation equations (4.11) as:

$$\begin{cases} \dot{x} = y \\ \dot{y} = z \\ \dot{z} = -ax - by - cz + au \\ u = h(x, p, q) \end{cases} \tag{5.5}$$

If p=q=1, and a=0.8, b=0.72, c=0.5, then system (5.5) has a 3-scroll chaotic attractor located on three subspaces, as shown in Fig. 5.11. On each subspace $\boldsymbol{W}_i$ ($-1 \leq i \leq 1$), the solutions are given:

$$\begin{cases} \boldsymbol{X}(t) = A_1 e^{\lambda t} + e^{\alpha t}(A_2 \cos(\beta t) + A_3 \sin(\beta t)] \\ \boldsymbol{Y}(t) = A_1 \lambda e^{\lambda t} + e^{\alpha t}[(A_2\alpha + A_3\beta)\cos(\beta t) + (A_3\alpha - A_2\beta)\sin(\beta t)] \\ \boldsymbol{Z}(t) = A_1 \lambda^2 e^{\lambda t} + e^{\alpha t}[(A_2\alpha^2 + 2A_3\alpha\beta - A_2\beta^2)\cos(\beta t) + (A_3\alpha^2 - 2A_2\alpha\beta - A_3\beta^2)\sin(\beta t)] \end{cases} \tag{5.6}$$

where $\boldsymbol{X}(0)$, $\boldsymbol{Y}(0)$ and $\boldsymbol{Z}(0)$ are the initial conditions;

$\overline{\boldsymbol{X}} = (x-1, y, z, u)^T$ for $\overline{\boldsymbol{X}} \in \boldsymbol{W}_1$;

$\overline{\boldsymbol{X}} = (x, y, z, u)^T$ for $\overline{\boldsymbol{X}} \in \boldsymbol{W}_0$;

$\overline{\boldsymbol{X}} = (x+1, y, z, u)^T$ for $\overline{\boldsymbol{X}} \in \boldsymbol{W}_{-1}$.

λ=λ_1, α and β are given by Eq. (4.14), and

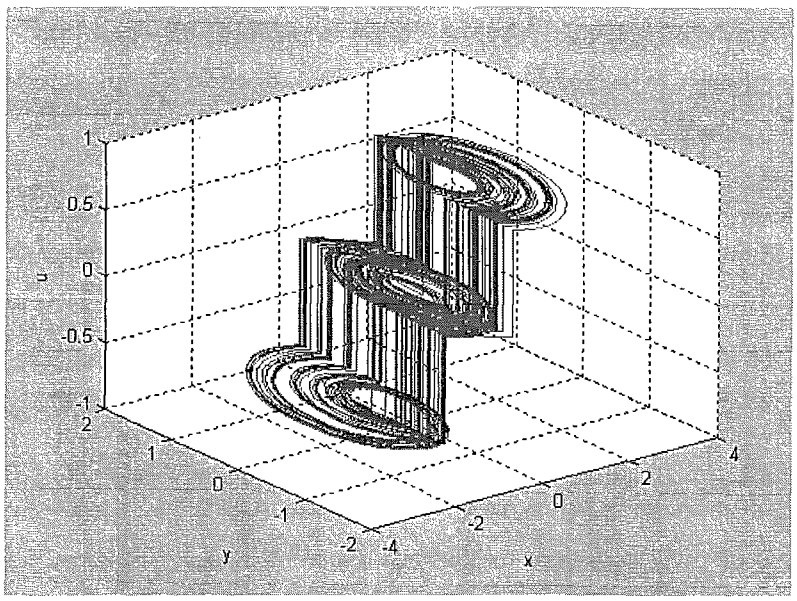

Fig. 5.11 Trajectory of a 3-scroll chaotic attractor of third-order systems case.

$$\begin{cases} A_1 = \dfrac{(\alpha^2+\beta^2)X(0)-2\alpha Y(0)+Z(0)}{(\lambda-\alpha)^2+\beta^2} \\ A_2 = \dfrac{(\lambda^2-2\alpha\lambda)X(0)+2\alpha Y(0)-Z(0)}{(\lambda-\alpha)^2+\beta^2} \\ A_3 = \dfrac{(\lambda\alpha^2-\lambda\beta^2-\lambda^2\alpha)X(0)-(\beta^2-\alpha^2+\lambda^2)Y(0)+(\alpha-\lambda)Z(0)}{\beta[(\lambda-\alpha)^2+\beta^2]} \end{cases}$$

Denote

$$\begin{pmatrix} \boldsymbol{X} \\ \boldsymbol{Y} \\ \boldsymbol{Z} \end{pmatrix} = \begin{pmatrix} g_1(t) \\ g_2(t) \\ g_3(t) \end{pmatrix} \begin{pmatrix} \boldsymbol{X}_0 \\ \boldsymbol{Y}_0 \\ \boldsymbol{Z}_0 \end{pmatrix}$$

Obviously, system (4.11) has four hysteresis switching planes:

$$\boldsymbol{M}_1 \equiv \{(x, y, z, u) \mid x=0\} \cap \boldsymbol{W}_1;$$

$$\boldsymbol{M}_2 \equiv \{(x, y, z, u) \mid x=1\} \cap \boldsymbol{W}_0;$$

$$\boldsymbol{M}_3 \equiv \{(x, y, z, u) \mid x=-1\} \cap \boldsymbol{W}_0;$$

$$\boldsymbol{M}_4 \equiv \{(x, y, z, u) \mid x=0\} \cap \boldsymbol{W}_{-1}.$$

and the corresponding switching rules are:

$$\overline{X}(t^+) = (0, y, z, 0) \subset \boldsymbol{W}_0 \quad \text{if} \quad \overline{X}(t) = (0, y, z, 1) \subset \boldsymbol{M}_1;$$

$$\overline{X}(t^+) = (1, y, z, 1) \subset \boldsymbol{W}_1 \quad \text{if} \quad \overline{X}(t) = (1, y, z, 0) \subset \boldsymbol{M}_2;$$

$$\overline{X}(t^+) = (-1, y, z, -1) \subset W_{-1} \text{ if } \overline{X}(t) = (-1, y, z, 0) \subset M_3;$$

$$\overline{X}(t^+) = (0, y, z, 0) \subset W_0 \text{ if } \overline{X}(t) = (0, y, z, -1) \subset M_4.$$

Now, define four specially grazing surfaces as shown in Fig. 5.12.

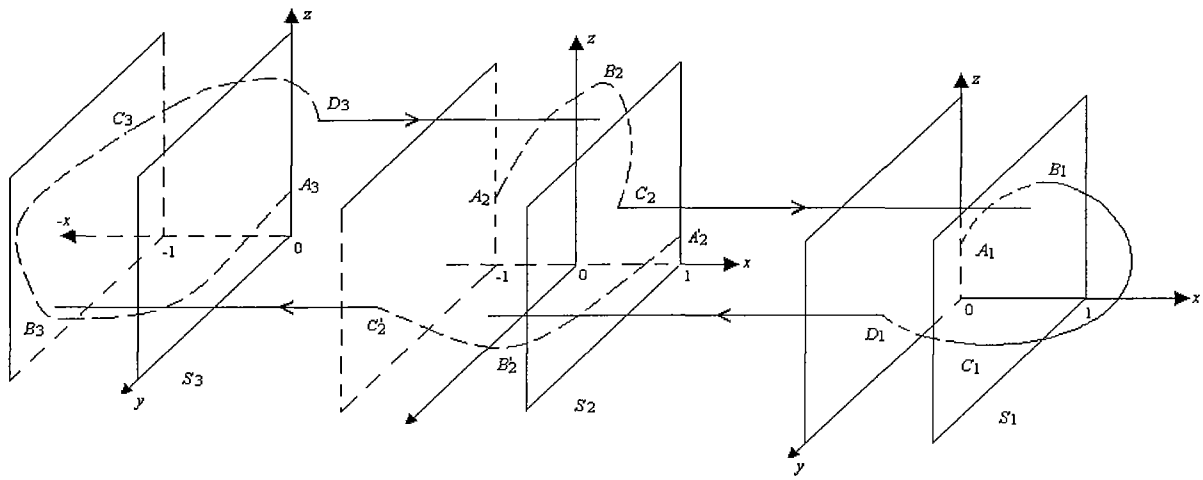

Fig. 5.12 Trajectories switching of 3-scroll of third-order systems case.

1) $\overrightarrow{A_1B_1C_1D_1}$ is a trajectory in W_1 that starts from A_1 $(0,0,a_1,1) \in M_1$ at $t = 0$, intersects $B_1(1, b_1, \bar{b}_1, 1) \in \{\overline{X} | x = 1, y < 0\} \in W_1$ at $t = t_1$ and reaches C_1 $(0, c_1, \bar{c}_1, 1) \in \overline{X}\{(x, y, z, u) | x = 1, y > 0\} \in W_1$ at $t = t_2$, and finally reaches D_1 $(0, d_1, \bar{d}_1, 1) \in M_1$ at $t = t_3$. Since the starting point A_1 lies in the line $\dot{x} = y = 0$, the trajectory $\overrightarrow{A_1B_1C_1D_1}$ grazes M_1 at A_1. Denote $S_1 = \{\overrightarrow{A_1B_1C_1D_1} \mid a_1 \in R\}$. Obviously, surface S_1 grazes the switching plane M_1 at z-axis.

2) $\overrightarrow{A_2B_2C_2}$ is a trajectory in W_0 that starts from A_2 $(-1,0,a_2,0) \in M_3$ at $t = 0$, intersects $B_2(0,b_2,\bar{b}_2,0) \in \{\overline{X} | x = 0, y < 0\} \in W_0$ at $t = t_4$ and reaches C_2 $(1,c_2,\bar{c}_2,0) \in M_2$ at $t = t_5$. The trajectory $\overrightarrow{A_2B_2C_2}$ grazes M_3 at A_2 since the starting point A_2 lies in the line $\dot{x} = y = 0$. Denote $S_2 = \{\overrightarrow{A_2B_2C_2} \mid a_2 \in R\}$. Clearly, surface S_2 grazes the switching plane M_3 at the line $M_3 \cap \{y=0\}$.

3) $\overrightarrow{A'_2B'_2C'_2}$ is a trajectory in W_0 that starts from $A'_2(1, 0, a'_2, 0) \in M_2$ at $t = 0$, intersects $B'_2(0, b'_2, \overline{b'_2}, 0) \in \{\overline{X} | x = 0, y > 0\} \in W_0$ at $t = t_6$ and reaches C'_2 $(-1, c'_2, \overline{c'_2}, 0) \in M_3$ at

$t = t_7$. The trajectory $\overrightarrow{A_2'B_2'C_2'}$ grazes $\boldsymbol{M}_2$ at A_2' since the starting point A_2' lies in the line $\dot{x} = y = 0$. Denote $\boldsymbol{S}_2' = \{\overrightarrow{A_2'B_2'C_2'} \mid a_2' \in R\}$. Obviously, surface $\boldsymbol{S}_2'$ grazes the switching plane $\boldsymbol{M}_2$ at line $\boldsymbol{M}_2 \cap \{y=0\}$.

4) $\overrightarrow{A_3B_3C_3D_3}$ is a trajectory in $\boldsymbol{W}_{-1}$ that starts from A_3 $(0,0,a_3,-1) \in \boldsymbol{M}_4$ at $t = 0$, intersects B_3 $(-1,b_3,\bar{b}_3,-1) \in \{\overline{X} \mid x=-1, y>0\} \in \boldsymbol{W}_{-1}$ at $t = t_8$ and reaches $C_3(-1,c_3,\bar{c}_3,-1) \in \{\overline{X} \mid x=-1, y<0\} \in \boldsymbol{W}_{-1}$ at $t = t_9$, and finally reaches $\boldsymbol{D}_3$ $(0,d_3,\bar{d}_3,-1) \in \boldsymbol{M}_3$ at $t = t_{10}$. Since the starting point A_3 lies in the line $\dot{x} = y = 0$, the trajectory $\overrightarrow{A_3B_3C_3D_3}$ grazes $\boldsymbol{M}_3$ at A_3. Denote $\boldsymbol{S}_3 = \{\overrightarrow{A_3B_3C_3D_3} \mid a_3 \in R\}$. Obviously, surface $\boldsymbol{S}_3$ grazes the switching plane $\boldsymbol{M}_3$ at z-axis.

Based on the above four grazing surfaces and four switching planes, define a special region of trajectories, by:

$$\Phi = \Phi_1 \cup \Phi_2 \cup \Phi_3$$

where Φ_1 : a region on $\boldsymbol{W}_1$ surrounded by $\boldsymbol{S}_1$ and $\boldsymbol{M}_1$;

Φ_2: a region on $\boldsymbol{W}_0$ surrounded by $\boldsymbol{S}_2$, $\boldsymbol{S}_2'$, $\boldsymbol{M}_2$ and $\boldsymbol{M}_3$;

Φ_3: a region on $\boldsymbol{W}_{-1}$ surrounded by $\boldsymbol{S}_3$ and $\boldsymbol{M}_4$.

It is noted that the parameters b_i, b_i', c_i, c_i', d_i, d_i' $(1 \le i \le 3)$ and b_2', $\bar{b}_2'$, c_2', $\bar{c}_2'$ can be regarded as functions of a, b, c for the given initial points A_1, A_2, A_2', A_3, and can be exactly calculated by using the exact solution (5.6) and the arriving time t_i $(1 \le i \le 10)$. Moreover, B_1 and B_3, C_1 and C_3, D_1 and D_3, B_2 and B_2', C_2 and C_2' are symmetric. Denote

$$\boldsymbol{P}_1 = \{(b_1,\bar{b}_1) \mid a_1 \in R\},\ \boldsymbol{N}_1 = \{(c_1,\bar{c}_1) \mid a_1 \in R\};$$

$$\boldsymbol{P}_2 = \{(b_2,\bar{b}_2) \mid a_2 \in R\},\ \boldsymbol{N}_2 = \{(b_2',\bar{b}_2) \mid a_2' \in R\};$$

$$\boldsymbol{P}_3 = \{(b_3,\bar{b}_3) \mid a_3 \in R\},\ \boldsymbol{N}_3 = \{(c_3,\bar{c}_3) \mid a_3 \in R\}.$$

and

$\boldsymbol{T}_1$: a region on $\boldsymbol{W}_1 \cap \{x=1\}$ surrounded by $\boldsymbol{P}_1$ and $\boldsymbol{N}_1$;

$\boldsymbol{T}_2$: a region on $\boldsymbol{W}_0 \cap \{x=0\}$ surrounded by $\boldsymbol{P}_2$, and $\boldsymbol{N}_2$;

$\boldsymbol{T}_3$: a region on $\boldsymbol{W}_{-1} \cap \{x=-1\}$ surrounded by $\boldsymbol{P}_3$ and $\boldsymbol{N}_3$.

It can be seen that the regions $\boldsymbol{T}_1$ and $\boldsymbol{T}_3$ are symmetrical. According to the switching rules and the exact analytic solution (5.6), one has the following conclusions: $\boldsymbol{\Phi}$ is an invariant set if the parameters a, b, c of system (4.11) satisfy:

$$[0, d_1(a,b,c,a_1), \bar{d}_1(a,b,c,a_1), 0] \in \boldsymbol{T}_2$$

and

$$[1, c_2(a,b,c,a_2), \bar{c}_2(a,b,c,a_2), 1] \in \boldsymbol{T}_1$$

where $a_1 \in R$ and $a_2 \in R$. In fact, all trajectories started from any point in $\boldsymbol{\Phi}$ will remain in $\boldsymbol{\Phi}$ as shown in Fig. 5.11. That is, $\boldsymbol{\Phi}$ is an invariant set. Although the switching rules are very simple, the generated trajectories are rather complex.

In the following, a two-dimensional Poincaré return map is rigorously derived for verifying the chaotic behaviours of 3-scroll chaotic attractors shown in Figure 5.5.

Consider a trajectory starting from the point $(0, y_0, z_0, 0) \in \boldsymbol{W}_0$ at $t = 0$. According to the solution (5.6), if there are no switchings in the boundaries $\boldsymbol{M}_2$ and $\boldsymbol{M}_3$, the trajectory must reach $\boldsymbol{M}_2$ and $\boldsymbol{M}_3$ at the positive time t_a and t_b separately. Here t_a and t_b are the first arriving times. Let $(1, y_1, z_1, 0) \in \boldsymbol{M}_2$ be the hit point, then one can calculate the arriving time t_a, y_1 and z_1 by using the exact solution (5.6). Similarly, for the hit point $(1, y_1', z_1', 0) \in \boldsymbol{M}_3$, one can calculate the arriving time t_b, y_1' and z_1'. In the following, first define a region by:

$$\boldsymbol{H}_0 = \left\{(0, y, z, 0) \in \boldsymbol{W}_0 \middle| \, t_a < t_b \right\} \tag{5.7}$$

Also, consider a trajectory starting from the point $(1, y_0, z_0, 1) \in \boldsymbol{W}_1$ at $t = 0$. Due to (5.6), it must reach $\boldsymbol{M}_1$ at some positive time t_c. Let $(1, \bar{y}_1, \bar{z}_1, 0) \in \boldsymbol{M}_1$ be the hit point, then one can calculate the arriving time t_c, $\bar{y}_1$ and $\bar{z}_1$ by using the exact solution (5.6). Thus, the following region is defined:

$$\boldsymbol{H}_1 = \left\{(1, y, z, 1) \in \boldsymbol{W}_1 \middle| \, (0, \bar{y}_1, \bar{z}_1, 0) \in \boldsymbol{H}_0 \right\} \tag{5.8}$$

Now consider the vector field in $\boldsymbol{W}_1$. Let E^r be the eigenspace corresponding to the real eigenvalue λ and let E^c be the eigenspace corresponding to the complex eigenvalues $\alpha \pm \beta i$. They are described by:

$$\begin{aligned} E^r &= \left\{(x, y, z) \middle| \lambda^2 (x-1) = \lambda y = z, x > 0 \right\} \\ E^c &= \left\{(x, y, z) \middle| (\alpha^2 + \beta^2)(x-1) - 2\alpha y + z = 0, x > 0 \right\} \end{aligned} \tag{5.9}$$

Denote $\Omega_1=W_1\cap\{x=1\}$, $\Omega_2=W_0\cap\{x=0\}$, $\Omega_3=W_{-1}\cap\{x=-1\}$. Consider a trajectory starting from an initial point $(1, y_0, z_0, 1)\in H_1$ At $t=0$, according to (5.6), it must reach the switching plane M_1 at some positive time t_1 as shown in Figure 5.13. In fact, since $\lambda<0$, the trajectory will tend to eigenspace E^c and spirally diverge at the eigenspace E^r with a positive exponential rate $e^{\alpha t}$. Let $(0, y_1, z_1, 1)$ be the hit point. From the switching rule and Eq. (5.8), the trajectory jumps onto $H_0\subset\Omega_2$ holding y_1, z_1 constant. That is, the hit point is $(0, y_1, z_1, 0)\in H_0$. Thus, according to Eqs. (5.7) and (5.8), the trajectory must reach the switching plane M_2 at some positive time t_2 as displayed in Fig. 5.13. Let $(1, y_2, z_2, 0)$ be the hit point. From the switching rule, this trajectory jumps onto Ω_1 holding y_2, z_2 constant. Thus, the hit point is $(0, y_2, z_2, 0)\in\Omega_1$.

On the other hand, consider a trajectory starting from a point $(1, y_0, z_0, 1)\in\Omega_1-H_1$ at $t=0$. According to Eq. (5.6), it must reach the switching plane M_1 at some positive time t_1. Let $(0, y_1, z_1, 1)$ be the hit point. According to the switching rule and Eq. (5.8), this trajectory jumps onto Ω_2-H_0 holding y_1, z_1 constant. That is, the hit point is $(0, y_1, z_1, 0)\in\Omega_2-H_0$. Due to Eq. (5.7), the trajectory must reach the switching plane M_3 at some positive time t_3 as shown in Fig. 5.13. Let $(-1, y_3, z_3, 0)$ be the hit point. According to the switching rule, this trajectory jumps onto Ω_3 holding y_3, z_3 constant. Thus, the hit point is $(-1, y_3, z_3, -1)\in\Omega_3$.

Notice the symmetry of the vector field in both W_1 and W_{-1}. Then, a trajectory starting from $(-1, y_3, z_3, -1)$ in W_{-1} is symmetric to that starting from $(1, -y_3, -z_3, 1)$ on Ω_1 in W_1. Now, one can define a two-dimensional Poincaré return map:

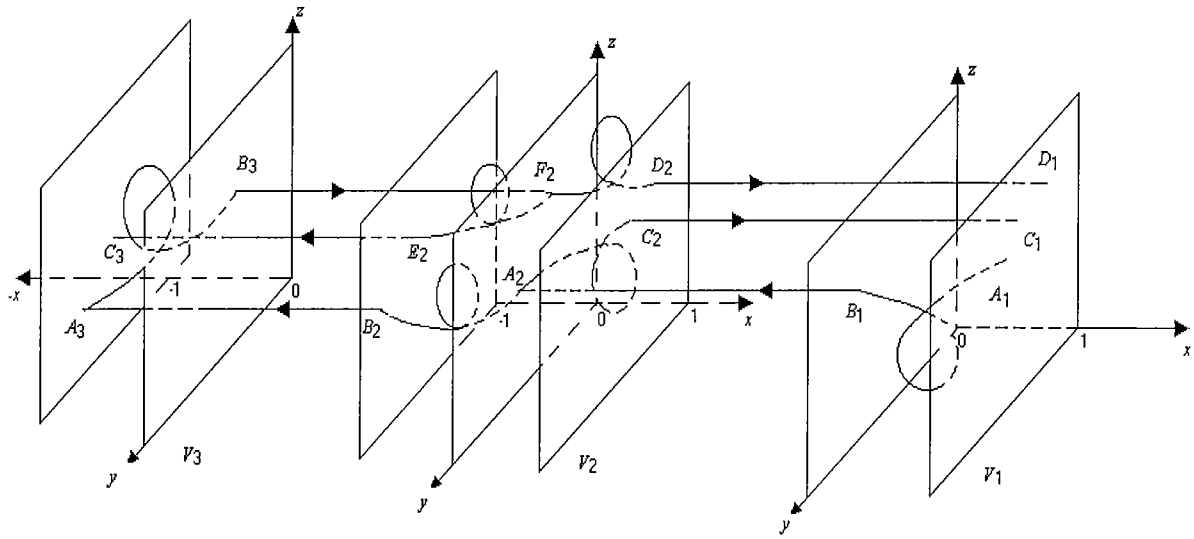

Fig. 5.13 Hysteresis phase space and Poincaré return map.

$$f:\Omega_1 \to \Omega_1,(y_0,z_0) \to \begin{cases}(y_2,z_2) & \text{for} \quad (y_0,z_0) \in \boldsymbol{H}_0 \\ (-y_3,-z_3) & \text{for} \quad (y_0,z_0) \in \Omega_1 - \boldsymbol{H}_0\end{cases} . \tag{5.10}$$

Clearly, one can formulate a rigorous mathematical description of this map by using the exact solution (5.6) as follows:

$$\begin{pmatrix}0\\ y_1\\ z_1\end{pmatrix} = \begin{pmatrix}g_1(t_1)\\ g_2(t_1)\\ g_3(t_1)\end{pmatrix}\begin{pmatrix}1\\ y_0\\ z_0\end{pmatrix} \tag{5.11-1}$$

$$\begin{pmatrix}1\\ y_2\\ z_2\end{pmatrix} = \begin{pmatrix}g_1(t_2-t_1)\\ g_2(t_2-t_1)\\ g_3(t_2-t_1)\end{pmatrix}\begin{pmatrix}0\\ y_1\\ z_1\end{pmatrix} \tag{5.11-2}$$

$$\begin{pmatrix}-1\\ y_3\\ z_3\end{pmatrix} = \begin{pmatrix}g_1(t_3-t_1)\\ g_2(t_3-t_1)\\ g_3(t_3-t_1)\end{pmatrix}\begin{pmatrix}0\\ y_1\\ z_1\end{pmatrix} \tag{5.11-3}$$

In actual calculations, one can use a numerical method, such as the Newton-Raphson method, to solve the equations. Moreover, the Jacobian matrix of this map f is described by:

$$Df = \begin{cases}\begin{pmatrix}\dfrac{\partial y_2}{\partial y_0} & \dfrac{\partial y_2}{\partial z_0}\\ \dfrac{\partial z_2}{\partial y_0} & \dfrac{\partial z_2}{\partial z_0}\end{pmatrix} & \text{for} \quad (y_0,z_0) \in \boldsymbol{H}_0 \\ -\begin{pmatrix}\dfrac{\partial y_3}{\partial y_0} & \dfrac{\partial y_3}{\partial z_0}\\ \dfrac{\partial z_3}{\partial y_0} & \dfrac{\partial z_3}{\partial z_0}\end{pmatrix} & \text{for} \quad (y_0,z_0) \in \Omega_1 - \boldsymbol{H}_0\end{cases} \tag{5.12}$$

Now, one can calculate the Lyapunov exponents λ_1 and λ_2 of the Poincaré map f. In fact, one can get the exact mathematical formulations for λ_1, λ_2 ($\lambda_1 \geq \lambda_2$) from Eqs. (5.11) and (5.12). However, the formulations are rather complex. In real calculations, one can use the numerical methods discussed in [48] to calculate λ_1, λ_2. When $0<\lambda_1<+\infty$, system (5.5) is chaotic. The maximum Lyapunov exponent of the 3-scroll chaotic attractor shown in Fig. 5.11 is $\lambda_1=0.0284>0$. Fig. 5.14 shows its Poincaré mapping at section $\dot{y}=0$.

5.3.4 3×3-Grid Scroll Chaotic Attractors via Third-Order Systems

Rewrite the 2D $n\times m$-grid scroll chaotic attractor generation equations (4.16) as:

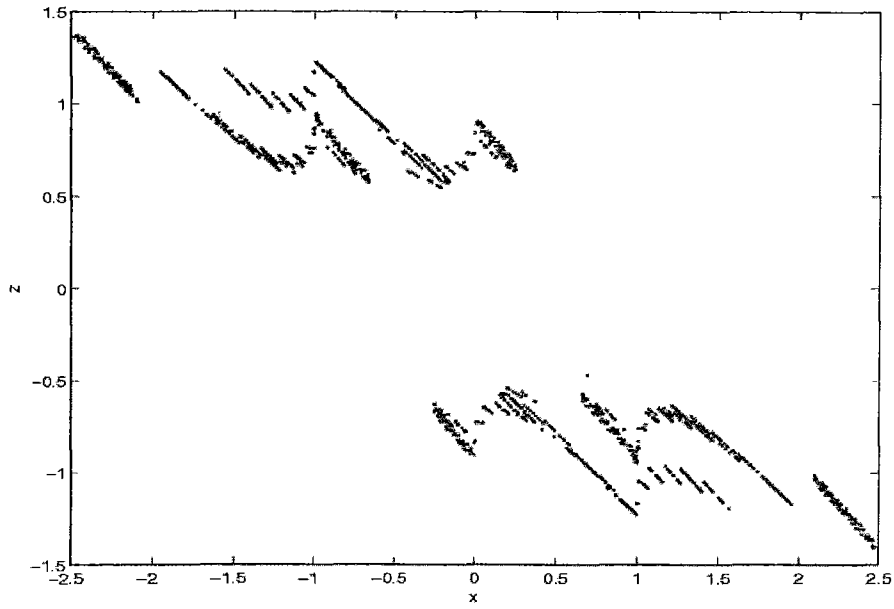

Fig. 5.14 Poincaré map at $\dot{y}=0$ of a 3-scroll attractor of third-order systems case.

$$\begin{cases} \dot{x} = y - v \\ \dot{y} = z \\ \dot{z} = -ax - by - cz + au + bv \\ u = h(x, p_1, q_1) \\ v = h(y, p_2, q_2) \end{cases} \tag{5.13}$$

This subsection briefly discusses the hysteresis switching dynamics of system (5.13). If $p_1=q_1=p_2=q_2=1$, and $a=0.8$, $b=0.72$, $c=0.5$, then system (5.13) has a 3×3-grid scroll chaotic attractor as shown in Fig. 5.15, which has nine equilibrium points, located in nine corresponding subspaces:

$$(i,j,0,\, i,j) \in \boldsymbol{W}_{(i,j)} \qquad -1 \le i,j \le 1$$

where $\boldsymbol{W}_{(i,j)}(-1 \le i,j \le 1)$ are defined by (4.17). Note that system (5.13) has a natural symmetry under the coordinates $(x, y, z) \rightarrow (-x, -y, -z)$, which persists for all values of the system parameters.

Similarly, one can find the exact solution (5.6) of the hysteresis based system (5.13), where

$$(\boldsymbol{X}, \boldsymbol{Y}, \boldsymbol{Z})^T = (x\text{-}i,\ y\text{-}j,\ z)^T \text{ for } \overline{\boldsymbol{X}} \in \boldsymbol{W}_{(i,j)}$$

in which $\overline{X} = (x, y, z, u, v)$ and $-1 \le i,j \le 1$. Define the switching planes of the nine subspaces: $\boldsymbol{W}_{(i,j)}(-1 \le i,j \le 1)$:

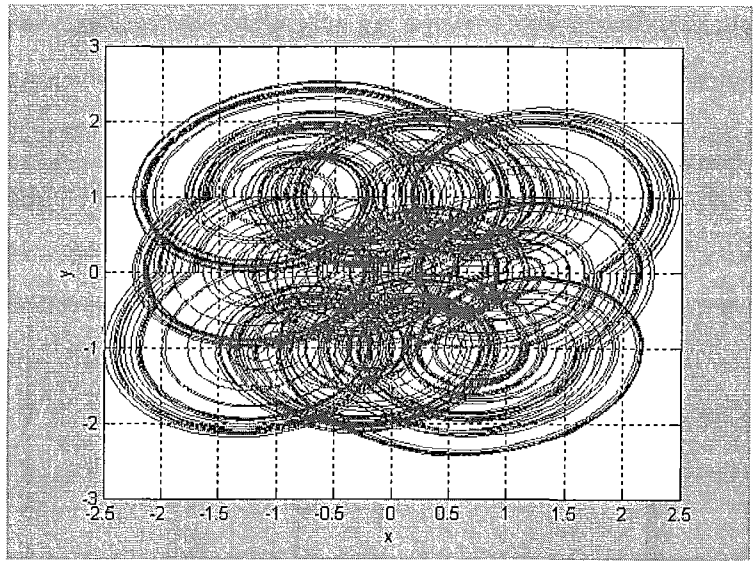

Fig. 5.15 Trajectory of a 3×3-grid scroll attractor of third-order systems case.

$W_{(1,1)}$: $M_1 \equiv \{(0, y, z, 1, 1) \mid y \geq 0\}$, $N_1 \equiv \{(x, 0, z, 1, 1) \mid x \geq 0\}$;

$W_{(0,1)}$: $M_2 \equiv \{(1, y, z, 0, 1) \mid y \geq 0\}$, $N_1 \equiv \{(-1, y, z, 0, 1) \mid y \geq 0\}$,

$P_2 \equiv \{(x, 0, z, 0, 1) \mid -1 \leq x \leq 1\}$;

$W_{(-1,1)}$: $M_3 \equiv \{(0, y, z, -1, 1) \mid y \geq 0\}$, $N_3 \equiv \{(x, 0, z, -1, 1) \mid x \leq 0\}$;

$W_{(1,0)}$: $M_4 \equiv \{(0, y, z, 1, 0) \mid -1 \leq y \leq 1\}$, $N_4 \equiv \{(x, 1, z, 1, 0) \mid x \geq 0\}$,

$P_4 \equiv \{(x, -1, z, 1, 0) \mid x \geq 0\}$;

$W_{(0,0)}$: $M_5 \equiv \{(1, y, z, 0, 0) \mid -1 \leq y \leq 1\}$, $N_5 \equiv \{(-1, y, z, 0, 0) \mid -1 \leq y \leq 1\}$,

$P_5 \equiv \{(x, 1, z, 0, 0) \mid -1 \leq x \leq 1\}$, $Q_5 \equiv \{(x, -1, z, 0, 0) \mid -1 \leq x \leq 1\}$;

$W_{(-1,1)}$: $M_6 \equiv \{(0, y, z, -1, 0) \mid -1 \leq y \leq 1\}$, $N_6 \equiv \{(x, 1, z, -1, 0) \mid x \leq 0\}$,

$P_6 \equiv \{(x, -1, z, -1, 0) \mid x \leq 0\}$;

$W_{(1,-1)}$: $M_7 \equiv \{(0, y, z, 1, -1) \mid y \leq 0\}$, $N_7 \equiv \{(x, 0, z, 1, -1) \mid x \geq 0\}$;

$W_{(0,-1)}$: $M_8 \equiv \{(1, y, z, 0, -1) \mid y \leq 0\}$, $N_8 \equiv \{(-1, y, z, 0, -1) \mid y \leq 0\}$,

$P_8 \equiv \{(x, 0, z, 0, -1) \mid -1 \leq x \leq 1\}$;

$W_{(-1,-1)}$: $M_9 \equiv \{(0, y, z, -1, -1) \mid y \leq 0\}$, $N_9 \equiv \{(x, 0, z, -1, -1) \mid x \leq 0\}$.

Thus, the switching rules are described by:

$W_{(1,1)}$: $\overline{X}(t^+) \in W_{(0,1)} \cap \{x = 0\}$ if $\overline{X}(t) \in M_1$, $\overline{X}(t^+) \in W_{(-1,1)} \cap \{y = 0\}$ if $\overline{X}(t) \in N_1$;

$W_{(0,1)}$: $\overline{X}(t^+) \in W_{(1,1)} \cap \{x = 1\}$, if $\overline{X}(t) \in M_2$, $\overline{X}(t^+) \in W_{(-1,1)} \cap \{x = -1\}$ if $\overline{X}(t) \in N_2$,

$\overline{X}(t^+) \in W_{(0,0)} \cap \{y = 0\}$, if $\overline{X}(t) \in P_2$;

$W_{(-1,1)}$: $\overline{X}(t^+) \in W_{(0,1)} \cap \{x = 0\}$ if $\overline{X}(t) \in M_3$, $\overline{X}(t^+) \in W_{(-1,0)} \cap \{y = 0\}$ if $\overline{X}(t) \in N_3$;

$W_{(1,1)}$: $\overline{X}(t^+) \in W_{(0,0)} \cap \{x = 0\}$, if $\overline{X}(t) \in M_4$, $\overline{X}(t^+) \in W_{(1,1)} \cap \{y = 1\}$ if $\overline{X}(t) \in N_4$,

$\overline{X}(t^+) \in W_{(0,-1)} \cap \{y = -1\}$, if $\overline{X}(t) \in P_4$;

$W_{(0,0)}$: $\overline{X}(t^+) \in W_{(1,0)} \cap \{x = 1\}$, if $\overline{X}(t) \in M_5$, $\overline{X}(t^+) \in W_{(-1,1)} \cap \{x = -1\}$ if $\overline{X}(t) \in N_5$,

$\overline{X}(t^+) \in \Omega_{(0,1)} \cap \{y = 1\}$, if $\overline{X}(t) \in P_5$, $\overline{X}(t^+) \in W_{(0,-1)} \cap \{y = -1\}$, if $\overline{X}(t) \in Q_5$;

$W_{(-1,0)}$: $\overline{X}(t^+) \in W_{(0,0)} \cap \{x = 0\}$, if $\overline{X}(t) \in M_6$, $\overline{X}(t^+) \in W_{(-1,1)} \cap \{y = 1\}$ if $\overline{X}(t) \in N_6$,

$\overline{X}(t^+) \in W_{(-1,-1)} \cap \{y = -1\}$, if $\overline{X}(t) \in P_6$;

$W_{(1,-1)}$: $\overline{X}(t^+) \in W_{(0,-1)} \cap \{x = 0\}$, if $\overline{X}(t) \in M_7$, $\overline{X}(t^+) \in W_{(1,0)} \cap \{y = 0\}$ if $\overline{X}(t) \in N_7$;

$W_{(0,-1)}$: $\overline{X}(t^+) \in W_{(1,-1)} \cap \{x = 1\}$, if $\overline{X}(t) \in M_8$, $\overline{X}(t^+) \in W_{(-1,-1)} \cap \{x = -1\}$ if $\overline{X}(t) \in N_8$,

$\overline{X}(t^+) \in W_{(0,0)} \cap \{y = 0\}$, if $\overline{X}(t) \in P_8$;

$W_{(-1,-1)}$: $\overline{X}(t^+) \in W_{(0,-1)} \cap \{x = 0\}$, if $\overline{X}(t) \in M_9$, $\overline{X}(t^+) \in W_{(-1,0)} \cap \{y = 0\}$ if $\overline{X}(t) \in N_9$.

where $\overline{X} = (x, y, z, u, v)$ and x, y, z are held constant during the switching.

Similarly, one can derive the conditions for chaos generation with an $n \times m$–grid scroll chaotic attractor by using a two-dimensional Poincaré return map.

5.3.5 3×3×3-Space Scroll Chaotic Attractors via Third-Order Systems

Rewrite the 3D $n \times m \times l$-space scroll chaotic attractor generation equations (4.18) as:

$$\begin{cases} \dot{x} = y - v \\ \dot{y} = z - w \\ \dot{z} = -ax - by - cz + au + bv + cw \\ u = h(x, p_1, q_1) \\ v = h(y, p_2, q_2) \\ w = h(z, p_3, q_3) \end{cases} \tag{5.14}$$

If $p_1=q_1=p_2=q_2=p_3=q_3=1$, and $a=0.8$, $b=0.72$, $c=0.6$, then system (5.14) has a 3×3×3-space scroll chaotic attractor, which has 27 equilibrium points, located in 27 corresponding subspaces:

$$(i, j, k, i, j, k) \in \boldsymbol{W}_{(i,j,k)} \text{ for } -1 \le i, j, k \le 1$$

where $\boldsymbol{W}_{(i,j,k)}$ ($-1 \le i, j, k \le 1$) are defined by (4.19). Note that system (5.14) has a natural symmetry under the coordinates $(x, y, z) \rightarrow (-x, -y, -z)$, which persists for all values of the system parameters.

It is easy to get the exact solution (5.6) of the hysteresis based system (5.14), where

$$(\boldsymbol{X}, \boldsymbol{Y}, \boldsymbol{Z})^T = (x-i,\ y-j,\ z-k)^T \text{ for } \overline{\boldsymbol{X}} \in \boldsymbol{W}_{(i,j,k)}$$

in which $\overline{\boldsymbol{X}} = (x, y, z, u, v, w)$ and $-1 \le i, j, k \le 1$.

Similarly, one can define the switching rules for system (5.14). Also, a two-dimensional Poincaré return map can be derived to prove that system (5.14) has chaotic behaviour with an $n \times m \times l$-space scroll chaotic attractor. The proof is similar but rather more complex, and is omitted here.

5.4 Dynamical Behaviour with Different Hysteresis Controllers

The multi-scroll chaotic attractor can be generated via continuous-time linear second-order or third-order systems and hysteresis function series controllers. It is especially noted that controlled systems have different dynamical behaviour with different hysteresis controllers. This subsection briefly investigates the dynamical behaviour of these kinds of hysteresis based chaotic systems.

5.4.1 Dynamical Behaviour of Second-Order Systems

There are three cases considered in this subsection:

1) Suppose $u = f(x,1,1)$ in system (4.5). Variation of the coefficients a or b and the corresponding dynamical behaviours are summarized in table 5.1.

Tab. 5.1 Dynamical behaviours of system (4.5).

b=0.125, a varies	a=1, b varies	Response property
	≤0.0027	one stable equilibrium point
≤0.479	≥0.181	divergent
≥0.480	[0.0028, 0.180]	chaotic

2) Suppose $v = f(y,1,1)$ in system (4.7). Variation of the coefficients a or b and the corresponding dynamical behaviours are summarized in table 5.2.

Tab. 5.2 Dynamical behaviours of system (4.7).

b=0.125, a varies	a=1, b varies	Response property
≤0	≤0	one stable equilibrium point
[0.002, 0.238]	≥0.256	divergent
≥0.239	[0, 0.255]	chaotic

3) Suppose $u = f(x,1,1)$, $v = f(y,1,1)$ in system (5.3). Variation of the coefficients a or b, and the corresponding dynamical behaviours are summarized in table 5.3.

Tab. 5.3 Dynamical behaviours of system (5.3).

b=0.125, a varies	a=1, b varies	Response property
≥16.0	≤0.004	one stable equilibrium point
≤0.26	≥0.30	divergent
[0.27, 15.0]	[0.005, 0.29]	chaotic

5.4.2 Dynamical Behaviour of Third-Order Systems

There are three cases considered in this subsection:

1) Suppose $u = h(x,1,1)$ in system (5.5). Variation of the coefficients a, b or c and the corresponding dynamical behaviours are summarized in table 5.4.

Tab. 5.4 Dynamical behaviours of system (5.5).

b=0.72, c=0.5, a varies	a=0.8, c=0.5, b varies	a=0.8, b=0.72, c varies	Response property
[0, 0.36]	≥1.6	≥1.12	one stable equilibrium point
< 0 or > 0.84	≤0.69	≤0.47	divergent
[0.37, 0.84]	[0.70, 1.59]	(0.48, 0.5), (0.52, 1.1)	chaotic
0.80, 0.84, 0.92, 0.99, [1.04, 1.18], 1.24,1.28,1.30,1.34.		[0.57, 0.59], [0.73, 0.77], [0.86, 0.93].	periodic windows

2) Suppose $u = h(x,1,1)$ and $v = h(y,1,1)$ in system (5.13). Variation of the coefficients a, b or c, and the corresponding dynamical behaviours are summarized as table 5.5.

Tab. 5.5 Dynamical behaviours of system (5.13).

b=0.72, c=0.5, a varies	a=0.8, c=0.5, b varies	a=0.8, b=0.72, c varies	Response property
[0, 0.36]	≥1.60	≥1.12	one stable equilibrium point
< 0 or > 1.00	≤0.56	≤0.39	divergent
0.37, 0.38, [0.49, 0.54], [0.59, 0.98].	[0.57, 1.59]	[0.4, 1.1]	chaotic
[0.39, 0.48], [0.55, 0.58], 0.99.		[0.61, 0.63], [0.74, 0.77], [0.87, 0.90], [0.93, 0.99].	periodic windows

3) Suppose $u = h(x,1,1)$, $v = h(y,1,1)$ and $w = h(z,1,1)$ in system (5.14). Variation of the coefficients a, b or c, and the corresponding dynamical behaviours are summarized as table 5.6.

Tab. 5.6 Dynamical behaviours of system (5.14).

b=0.72, c=0.6, a varies	a=0.8, c=0.6, b varies	a=0.8, b=0.72, c varies	Response property
[0, 0.43]	≥1.34	≥1.12	one stable equilibrium point
< 0 or ≥0.94	≤0.51	≤0.51	divergent
[0.44, 0.93]	[0.53, 1.33]	[0.52, 1.11]	chaotic
[0.48, 0.60], [0.71, 0.72].		[0.74, 0.77], [0.87, 0.90].	periodic windows
	0.52		limit cycle

5.4.3 Remarks

From the analysis in the above two subsections, it has been shown that the considered hysteresis based systems can have a stable equilibrium point, or they can be chaotic or divergent dependent on which hysteresis controllers is used. Furthermore:

1) In the second-order systems case: when parameter a is fixed and b is varied, the 1D horizontal n-scroll, vertical n-scroll and 2D $n \times m$-grid scroll chaotic attractors have similar characteristics; when parameter b is small, the systems have a stable equilibrium point; when parameter b is increased, the systems are chaotic; when parameter b is very large, the systems are divergent.

2) In the third-order systems case, in addition to the rules for the second-order systems case, periodic windows and sometimes limit cycles appear. When one of the parameters varies, systems (5.5), (5.13) and (5.14) have similar characteristics and some of the boundary values are the same.

Since the hysteresis based system is very diverse, there may be many unknown dynamical behaviours to be observed, and this deserves further investigation in the future.

5.5 Summary

The complex dynamical behaviour of the multi-scroll chaos generation system has been studied in this chapter. The dynamical mechanics of multi-scroll chaotic attractor generation have been confirmed theoretically. The main conclusions of this chapter are:

1) An unstable limit cycle bounds a basin of attraction for the multi-scroll chaotic attractor in the second-order system case. The size of the basin of attraction is determined by the parameters of the hysteresis based systems.

2) There exists a non-ordinary attractor for chaos generation in the second-order system case.

3) A rigorously derived two-dimensional Poincaré map and the Lyapunov exponent verifying the chaotic behaviours in the third-order system case.

The hysteresis chaotic generator may find wide ranging real-world engineering applications because hysteresis based chaotic systems possess complex dynamical behaviours with relatively simple models.

Chapter 6

Circuit Implementation of the Multi-Scroll Chaotic Attractor

6.1 Introduction

Over the past few years, a number of applications of chaotic systems to cryptography and secure information processing, liquid mixing, chemical reactions, and so on have surfaced in the engineering community. One major problem in the application of chaos based systems is their hardware implementation. Generating complex chaotic attractors with simple electronic circuits has attracted increasing attention. The implementation of circuitry to model hysteresis based chaotic generators has been widely studied [56, 59, 62, 64, 67-70, 75, 77]. In addition to implementing a single and double scroll chaotic attractors, Saito also implemented a 2×2-scroll chaotic attractor with a two-port chaotic oscillator [70]. A multi-scroll generation scheme was proposed by Varrientos and Sanchez-Sinencio [77]. In their scheme it was shown that by constructing more than one differential hysteresis comparators and placing them in parallel, two or more different hysteresis outputs could be generated. Their experimental results only show limited chaotic scrolls due to the physical constraint that the differential hysteresis comparators are difficult to implement, particularly because when more comparators are needed the resistors have to be adjusted simultaneously to maintain the synchrony.

The multi-scroll chaotic attractors proposed in Chapter 4 have more complicated dynamical behaviours and a wide range of basin of attraction. The chaotic behaviours have been confirmed mathematically in Chapter 5. In order to verify the chaotic attractors experimentally, a novel double-hysteresis block is proposed, and the ideal double-hysteresis series are constructed via a systematic method using basic building blocks. A new circuit is designed for generating 1D n-scroll chaotic attractors in the directions of the state variables, and 2D $n \times m$-grid scroll chaotic attractors in the phase plane via linear second-order systems and double-hysteresis series. Circuit implementation and the oscilloscope illustrated

waveforms of multi-scroll chaotic attractors and the output of the double-hysteresis series are used to verify the effectiveness of this design.

This chapter is organized as follows. Section 6.2 proposes a design scheme for a double-hysteresis building block and double-hysteresis series. Multi-scroll chaotic attractors via linear second-order systems and double-hysteresis series are designed in section 6.3. Experimental results are shown in section 6.4. Section 6.5 is the summary of this chapter.

6.2 Double-Hysteresis Series and its Implementation

The double-hysteresis function is the basis for generating multi-scroll chaotic attractors. In this section, the design of the ideal double-hysteresis function and its series are given. The mathematical model, the circuit structure and the operational principle of the double-hysteresis series are also studied.

Definition 6.1: Double-hysteresis function is defined as the superimposition of two hysteresis functions, which described as:

$$u = h_1(x) + h_{-1}(x) \tag{6.1}$$

Eq. (6.1) is a special case when p=q=1 in Eq. (4.2).

Definition 6.2: Double-hysteresis series is defined as:

$$u_0 = -h(u_i, k) \tag{6.2}$$

where u_i and u_0 are the input and output of the double-hysteresis series, respectively, and k is the number of the double-hysteresis functoin.

It should be noted that the double-hysteresis series is a special case of the hysteresis function series described by Eq. (4.2) where p=q=k.

6.2.1 Building Block of the Double-Hysteresis Function

In this subsection, an electronic circuit is designed to implemente the double-hysteresis function.

The block diagram of the double-hysteresis building block is shown in Fig. 6.1. It consists of operational amplifier, diode and resistor.

In Fig. 6.1, suppose the voltages corresponding to the two diodes (D1, D2) being on and off are U_{on} and U_z, respectively. The output of two operational amplifiers U1B and U1C, are u_1 and u_2, and are switched between two different values, respectively:

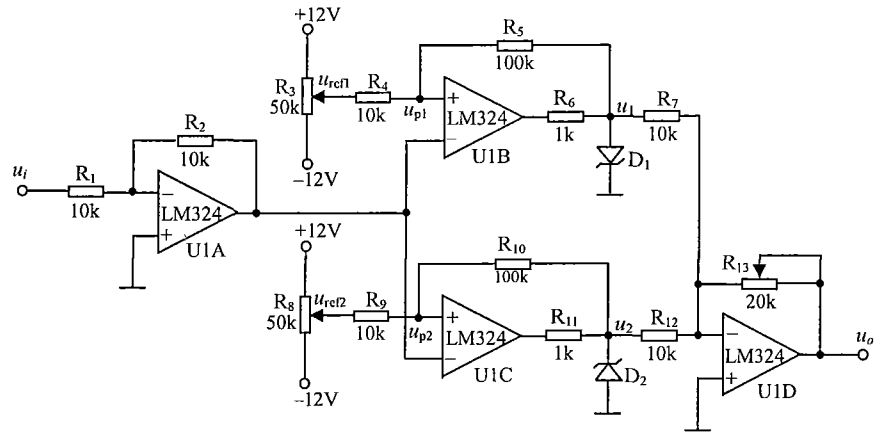

Fig. 6.1 Block diagram of double-hysteresis building block.

$$u_1 = \begin{cases} U_{on} & if\ D_1\ is\ on \\ -U_z & if\ D_1\ is\ off \end{cases}$$

$$u_2 = \begin{cases} -U_{on} & if\ D_2\ is\ on \\ U_z & if\ D_2\ is\ off \end{cases}$$

In this design, a Zener diode is selected, and when U_Z=7V, the corresponding voltage for the diodes to work is U_{on}=0.5V. By applying Kirchhoff's Current Law (KCL) to Fig. 6.1, one has:

$$\begin{cases} (\frac{1}{R_4}+\frac{1}{R_5})u_{P1} - \frac{1}{R_4}U_{ref1} - \frac{1}{R_5}u_1 = 0 \\ (\frac{1}{R_9}+\frac{1}{R_{10}})u_{P2} - \frac{1}{R_9}U_{ref2} - \frac{1}{R_{10}}u_2 = 0 \end{cases}$$

and the threshold voltages of u_1 for switching U1B are obtained as:

$$\begin{cases} U_{T11} = -\dfrac{R_5}{R_4+R_5}U_{ref1} - \dfrac{R_4}{R_4+R_5}u_z \\ U_{T12} = -\dfrac{R_5}{R_4+R_5}U_{ref1} + \dfrac{R_4}{R_4+R_5}U_{on} \end{cases}$$

where U_{T11} and U_{T12} are the two switching values of the output of U1B shown in Fig. 6.2, which represents the characteristics of voltage transmission of the two hysteresis units.

The threshold voltages of u_2 for switching U1C are given by:

$$\begin{cases} U_{T21} = -\dfrac{R_{10}}{R_9 + R_{10}} U_{ref2} - \dfrac{R_9}{R_9 + R_{10}} U_z \\ U_{T22} = -\dfrac{R_{10}}{R_9 + R_{10}} U_{ref2} + \dfrac{R_9}{R_9 + R_{10}} U_{on} \end{cases}$$

where U_{T21} and U_{T22} are the two switching values of the output of U1C shown in Fig. 6.2.

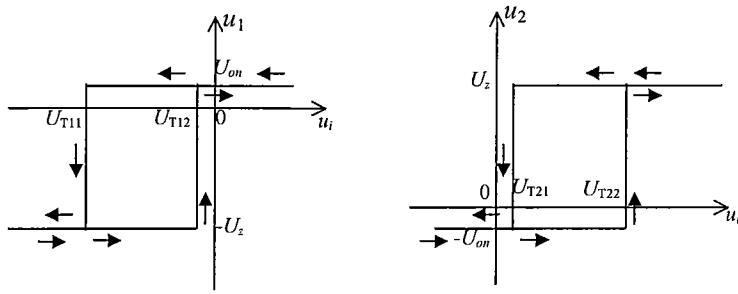

Fig. 6.2 The characteristics of voltage transmission for two hysteresis functions.

If U_{T12}=U_{T21}=0 (achieved by adjusting $R3$ and $R8$ in Fig. 6.1), then ideal double-hysteresis characteristics can be obtained. The characteristics of the voltage transfer for the double-hysteresis function is depicted in Fig. 6.3. The output of the circuit in Fig. 6.1, u_0, is switched among three values: $k(u_z-u_{on})$, 0, $k(-u_z+u_{on})$, where k=R_{13}/R_{12}=R_{13}/R_7. The oscilloscope depiction of the double-hysteresis function is shown in Fig. 6.4.

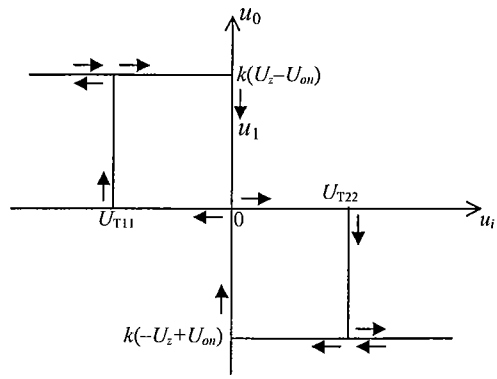

Fig. 6.3 Characteristics of voltage transmission for the double-hysteresis function.

6.2.2 Implementation of Double-Hysteresis Series

The double-hysteresis series is constructed by combining double-hysteresis building blocks. If more double-hysteresis blocks are connected in parallel, then the output of the double-hysteresis series can be obtained.

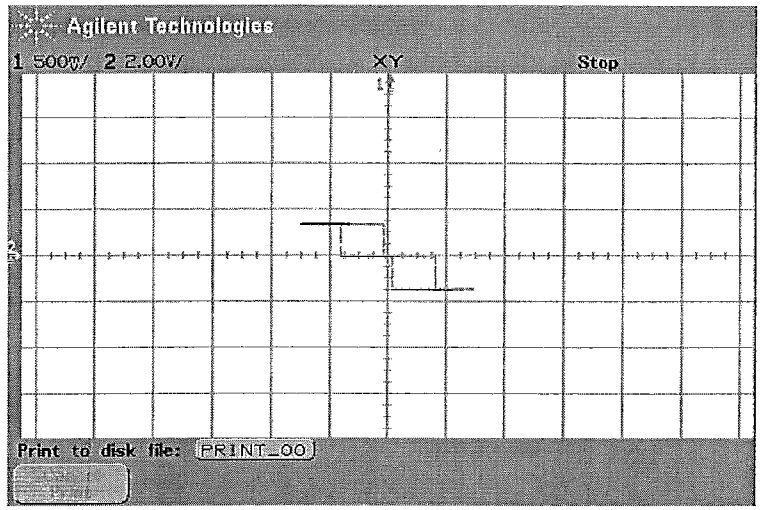

Fig. 6.4 The oscilliscope depiction of the double-hysteresis function.

One can construct any number of double-hysteresis series by setting different values of k in the double-hysteresis series $h(x, k)$. If k=4, four double-hysteresis series (eight-hysteresis) can be obtained. The circuit diagram for the eight-hysteresis case is shown in Fig. 6.5, whose input u_i is the state variable x, and output u_0 has four double-hysteresis series composed of eight hysteresis functions.

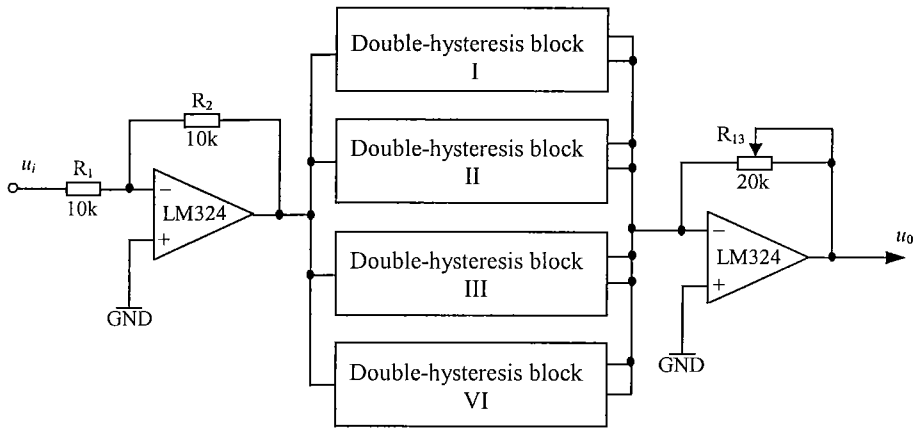

Fig. 6.5 Block diagram of eight-hysteresis series.

6.3 Multi-Scroll Chaos Generator

Some multi-scroll chaotic attractors via linear second-order systems and double-hysteresis series are generated experimentally and the results are reported in this section. These results verify the proposed systematic design scheme in chapter 4 experimentally. The circuit equations and the operation principles of the blocks are also given in this section.

6.3.1 Generating Chaotic Attractors

By replacing the hysteresis function series Eq. (4.2) with the double-hysteresis series Eq. (6.1) in system (4.5), the new system equations become:

$$\begin{cases} \dot{x} = y \\ \dot{y} = -ax + by + ah(x,k) \end{cases} \tag{6.3}$$

and the1D horizontal n-scroll (n=2k+1) chaotic attractors can be obtained from system (6.3).

Similarly, replacing hysteresis function series with double-hysteresis series in system (4.7), then the new system equations become:

$$\begin{cases} \dot{x} = y - h(y,k) \\ \dot{y} = -ax + by - bh(y,k) \end{cases} \tag{6.4}$$

and the 1D vertical n-scroll (n=2k+1) chaotic attractors can be obtained from system (6.4).

The n×m–grid scroll chaotic attractors (n=2k+1, m=2l+1) can be generated by replacing the hysteresis function series with double-hysteresis series in system (4.9):

$$\begin{cases} \dot{x} = y - h(y,l) \\ \dot{y} = -ax + by + ah(x,k) - bh(y,l) \end{cases} \tag{6.5}$$

6.3.2 Circuit Implementation

The circuit diagram for generating multi-scroll chaotic attractors is shown in Fig. 6.6. There are two basic circuit cells: The upper cell comprises the linear portion of the system. U2A, R_{25}, C_1 and U2B, R_{26}, C_2 in the upper cell implement the two integers of the continuous-time linear second-order system. And U2C is a buffer. The integrating constant of the first integer is $\tau_1 = R_{25}C_1 = 100k\Omega \cdot 0.01\mu F = 1\text{ms}$, and the second is $\tau_2 = R_{26}C_2 = 100k\Omega \cdot 0.001\mu F = 0.1\text{ms}$.

The linear portion of the system is designed, with the complex conjugate poles being located in the right-half plane. This would normally lead to an unstable response. With the help of the double-hysteresis series for bounding the output trajectory, a chaotic response can be created.

There are two double-hysteresis series $h(V_{C1}, k_1)$ and $h(V_{C2}, k_2)$ in the lower cell. The input of the two double-hysteresis series are the state variables, V_{C1} and V_{C2}, which corresponds to x and $-y$ in Eqs. (6.3)~(6.5), respectively, that is, $V_{C1} = x$ and $V_{C2} = -y$; the output of the double-hysteresis series, $-u = -h(V_{C1}, k_1)$ and $v = -h(V_{C2}, k_2)$, are fed-back to the linear part in the upper cell.

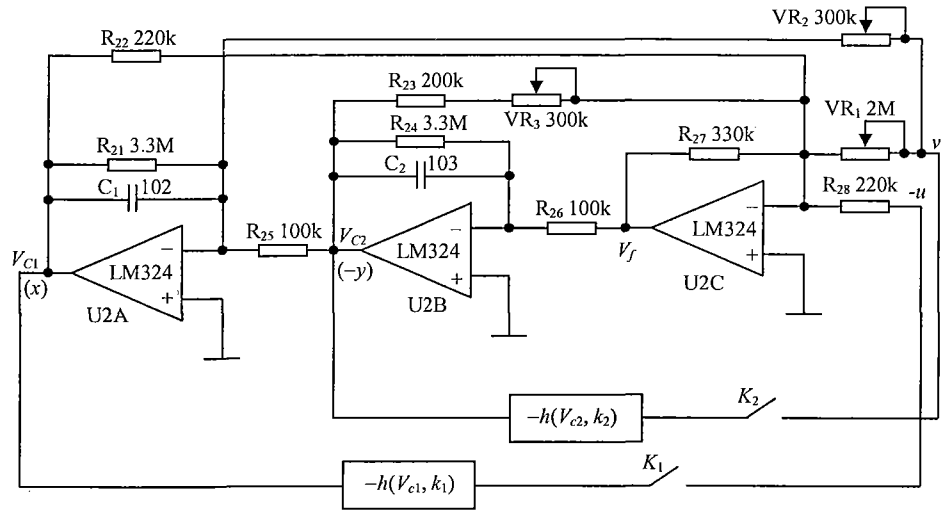

Fig. 6.6 Circuit diagram of multi-scroll chaos generator.

When switch K_1 is on and K_2 is off, the horizontal n-scroll ($n=2k_1+1$) chaotic attractors can be observed; when K_2 is on and K_1 is off, the vertical n-scroll ($n=2k_2+1$) chaotic attractors can be observed; when both K_1 and K_2 are on, the 2D $n\times m$-grid scroll chaotic attractors can be observed.

6.4 Experimental Results

Applying the KCL to Fig. 6.6, the following circuit equations can be obtained:

$$\begin{cases} -sC_1V_{C1} - \dfrac{1}{R_{21}}V_{C1} - \dfrac{1}{R_{25}}V_{C2} - \dfrac{1}{VR_2}v = 0 \\ -sC_2V_{C2} - \dfrac{1}{R_{24}}V_{C2} - \dfrac{1}{R_{26}}V_f = 0 \\ \dfrac{1}{R_{27}}V_f - \dfrac{1}{R_{28}}u - \dfrac{1}{VR_1}v - \dfrac{1}{R_5+VR_3}V_{C2} - \dfrac{1}{R_{22}}V_{C1} = 0 \end{cases} \tag{6.6}$$

where VR_1, VR_2 and VR_3 are potentiometers; V_{C1}, V_{C2} and V_f are node voltages, shown in Fig. 6.6; u and v are the outputs of two double-hysteresis series.

Eq. (6.6) can be reformulated as:

$$\begin{cases} V_{C2} = -R_{25}(sC_1 + \dfrac{1}{R_{21}})V_{C1} - \dfrac{R_{25}}{VR_2}(-u) \\ V_{C1} = R_{22}[\dfrac{R_{26}}{R_{27}}(sC_2 + \dfrac{1}{R_{24}}) - \dfrac{1}{R_{23}+VR_3}]V_{C2} - \dfrac{R_{22}}{VR_1}(-u) - \dfrac{R_{22}}{R_{28}}v \end{cases} \tag{6.7}$$

By choosing circuit parameters properly, and adjusting the potentiometers in Fig. 6.6, Eq. (6.7) can be written the same as Eqs. (6.3) ~ (6.5) which generates 1D n-scroll horizontal and vertical chaotic attractors and 2D $n\times m$-grid scroll chaotic attractors, respectively.

In all the experiments, the voltage supplies to the active devices are ±12V. The types of operational amplifier and diodes, and the values of resistors and capacitors are shown in Fig. 6.1 and Fig. 6.6, respectively. A digital storage oscilloscope was used to record the waveforms. The two connectors of the oscilloscope are $x=V_{C1}$, $-y=V_{C2}$. The scales for each measurement are shown on the upper-left corners of the diagrams. The oscilloscope shows pictures illustrating the following three cases.

Case 1. 1D n-scroll chaotic attractors.

When switch K_1 is on and K_2 is off, and $u = h(V_{C1}, k_1)$ (k_1=1, 2, 3, 4), the oscilloscope illustrates the 1D horizontal n-scroll chaotic attractors as shown in Fig. 6.7.

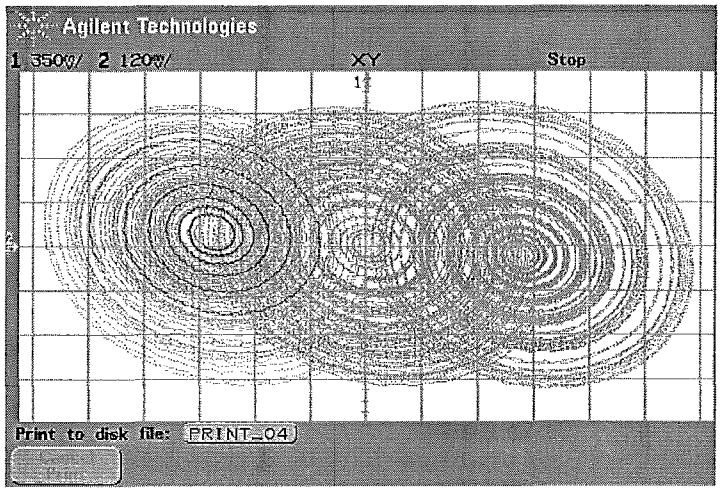

(a)

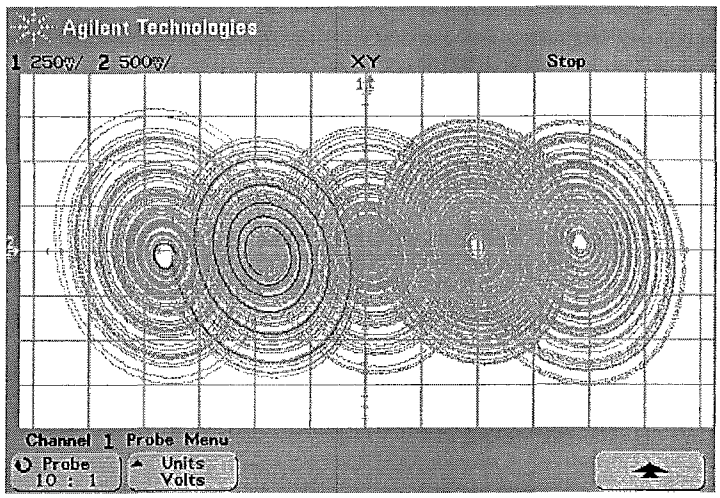

(b)

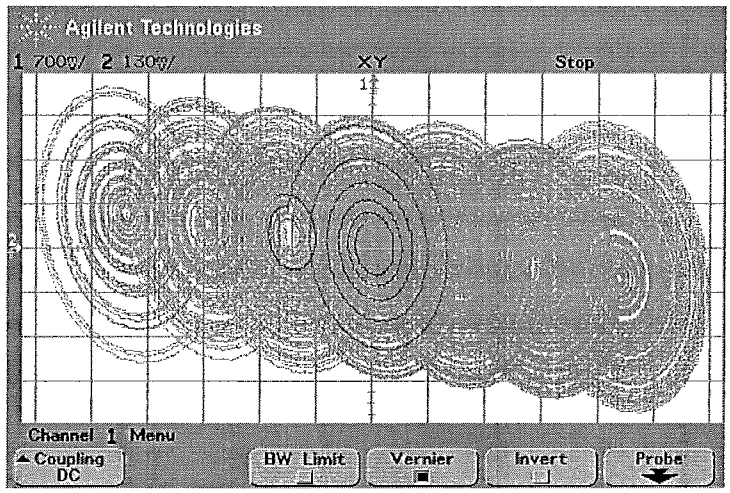

(c)

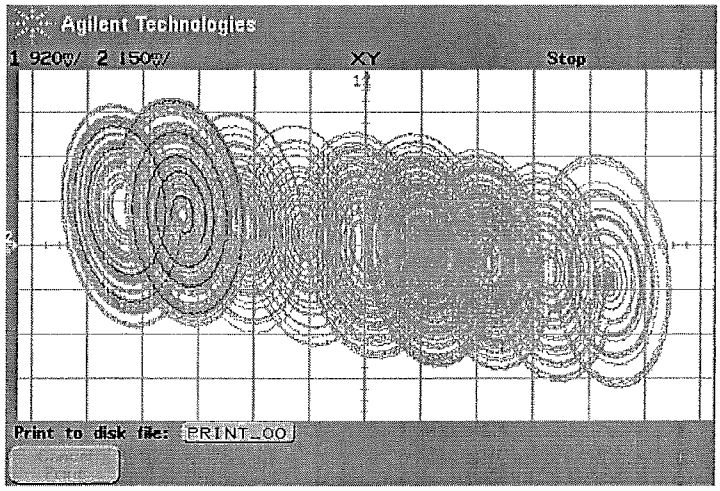

(d)

Fig. 6.7 Oscilloscope illustrated 1D n-scroll chaotic attractors.
(a) 3-scroll; (b) 5-scroll; (c) 7-scroll; (d) 9-scroll.

Case 2. 2D $n\times m$-grid scroll chaotic attractors.

When both switches K_1 and K_2 are on, and $u = h(V_{C1}, k_1)$ (k_1=1, 2, 3, 4), $v = h(V_{C2}, 1)$, the oscilloscope illustrates the 2D $n\times$3-grid scroll chaotic attractors as shown in Fig. 6.8.

If $u = h(V_{C1}, k_1)$ (k_1=2, 3) and $v = h(V_{C2}, 2)$, the oscilloscope illustrates 5×5-, and 7×5-grid scroll chaotic attractors as shown in Fig. 6.9 (a) and (b). If $u = h(V_{C1}, 4)$ and $v = h(V_{C2}, k_2)$ (k_2=3, 4), the oscilloscope illustrates 9×7-, and 9×9-grid scroll chaotic attractors as shown in Fig. 6.9 (c) and (d).

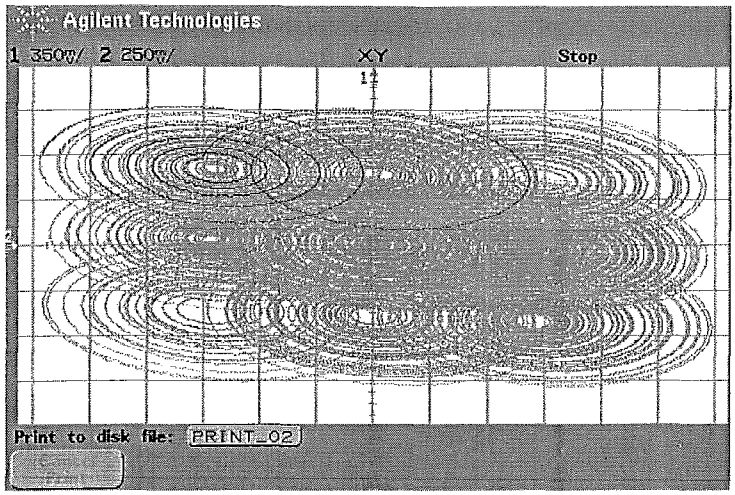
Agilent Technologies
1 350mV/ 2 250mV/
XY
Stop
Print to disk file: PRINT_02

(a)

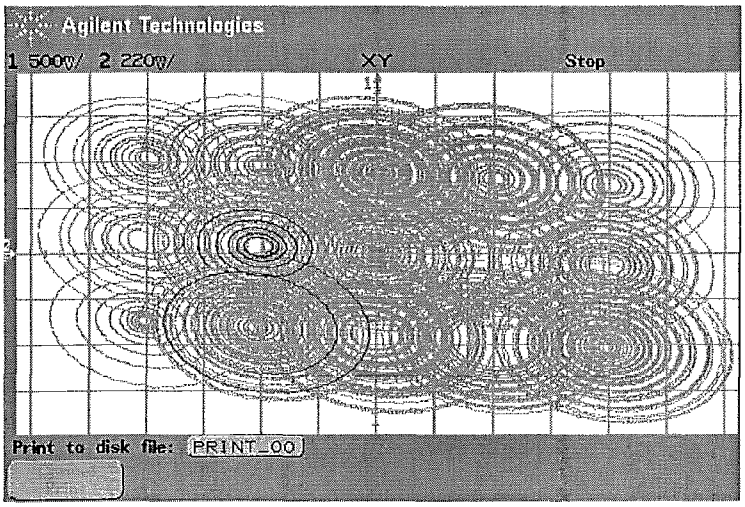
Agilent Technologies
1 500mV/ 2 220mV/
XY
Stop
Print to disk file: PRINT_00

(b)

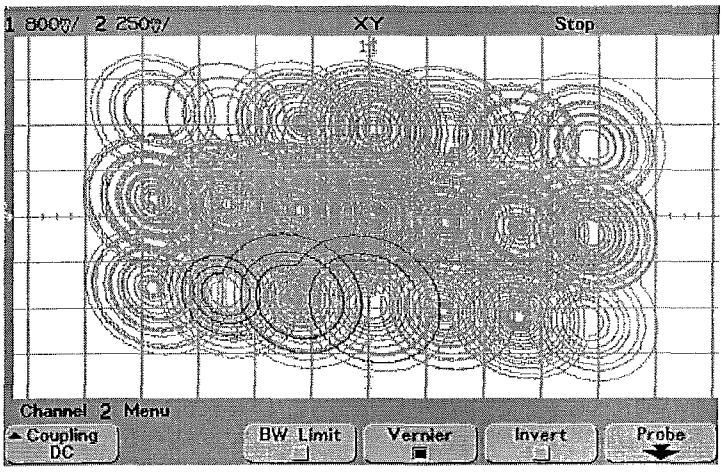
1 800mV/ 2 250mV/
XY
Stop
Channel 2 Menu
Coupling
DC
BW Limit
Vernier
Invert
Probe

(c)

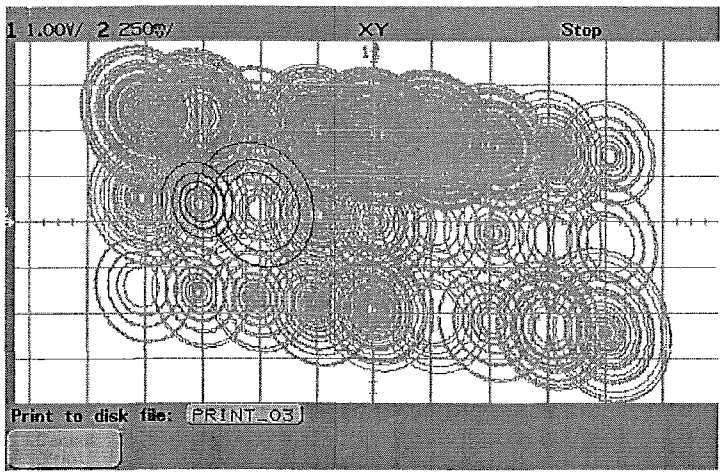

(d)

Fig. 6.8 Oscilloscope illustrated 2D n×3-grid scroll chaotic attractors. (a) 3×3-scroll; (b) 5×3-scroll; (c) 7×3-scroll; (d) 9×3-scroll.

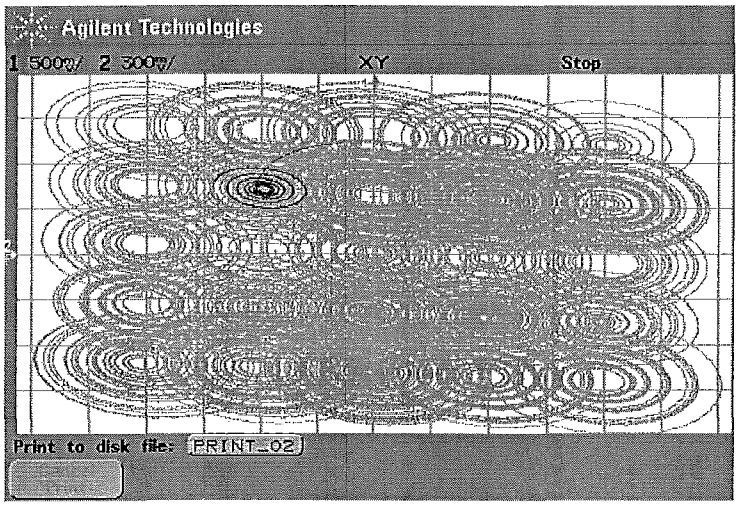

(a)

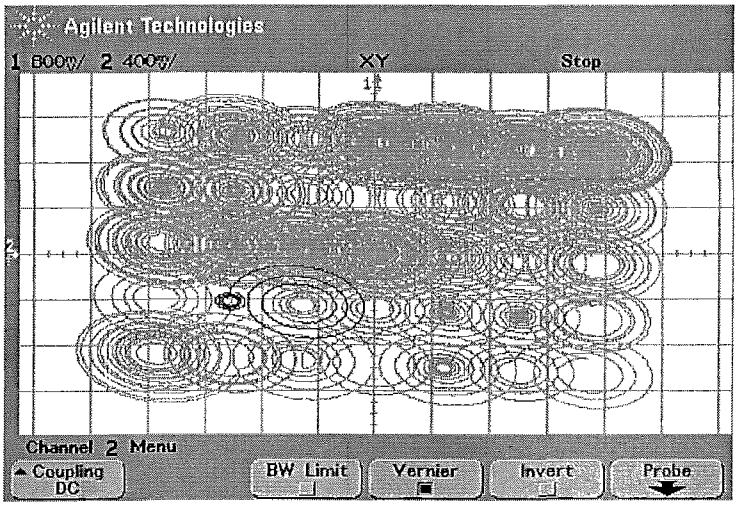

(b)

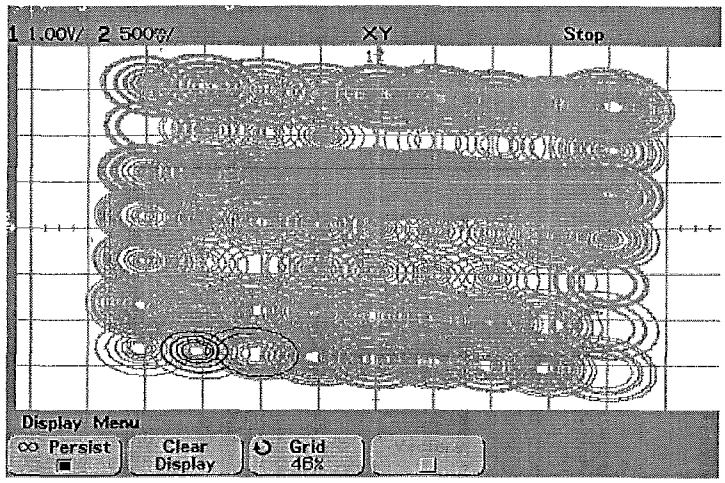

(c)

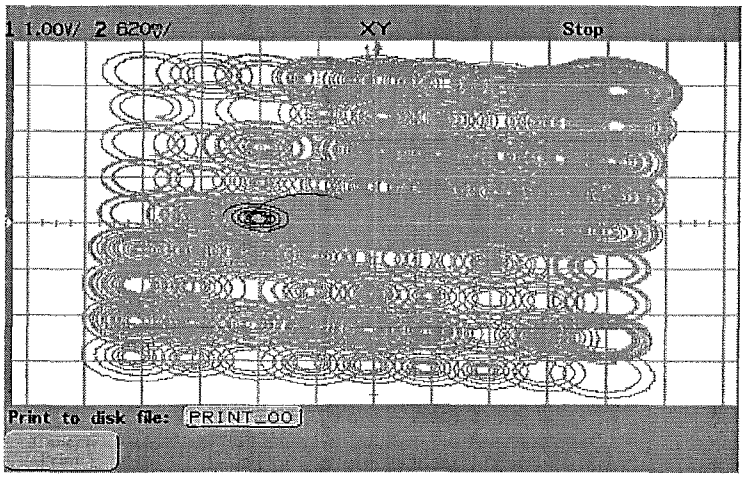

(d)

Fig. 6.9 Oscilloscope illustrated 2D $n\times m$-grid scroll chaotic attracors.
(a) 5×5-scroll; (b) 7×5-scroll; (c) 9×7-scroll; (d) 9×9-scroll.

Case 3. The phase trajectories of the double-hysteresis series $h[V_{C1}\ (V_{C2}), k]$, (k =2, 3, 4) for generating multi-scroll chaotic attractors are shown in Fig. 6.10.

It is noted that, the advantage of the proposed chaos oscillators is that the scroll number can be increased to any number very easily using the double-hysteresis building blocks. The 1D n-scroll chaotic attractors and the 2D $n\times m$-grid scroll chaotic attractors can be placed anywhere, and cover any chosen area of the phase plane.

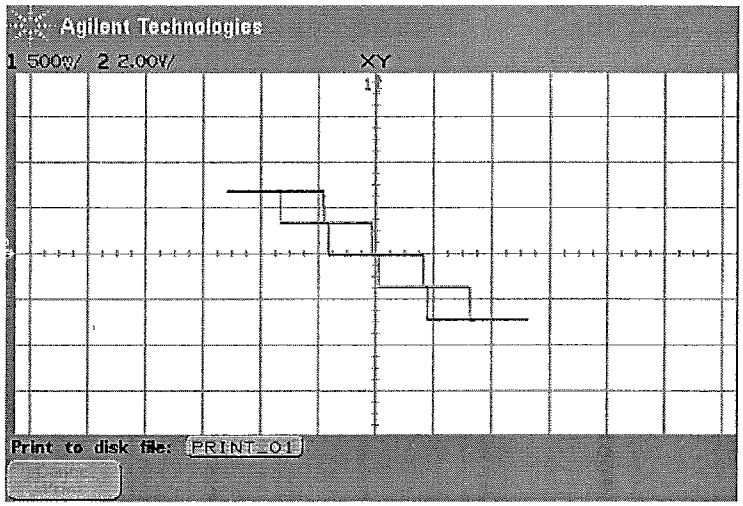

(a)

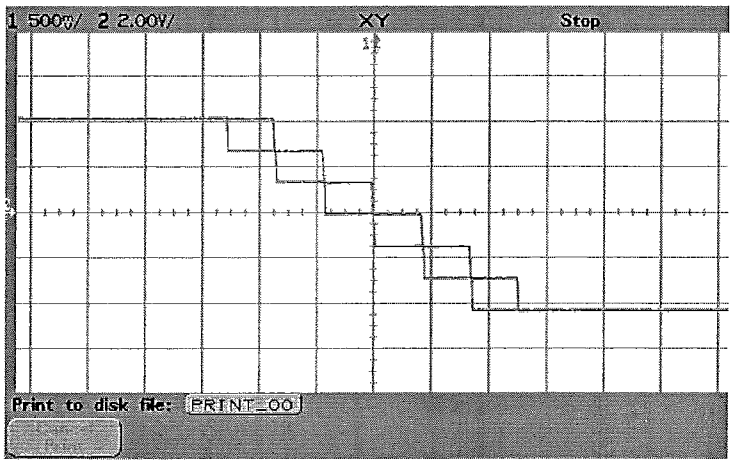

(b)

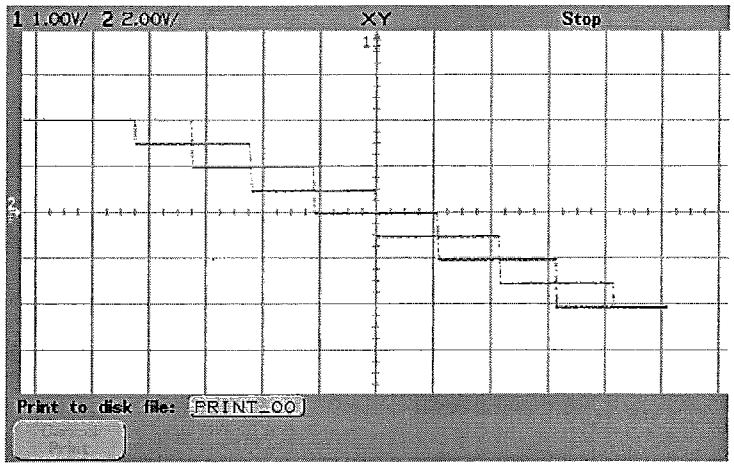

(c)

Fig. 6.10 Oscilloscope illustrated outputs of double-hysteresis series. (a) k=2; (b) k=3; (c) k=4.

6.5 Summary

In this chapter, a novel double-hysteresis block has been proposed to realize multi-scroll chaotic attractors. We have shown that with the proposed scheme: 1D n-scroll chaotic attractors in the directions of state variables, 2D $n \times m$-grid scroll chaotic attractors in the phase plane via continuous-time linear second-order system and double-hysteresis series can be easily implemented. The main characteristics of the chaos generators are:

1) The number of scroll in the horizontal and vertical direction can be changed separately by choosing the number of double-hysteresis feedback of two state variables, and can be increased arbitrarily without any technical problem.

2) The scrolls can be placed anywhere and cover any chosen area of the phase plane. The position of the equilibrium points can be adjusted by changing the parameters of hysteresis feedback.

These proposed multi-scroll chaotic oscillators may find potential applications in engineering due to their complex dynamical behaviours and their comparatively simple circuitry implementation.

Chapter 7

Conclusions and Future Research

In this thesis systematic methods for generating multi-scroll chaotic attractors via continuous-time linear second-order and third-order systems with a hysteresis function series have been proposed. The theoretical development, dynamical analyses, numerical simulations and circuit implementations have demonstrated the effectiveness of the multi-scroll chaos generation scheme. The conclusions are drawn and future research directions are suggested in this chapter.

7.1 Conclusions

This research proposes several systematic methods for generating the multi-scroll chaotic attractors. The following results have been achieved:

1) The concept of the chaotic stability margin has been proposed. The dynamical behaviours of the hysteresis based system have been demonstrated in detail. A hysteresis based chaotic system with the maximum chaotic stability margin has been designed.

2) A method for calculating the limit cycle which bounds the basin of attraction in the hysteresis based system has been proposed. The analytic solutions for trajectory boundaries have been presented.

3) 1D n-scroll chaotic attractors in the directions of the state variables, 2D $n \times m$-grid scroll chaotic attractors in the phase plane have been generated via continuous-time linear second-order systems and the hysteresis function series. 1D n-scroll, 2D $n \times m$-grid scroll and 3D $n \times m \times l$-space scroll chaotic attractors have been generated via continuous-time linear third-order systems and the hysteresis function series.

4) An unstable limit-cycle defines the boundary of the basin of attraction for the multi-scroll chaotic attractors in the second-order systems case. The size of the basin of attraction increases with the increase in the number of hysteresis function series.

The higher the scroll number, the greater the stability margin the system has.

5) Multi-scroll chaotic behaviours have been confirmed theoretically and it has been shown that an ordinary attractor exists in the second-order systems case. A two-dimensional Poincaré map has been rigorously derived, and the Lyapunov exponent has been applied to verify the chaotic behaviour in the third-order systems case.

6) Based on the proposed double-hysteresis building block, the circuit implementation of multi-scroll chaotic oscillators via second-order systems and the double-hysteresis series have been designed. The numbers of scroll and the positions of equilibrium points can be designed arbitrarily. And the scrolls can be placed anywhere and cover any chosen area of the phase plane.

7.2 Future Research

The field of anti-control of chaos is presently fast booming, and may lead to some important applications in the near future.

The chaotic behaviours of the multi-scroll chaotic attractors in this study have been rigorously proven theoretically. The circuit for a chaotic generator via a linear second-order systems and a hysteresis function series has been implemented. There are some issues that can be further dealt with both in theory and in applications and are worth further investigation:

1) The n-scroll attractors and the grid-type attractors possess some interesting properties, which may be used for image processing applications. Future work can focus on the study of the multi-scroll chaotic attractors for representing digital codes or images for information transmission or storage.

2) The concept of *chaos stability margin* may be further investigated and applied to define the likelihood of generating a particular pattern or image (e.g., a scroll representing a pixel). In other words, it may be interesting to look into the problem of controlling the chaos generating process such that scrolls at particular grid locations can be guaranteed or shut down permanently, as required for representing a digital code or image.

3) As the heart is basically a second-order system, electronic simulations of hysteresis chaos help us to study the heart under arrhythmic behaviour. Chaotic behaviour should be able to represent heart fibrillations. Further theoretic research can be focused on

this topic with the view of suppressing arrhythmic heart behaviour;

4) The design criteria of multi-scroll chaotic attractors via linear second-order systems with hysteresis function series can be further studied. An open question is that is it possible to design a multi-scroll chaotic attractor with maximum stability margin?

5) The circuit implementation of the multi-scroll chaotic attractor is based on the double-hysteresis function, the scroll number can only be odd numbers. How to implement the case with an even number scrolls is another open question;

6) The complex dynamical behaviours of multi-scroll chaos generation with respect to the variation of parameters can be explored further;

7) The circuit implementation of chaos generators via linear third-order systems and the hysteresis function series need to be explored;

8) How to synchronize two identical multi-scroll chaotic generators, and study the possibility of using it in engineering areas;

9) The VLSI design and implementation of the multi-scroll chaotic generators.

Further results along the above directions will further enrich the study of the anti-control of chaos, thus enhancing the application of the anti-control of chaos research in practical situations.

Bibliography

[1] T. Matsumoto, "A chaotic attractor from Chua's circuit," *IEEE Trans. Circuits Syst. I*, vol. 31, no. 12, pp. 1055-1058, 1984.

[2] G. Q. Zhong and F. Ayrom, "Experimental confirmation of chaos from Chua's circuit," *Int. J. Circuit Theory Appl.*, vol. 13, no. 11, pp. 93-98, 1985.

[3] T. Matsumoto, L. O. Chua and M. Komuro, "The double scroll," *IEEE Trans. Circuits Syst. I*, vol. 32, no.8, pp. 797-818, 1985.

[4] L. O. Chua, M. Komuro and T. Matsumoto, "Double scroll family," *IEEE Trans. Circuits Syst. I*, vol. 33, no. 11, pp. 1072-1118, 1986.

[5] A. L. Fradkov and A. Y. Pogromsky, *Introduction to Control of Oscillations and Chaos*, World Scientific, Singapore, 1998.

[6] M. P. Kennedy, "Three steps to chaos – part I: evolution," *IEEE Trans. Circuits Syst. I*, vol. 40, no. 10, pp. 640-656, 1993.

[7] M. P. Kennedy, "Three steps to chaos – part II: a Chua's circuit primer," *IEEE Trans. Circuits Syst. I*, vol. 40, no. 10, pp. 657-674, 1993.

[8] G. Chen and X. Dong, *From Chaos to Order: Methodologies, Perspectives and Applications*, World Scientific, Singapore, 1998.

[9] E. Ott, C. Grebogi and J. A. Yorke, "Controlling chaos," *Phys. Rev. Lett.*, vol. 64, no. 11, pp. 1196-1199, 1990.

[10] L. M. Pecoar and T. L. Carroll, "Synchronization in chaotic systems," *Phys. Rev. Lett*, vol. 64, no. 8, pp. 821-824, 1990.

[11] T. L. Carroll and L. M. Pecoar, "Synchronizing chaotic circuits," *IEEE Trans. Circuits Syst. I*, vol. 38, no. 4, pp. 453-456, 1991.

[12] K. M. Cuomo and A. V. Oppenheim, "Circuit implementation of synchronized chaos with application to communications," *Phys. Rev. Lett*, vol. 71, no.1, pp. 65-68, 1993.

[13] C. P. Silva, "Shil'nikov theorem – a tutorial," *IEEE Trans. Circuits Syst. I*, vol. 40, no. 10, pp. 675-682, 1993.

[14] R. C. Hilborn, *Chaos and Nonlinear Dynamics*, Oxford University Press, New York Oxford, 1994.

[15] T. Y. Li and J. A. Yorke, "Period three implies chaos", *The American Mathematical Monthly*, vol. 82, no. 10, pp. 985-992, 1975.

[16] J. M. Cruz and L. O. Chua, "An IC chip of Chua's circuit," *IEEE Trans. Circuits Syst. II*, vol. 40, no. 10, pp. 614-625, 1993.

[17] P. Arena, S. Baglio, L. Fortuna and G. Manganaro, "Chua's circuit can be generated by CNN cells," *IEEE Trans. Circuits Syst. I*, vol. 42, no. 2, pp. 123-125, 1995.

[18] M. P. Kennedy, "On the relationship between the chaotic Colpitts oscillator and Chua's oscillator," *IEEE Trans. Circuits Syst. I*, vol. 42, no. 6, pp. 376-379, 1995.

[19] A. S. Elwakil and M. P. Kennedy, "Improved implementation of Chua's chaotic oscillator using the current feedback op amp," *IEEE Trans. Circuits Syst. I*, vol. 47, no. 1, pp. 76-79, 2000.

[20] A. S. Elwakil and M. P. Kennedy, "Generic RC realization of Chua's circuit," *Int. J. Bifurcat. Chaos*, vol. 10, no. 8, pp. 1981-1985, 2000.

[21] A. S. Elwakil and A. M. Soliman, "Current mode chaos generator," *Electron. Lett.*, vol. 33, no. 20, pp. 1661-1662, 1997.

[22] A. S. Elwakil and A. M. Soliman, "Current conveyor chaos generators," *IEEE Trans. Circuits Syst. I*, vol. 46, no. 3, pp. 393-398, 1999.

[23] A. S. Elwakil and M. P. Kennedy, "High frequency RC chaos generator," *Proc. of the IEEE Symp. Electronics, Circ., and Syst.*, vol. 2, pp. 513-516, Lisboa, Portugal, 1998.

[24] A. S. Elwakil and M. P. Kennedy, "High frequency Wien-type chaotic oscillator," *Electron. Lett.*, vol. 34, no. 12, pp. 1161-1162, 1998.

[25] G. M. Maggio, O. De Feo and M. P. Kennedy, "Nonlinear analysis of the Colpitts oscillator and applications to design," *IEEE Trans. Circuits Syst. I*, vol. 46, no. 9, pp. 1118-1129, 1999.

[26] A. S. Elwakil and M. P. Kennedy, "A semi-systematic procedure for producing chaos from sinusoidal oscillators using diode-inductor and FET-capacitor composites," *IEEE Trans. Circuits Syst. I*, vol. 47, no. 4, pp. 582-590, 2000.

[27] A. S. Elwakil and K. N. Salama, and M. P. Kennedy, "A system for chaos generation and its implementation in monolithic form," *Proc. of the IEEE Symp. Circuits. Syst.*, vol. 5, pp. 217-220, Geneva, Switzerland, 2000.

[28] A. S. Elwakil and M. P. Kennedy, "Chaotic oscillators derived from Saito's double-screw hysteresis oscillator," *The Institute of Electronics, Information and*

Communication Engineering, Trans. Fundamentals, vol. E82-A, no. 9, pp. 1769-1775, 1999.

[29] A. S. Elwakil and M. P. Kennedy, "Systematic realization of a class of hysteresis chaotic oscillators," *Int. J. Circuit Theory Appl.*, vol. 28, pp. 319-334, 2000.

[30] A. S. Elwakil and M. P. Kennedy, "Construction of classes of circuit-independent chaotic oscillators using passive-only nonlinear devices," *IEEE Trans. Circuits Syst. I*, vol. 48, no. 3, pp. 289-307, 2001.

[31] J. A. K. Suykens and J. Vandewalle, "Generation of n-double scrolls (n=1,2,3,4,....)," *IEEE Trans. Circuits Syst. I*, vol. 40, no. 11, pp. 861-867, 1993.

[32] M. E. Yalçin, S. Ozoguz, J. A. K. Suykens and J. Vandewalle, "n-scroll chaos generators: a simple circuit model," *Electron. Lett.*, vol. 37, no. 3, pp. 147-148, 2001.

[33] M. E. Yalçin, J. A. K. Suykens and J. Vandewalle, "Experimental confirmation of 3- and 5- scroll attractors from a generalized Chua's circuit," *IEEE Trans. Circuits Syst. I*, vol. 47, no. 3, pp. 425-429, 2000.

[34] M. E. Yalçin, J. A. K. Suykens and J. Vandewalle, "Families of scroll grid attractors," *Int. J. Bifurcat. Chaos*, vol. 12, no. 1, pp. 23-41, 2002.

[35] G. Chen and T. Ueta, "Yet another chaotic attractor," *Int. J. Bifurcat. Chaos*, vol. 9, no. 7, pp. 1465-1466, 1999.

[36] T. Ueta and G. Chen, "Bifurcation analysis of Chen's attractor," *Int. J. Bifurcat. Chaos*, vol. 10, no. 8, pp. 1917-1931, 2000.

[37] X. Yu and Y. Xia, "Detecting unstable periodic orbits in Chen's chaotic attractor," *Int. J. Bifurcat. Chaos*, vol. 10, no. 8, pp. 1987-1991, 2000.

[38] J. Lü, T. Zhou and S. Zhang, "Controlling the Chen attractor using linear feedback based on parameter identification," *Chinese Phys.*, vol. 11, no. 1, pp. 12-16, 2002.

[39] G. Q. Zhong and K. S. Tang, "Circuitry implementation and synchronization of Chen's attractor," *Int. J. Bifurcat. Chaos*, vol. 12, no. 6, pp. 1423-1427, 2002.

[40] J. Lü and G. Chen, "A new chaotic attractor coined," *Int. J. Bifurcat. Chaos*, vol. 12, no. 3, pp. 659-661, 2002.

[41] J. Lü, G. Chen, D. Cheng and S. Celikovsky, "Bridge the gap between the Lorenz system and the Chen system," *Int. J. Bifurcat. Chaos*, vol. 12, no. 12, pp. 2917-2926, 2002.

[42] J. Lü, G. Chen and S. Zhang, "Dynamical analysis of a new chaotic attractor," *Int. J. Bifurcat. Chaos*, vol. 12, no. 5, pp. 1001-1015, 2002.

[43] F. Han, Y. Wang, X. Yu and Y. Feng, "Experimental confirmation of a new chaotic attractor," *Chaos, Solitons & Fractals*, vol. 21, no. 1, pp. 69-74, 2004.

[44] X. Q. Wu and J. Lü, "Parameter identification and backstepping control of uncertain Lü system," *Chaos, Solitons & Fractals*, vol. 18, no. 4, pp. 721-729, 2003.

[45] J. Lü, X. Yu and G. Chen, "Generating chaotic attractors with multiple merged basins of attraction: a switching piecewise-linear control approach," *IEEE Trans. Circuits Syst. I*, vol. 50, no. 2, pp. 198-207, 2003.

[46] J. Lü, G. Chen and D. Z. Cheng, "A new chaotic system and beyond: the general Lorenz-like system," *Int. J. of Bifurcat. Chaos*, vol. 14, no. 5, pp. 1507-1537, 2004.

[47] J. Lü, X. Yu, G. Chen and D. Cheng, "Characterizing the synchronizability of small-world dynamical networks," *IEEE Trans. Circuits Syst. I*, vol. 51, no.4, pp. 787-796, 2004.

[48] G. Chen and J. Lü, *Dynamics of Lorenz System Family: Analysis, Control and Synchronization*, Science Press (in Chinese), Beijing, China, 2003.

[49] K. S. Tang, G. Q. Zhong, G. Chen and K. F. Man, "Generation of n-scroll attractors via sine function," *IEEE Trans. Circuits Syst. I*, vol. 48, no. 11, pp. 1369-1372, 2001.

[50] K. S. Tang, K. F. Man, G. Q. Zhong and G. Chen, *Some New Circuit Design for Chaos Generation, Chaos in Circuits and Systems* (G. Chen and T. Ueta, eds.), pp. 171-190, World Scientific, Singapore, 2002.

[51] G. Q. Zhong, K. F. Man and G. Chen. "A systematic approach to generating n-scroll attractors," *Int. J. Bifurcat. Chaos*, vol. 12, no. 12, pp. 2907-2915, 2002.

[52] X. F. Wang and G. Chen, "Chaotification via arbitrarily small feedback controls: Theory, Methods and Applications," *Int. J. of Bifurcat. Chaos*, vol. 10, no. 3, pp. 549-570, 2000.

[53] X. F. Wang, G. Chen and X. Yu, "Anticontrol of chaos in continuous-time systems via time-delay feedback. *Chaos*, vol. 10, no. 4, pp. 771-779, 2000.

[54] U. F. Moreno, P. L. D. Peres and I. S. Bonatti, "Analysis of piecewise-linear oscillators with hysteresis," *IEEE Trans. Circuits Syst. I*, vol. 50, no. 8, pp. 1120-1124, 2003.

[55] M. P. Kennedy and L. O. Chua, "Hysteresis in electronic circuits: a circuit theorist's perspective," *Int. J. Circuit Theory Appl.*, vol. 19, pp. 471-515, 1991.

[56] R. W. Newcomb and S. Sathyan, "An RC op amp chaos generator," *IEEE Trans. Circuits Syst. I*, vol. 30, no. 1, pp. 54-56, 1983.

[57] R. W. Newcomb and N. El-Leithy, "A binary hysteresis chaos generator," *Proc. of the IEEE Symp. Circuits. Syst.*, pp. 856-859, Montreal, Canada, 1984.

[58] R. W. Newcomb and N. El-Leithy, "Chaos generation using binary hysteresis," *Circuit System, Signal Processing*, vol. 5, no. 3, pp. 321-341, 1986.

[59] T. Saito, "On a hysteresis chaos generator," *Proc. of the IEEE Symp. Circuits. Syst.*, pp. 847-849, Kyoto, Japan, 1985.

[60] T. Saito, "The hysteresis chaos generator family, " *Proc. of the IEEE Symp. Circuits. Syst.*, vol. 1, pp. 15-18, Espoo, Finland, 1988.

[61] T. Saito, "An approach toward higher dimensional hysteresis chaos generators," *IEEE Trans. Circuits Syst. I*, vol. 37, no. 3, pp. 399-409, 1990.

[62] T. Saito, "Reality of chaos in four-dimensional hysteresis circuits," *IEEE Trans. Circuits Syst. I*, vol. 38, no. 12, pp. 1517-1524, 1991.

[63] K. Mitsubori and T. Saito, "A four-dimensional plus hysteresis chaos generator", *IEEE Trans. Circuits Syst. I*, vol. 41, no. 12, pp. 782-789, 1994.

[64] T. Suzuki and T. Saito, "On fundamental bifurcations from a hysteresis hyperchaos generator," *IEEE Trans. Circuits Syst. I*, vol. 41, no. 12, pp. 876-884, 1994.

[65] T. Saito and S. Nakagawa. "Chaos from a hysteresis and switched circuit," *Phil. Trans. R. Soc. Lond. A*, vol. 353, pp. 47-57, 1995.

[66] T. Saito and K. Mitsubori, "Control of chaos from a piecewise linear hysteresis circuit," *IEEE Trans. Circuits Syst. I*, vol. 42, no. 3, pp. 168-172, 1995.

[67] S. Nakagawa and T. Saito, "An RC OTA hysteresis chaos generator," *IEEE Trans. Circuits Syst. I*, vol. 43, no. 12, pp. 1019-1021, 1996.

[68] S. Nakagawa and T. Saito, "Design and control of RC VCCS 3-D hysteresis chaos generator," *IEEE Trans. Circuits Syst. I*, vol. 45, no. 2, pp. 182-186, 1998.

[69] T. Tsubone and T. Saito, "Hyperchaos from a 4-D manifold piecewise-linear system," *IEEE Trans. Circuits Syst. I*, vol. 45, no. 9, pp. 889-894, 1998.

[70] M. Kataoka and T. Saito, "A two-port VCCS chaotic oscillator and quad screw attractor," *IEEE Trans. Circuits Syst. I*, vol. 48, no. 2, pp. 221-225, 2001.

[71] M. Parodi, M. Storace and S. Cincotti, "A PWL ladder circuit which exhibits hysteresis," *Int. J. Circuit Theory Appl.*, vol. 22, pp. 513-526, 1994

[72] M. Parodi, M. Storace and S. Cincotti, "Static and dynamic hysteresis features in a PWL circuit," *Int. J. Circuit Theory Appl.*, vol. 24, pp. 183-199, 1996.

[73] M. Storace, M. Parodi and D. Robatto, "A hysteresis-based chaotic circuit: dynamics and applications," *Int. J. Circuit Theory Appl.*, vol. 27, pp. 527-542, 1999.

[74] M. Storace and M. Parodi, "Simple realization of hysteresis chaos generator," *Electron. Lett.*, vol. 34, no. 1, pp. 10-11, 1998.

[75] F. Bizzarri and M. Storace, "RC op-amp implementation of hysteresis chaotic oscillator," *Electron. Lett.*, vol. 37, no. 4, pp. 209-210, 2001.

[76] F. Bizzarri and M. Storaec, "Bifurcation analysis of a PWL chaotic circuit based on hysteresis through a one-dimensional map," *Int. J. Bifurcat. Chaos*, vol. 11, no. 7, pp. 1911-1927, 2001.

[77] J. E. Varrientos and E. Sanchez-Sinencio, "A 4-D chaotic oscillator based on a differential hysteresis comparator," *IEEE Trans. Circuits Syst. I*, vol. 45, no. 1, pp. 3-10, 1998.

[78] F. Dachselt and W. Schwarz, "Chaos and cryptography," *IEEE Trans. Circuits Syst. I*, vol. 48, no. 12, pp. 1498-1599, 2001.

[79] T. Yang, C. W. Wu and L. O. Chua, "Cryptography based on chaotic systems," *IEEE Trans. Circuits Syst. I*, vol. 44, no. 5, pp. 469-472, 1997.

[80] D. Frey, "On adaptive chaotic encoding," *IEEE Trans. Circuits Syst. I*, vol. 45, no. 11, pp. 1200-1205, 1998.

[81] K. Li, Y. C. Soh and Z. G. Li, "Chaotic cryptosystem with high sensitivity to parameter mismatch," *IEEE Trans. Circuits Syst. I*, vol. 50, no. 4, pp. 579-583, 2003.

[82] R. Jauregui-Ortiz and G. Solís-Perales, " A chaos-based communication scheme via robust asymptotic feedback," *IEEE Trans. Circuits Syst. I*, vol. 48, no. 10, pp. 1161-1169, 2001.

[83] F. C. M. Lau, M. M. Yip, C. K. Tse and S. F. Hau, "A multiple-access technique for differential chaos-shift-keying," *IEEE Trans. Circuits Syst. I*, vol. 49, no. 1, pp. 96-104, 2002.

[84] V. Varadan and H. Leung, "Design of piecewise maps for chaotic spread-spectrum communications using genetic programming," *IEEE Trans. Circuits Syst. I*, vol. 49, no. 11, pp. 1543-1553, 2002.

[85] K. Murali, H. Leung and H. Y. Yu, "Design of noncoherent receiver for analog spread-spectrum communication based on chaotic masking," *IEEE Trans. Circuits Syst. I*, vol. 50, no. 3, pp. 432-441, 2003.

[86] G. Kolumban, M. P. Kennedy and L. O. Chua, "The role of synchronization in digital communication using chaos: Part I, Fundamentals of digital communications," *IEEE Trans. Circuits Syst. I*, vol. 44, no. 10, pp. 927-936, 1997.

[87] G. Kolumbán, M. P. Kennedy and L. O. Chua, "The role of synchronization in digital communications using chaos – Part II: Chaotic modulation and chaotic synchronization," *IEEE Trans. Circuits Syst. I*, vol. 45, no. 11, pp. 1129-1140, 1998.

[88] G. Kolumbán, M. P. Kennedy and L. O. Chua, "The Role of synchronization in digital communications using chaos – Part III: Performance bounds for correlation receivers," *IEEE Trans. Circuits Syst. I*, vol. 47, no. 12, pp. 1673-1683, 2000.

[89] S. Tang, H. F. Chen, S. K. Hwang and J. M. Liu, "Message encoding and decoding through chaos modulation in chaotic optical communications," *IEEE Trans. Circuits Syst. I*, vol. 49, no. 2, pp. 163-169, 2002.

[90] W. M. Tam, F. C. M. Lau, C. K. Tse and M. M. Yip, "An approach to calculating the bit-error rate of a coherent Chaos-Shift-Keying digital communication system under a noisy multiuser environment," *IEEE Trans. Circuits Syst. I*, vol. 49, no. 2, pp. 210-223, 2002.

[91] T. Yang and L. O. Chua, "Impulsive stabilization for control and synchronization of chaotic systems: theory and application to secure communication," *IEEE Trans. Circuits Syst. I*, vol. 44, no. 10, pp. 976-988, 1997.

[92] A. S. Dmitriev, A. I. Panas and D. Y. Puzikov, "Wideband and ultra wideband direct chaotic communications," *Proc. of the first IEEE Symp. Circuits Syst. for Communications*, pp. 291-295, St. Petersburg, Russia, 2002.

[93] B. E. Kyarginsky, N. A. Maximov, A. I. Panas and S. O. Starkov, "Wideband microwave chaotic oscillators," *Proc. of the first IEEE Symp. Circuits Syst. for Communications*, pp. 296-299, St. Petersburg, Russia, 2002.

[94] H. D. Chiang, C. W. Liu, P. P. Varaiya, F. F. Wu and M. G. Lauby, "Chaos in a simple power system," *IEEE Trans. Power Syst.*, vol. 8, no. 4, pp. 1407-1417, 1993.

[95] H. O. Wang, E. H. Abed and A. M. A Hamdan, "Bifurcation, chaos and crises in voltage collapse of a model of power system," *IEEE Trans. Circuits Syst. I*, vol. 41, no. 3, pp. 294-302, 1994.

[96] M. Gilli, "Strange attractors in delayed cellular neural networks," *IEEE Trans. Circuits Syst. I*, vol. 47, no. 11, pp. 849-853, 1993.

[97] F. Zou and J. A. Nossek, "Bifurcation and chaos in cellular neural networks," *IEEE Trans. Circuits Syst. I*, vol. 40, no. 3, pp. 166-173, 1993.

[98] H. Lu, Y. He and Z. He, "A chaos-generator: analyses of complex dynamics of a cell equation in delayed cellular neural networks," *IEEE Trans. Circuits Syst. I*, vol. 45, no. 2, pp. 178-181, 1998.

[99] H. H. C. Iu and C. K. Tse, "A study of synchronization in chaotic autonomous Ćuk DC/DC converters," *IEEE Trans. Circuits Syst. I*, vol. 47, no. 6, pp. 913-918, 2000.

[100] Z. Li, J. B. Park, Y. H. Joo, B. Zhang and G. Chen, "Bifurcations and chaos in a permanent-magnet synchronous motor," *IEEE Trans. Circuits Syst. I*, vol. 49, no. 3, pp. 383-387, 2002.

[101] J. M. Ottino, F. J. Muzzio, M. Tjahjadi, J. G. Franjione, S. C. Jana and H. A. Kusch, "Chaos, symmetry and self-similarity: Exploiting order and disorder in mixing process," *Science*, vol. 257, pp. 754-760, 1992.

[102] R. S. Mackay, *Some Thoughts on Chaos in Engineering, in Towards the Harnessing of Chaos*, (M. Yamaguti ed.), pp. 73-82, Elsevier Sci., New York, 1994.

[103] A. Garfinkel, M. L. Spano, W. L. Ditto and J. N. Weiss, "Controlling cardiac chaos," *Science*, vol. 257, pp. 1230-1235, Aug. 1992.

[104] A. L. Goldberger and B. J. West, "Applications of nonlinear dynamics to clinical cardiology," *Ann. New York Acad. Sci.*, vol. 504, pp. 195-213, 1987.

[105] S. J. Schiff, K. Jerger, D. H. Duong, T. Chang, M. L. Spano and W. L. Ditto, "Controlling chaos in the brain," *Nature*, vol. 370, pp. 615-620, Aug. 1994.

[106] M. P. Dafilis, D. T. J. Liley and P. J. Cadusch, "Robust chaos in a model of the electroencephalogram: implications for brain dynamics," *Chaos*, vol. 11, no. 3, pp. 714-717, 2001.

[107] H. –W. Lorenz, *Nonlinear Dynamical Economics and Chaotic Motion*, Springer-Verlag, Berlin, 1989.

[108] A. Medio, "Continuous-time models of chaos in economics," *Journal of Economic Behaviour and Organization*, vol. 16, pp. 115-151, 1991.

[109] H. –W. Lorenz, "Complexity in deterministic, nonlinear business cycle models – foundations, empirical evidence, and predictability," in *Nonlinear Dynamics in Economics and Social Science*, vol. 399, pp. 17-52, Springer-Verlag, Berlin, 1993.

[110] S. Ozoguz and N. S. Sengor, "Modified log-domain oscillator for chaos," *Proc. of the first IEEE Symp. Circuits Syst. for Communications*, pp. 287-290, St. Petersburg, Russia, 2002.

[111] T. Munakata, S. Sinha and W. L. Ditto, "Chaos computing: implementation of fundamental logical gates by chaotic elements," *IEEE Trans. Circuits Syst. I*, vol. 49, no. 11, pp. 1629-1633, 2002.

[112] L. O. Chua, *Introduction to Nonlinear Network Theory*, McGRAW – Hill Book Company, New York, 1969.

[113] S. Wiggins, *Introduction to Applied Nonlinear Dynamic Systems and Chaos Texts in Applied Mathematics*, vol. 2, Springer-Verlag, New York, 1990.

[114] W. R Kolk and R. A. Lerman, *Nonlinear System Dynamics*, Van Nostrand Reinhold, New York, 1992.

[115] M.J. Ogorzalek, "Taming chaos – Part I: Control," *IEEE Trans. Circuits Syst. I.* vol. 40, no. 10, pp. 591-601, 1993.

[116] T. Kapitaniak, *Controlling Chaos, Theoretical and Practical Methods in Nonlinear Dynamics*, Academic Press, London, 1996.